Senior Thesis

CRUSTAL ANALYSIS OF VENUS FROM MAGELLAN SATELLITE OBSERVATIONS AT ATALANTA PLANITIA, BETA REGIO, AND THETIS REGIO

by

Timothy E. Leftwich

1998

Submitted as partial fulfillment of the requirements for the degree of Bachelor of Science
in Geological Sciences at The Ohio State University,
Spring Quarter, 1998

Approved by:

Dr. Ralph R. B. vonFrese

Abstract

As a result of NASA's Magellan satellite mission, serious questions have arisen concerning the crust of Venus. Venus is very similar to Earth in size and composition, yet different in tectonic style and internal dynamics. For example, the primary mode of heat loss appears to be hot-spot volcanism (Head et al., 1992), whereas on Earth it is plate tectonics and plate boundary volcanism. The relatively young and unmodified appearance of most Venusian craters and their largely random distribution has led some researchers to conclude that a global resurfacing event occurred between 300 to 1000 Ma (Schaber et al., 1992). The possible correlation between modified craters and low crater density with volcanically and tectonically active regions supports the notion that ongoing volcanic activity may represent the primary mode of planetary resurfacing (Phillips et al., 1992; Head et al., 1992). An alternative hypothesis suggests that perhaps volcanism is ongoing on Venus, but at a reduced rate subsequent to a global resurfacing event (Price et al., 1996). Understanding the crustal properties of the different tectonic regions, including the crustal plateaus and their relationships to cold spots and hot spots, is important for developing meaningful models of Venusian tectonics and internal dynamics. A discrete model for the structure and properties of the Venusian crust is essential in constraining models for the tectonic and resurfacing history of Venus.

In this paper, I investigate an improved quantitative method for interpreting attributes of the Venusian crust from spherical harmonic topographic and gravity models. I use spectral correlation theory to compare gravity effects of topography against free-air gravity anomalies for the tectonically disparate regions of Atalanta Planitia, Beta Regio, and Thetis Regio. For all three areas, observed free-air gravity anomaly magnitudes are much smaller than the gravity effects modeled from topographic relief and there is strong positive correlation between free-air gravity anomalies, topography, and terrain gravity effects. Adjusting terrain gravity effects for correlated free-air gravity anomalies yield compensated effects that I use to estimate Moho relief and crustal thickness variations of the three study regions.

For Atalanta Planitia, the crust appears to be relatively thin with peripherally thickened crust associated with concentric ridge belts and tessera terrain. Crustal thickness may increase rapidly between the interior of this lowland plain and the adjacent periphery and highlands. For Beta Regio and Thetis Regio, crustal thicknesses may approach 40 km and 50 km, respectively. Beta Regio, with its large free-air gravity anomalies and apparent structurally related terrain-decorrelated gravity component, may be a partially compensated region. The lack of anticorrelated topographic and gravity features in these disparate tectonic environments is consistent with a largely undifferentiated and dynamically supported crust, which is ubiquitously distributed over the study regions and possibly the entire planet.

Table of Contents

I. Introduction

Satellite observer missions that map topography and gravity fields are providing additional constraints on the internal dynamics and structure of the Earth and other planetary bodies. Mass distribution within a planetary body tends to equilibrate and hence minimize its mean free-air gravity anomaly. If the gravity field generated by topography is greater than the observed gravity field, then topography plays a role in the isostatic compensation of the crust. Where the topographic gravity effect is less than the observed field, there must be another source to the anomalous field within the interior of the planet. This concept provides a basis for determining local states of crustal isostatic adjustment, crustal stresses, and structure from relationships between topographic gravity effects and the ambient gravity field. Correlative and noncorrelative features of topographic gravity effects and free-air gravity anomalies can be used to infer crustal structure and mass variations within the context of an appropriate compensation model. In this paper, I investigate a quantitative method for modeling the Venusian crust using spectral correlation theory to separate the correlative and noncorrelative features in topographic gravity effects and the free-air gravity anomalies (von Frese et al., 1997 & 1998). In particular, I investigate the utility of this approach for obtaining insight on the crustal properties of Atalanta Planitia, Beta Regio, and Thetis Regio using Magellan and earlier satellite observations.

A better understanding of crustal structure is central to the development of meaningful models of the internal dynamics and tectonic history of Venus. A range of geological models have been invoked to explain the gravity and topography observations of Venus that were obtained by the Magellan satellite. For example, a thin thermal lithosphere in hot-spot regions supports theories that volcanism and rifting are contemporary and volcanic resurfacing is ongoing while a thicker thermal lithosphere is predicted by the convective lid theory with periodic volcanic resurfacing (Smrekar et al., 1997). Whether or not crustal highlands are related to mantle downwelling, are remnants

of depleted hot-spot mantle plumes, or are of differing origins might be inferred by how closely related the crustal structure of these highlands is to the crustal structures of lowlands and volcanic highlands. A detailed analysis of the gravity field data, topography, and imagery from Magellan and earlier investigations is needed, especially in lowland plains such as Atalanta Planitia, to better constrain theories regarding Venusian heat loss and mantle convection and related tectonic features.

Previous studies have inferred the lack of a weak asthenosphere for Venus from deep apparent depths of compensation (e.g., Sjorgren et al., 1997), anomalous density waves (Zharkov, 1992b), and analysis of geochemical properties (Mackwell et al, 1998; Williams and Pan, 1990). An anhydrous mantle on Venus would mean a strongly viscous mantle (Kaula, 1990), a stiff elastic crust that is tightly coupled to the mantle (Mackwell et al., 1998), and consequently surface tectonics that are controlled by mantle convection. Such a viscous mantle would lead to less vigorous mantle convection than on Earth and hence relatively retarded rates of tectonic activity and continent accumulation (Kaula, 1990). Venus has 10% lower gravity than Earth, which also results in lower stress levels in the Venusian crust. Therefore, Venus at present may have a relatively strong crust that is being stressed at lower rates than on Earth as a consequence of being tightly coupled to a slowly convecting viscous mantle. Mantle convection is likely to be manifested by regionally intermittent hotspot development between interconnected downwellings and neutrally buoyant regions. Crustal plateau development may occur as a consequence of hotspot extinction (e.g., Hansen et al., 1997), compressional strain associated with downwelling mantle, or as remnants of an earlier mode of Venusian tectonics.

Whether Venus has undergone a catastrophic resurfacing event, or is undergoing periodic resurfacing, or is in a fundamentally different state now than when many of the features revealed by Magellan were formed, are questions for which a better understanding of the crustal structure and properties is required. My study investigates the use of correlative terrain gravity and free-air gravity anomaly features to model better

the thickness and isostatic properties of the Venusian crust. Improved crustal modeling for Venus may help to impose new constraints on the fundamental theories for its internal dynamics and tectonics, and thereby enhance the utility of Magellan topography and gravity data.

The Magellan satellite mission to Venus provided high-resolution imagery from its synthetic aperture radar (SAR), improved altimetry, and improved gravity field models from line-of-sight (LOS) tracking observations. Over 90% of the Venusian surface was imaged by Magellan's radar. Accuracy for relative topographic elevations from Magellan's altimetry approaches 5 meters, depending on the roughness of the terrain, although orbital uncertainties constrain absolute certainty to only about 50 meters. In extremely rough topography, measurement uncertainties are limited to about 88 meters (Pettengill et al., 1991).

Venusian gravity and topography data have been synthesized into spherical harmonic models that incorporate Magellan and earlier observations. These models provide convenient data sets for this analysis with accuracies that reflect the original data observations (Sjorgren et al., 1997). The development of the spherical harmonic topographic model to degree 360 was discussed by Rappaport and Plaut [1994]. A spherical harmonic gravity model to degree 90 was developed by Sjogren et al. [1996] with a maximum radial error of 20 milligals. However, for this study an improved gravity model to degree 120, which was subsequently developed by A. S. Konopliv, was obtained from the Planetary Data System at Washington University at St. Louis, Missouri (http://pds.geophys/pds). The maximum radial gravity error for this model is within the 20 milligal error envelop that was estimated for the previous model (Konopliv, 1998 - private communication).

In this study, I investigate the crustal properties and thickness (i.e., Moho) of three geologically disparate regions using spectral correlation analysis of the gravity effects of the Venusian terrain against free-air gravity anomalies. In particular, I consider

64°-by-64° areas at 1° grid spacing that are inclusive of a representative lowland plain (i.e., Atalanta Planitia), a volcanic highland (i.e., Beta Regio), and a complexly ridged highland (i.e., Thetis Regio). The study regions are labeled in the global topographic relief map of figure 1.

A discrete least squares model of the gravity effects of the topography, or terrain gravity effects, is obtained utilizing Gauss-Legendre quadrature integration (von Frese et al, 1981). The terrain gravity effects are compared to the corresponding free-air gravity anomalies for the correlation spectrum. Spectral correlation filters are then implemented to extract terrain-correlated and terrain-decorrelated components of the free-air gravity anomalies. Subtracting the terrain-correlated free-air gravity components from the terrain gravity effects yields compensated terrain gravity effects that provide insight on possible isostatic properties of the crust. Because the compensated terrain gravity effects are not evident in the ambient free-air gravity field, an annihilating gravity effect can be inferred, which can be interpreted for mantle relief or crustal thickness variations assuming an appropriate compensation model and *a priori* constraints on the density contrast between crust and mantle.

This methodology was developed for the crustal analysis of the Mare Orientale, which is the largest impact crater on the Moon (von Frese et al., 1997c). It was tested and validated in crustal studies of the Antarctic (von Frese et al., 1997b), East Asia (Tan and von Frese, 1997), and Ohio (Kim, 1996), with Moho relief having been found to be within 10% of that observed by large offset seismic studies. In the following sections, I describe the derivation of crustal models that satisfy the independently derived topography and gravity data. I explore the derived crustal models in the context of the geology, and regional tectonics for the study areas as revealed by Magellan and earlier satellite observations, and discuss the utility of this approach for developing additional insight on the tectonic history of Venus.

II. Spectral Correlation Modeling of the Venusian Crust

The wavenumber correlation spectrum (von Frese et al., 1997) between Fourier transforms of the terrain gravity effects (**T**) and the free-air gravity anomalies (**F**) is given by:

$$CC(k)=cos(\Delta\theta k)=Re[\mathbf{F}(k)/\mathbf{T}(k)]\ [|\mathbf{T}(k)|/|\mathbf{F}(k)|], \qquad (1)$$

where $CC(k)$ is the correlation coefficient between the kth wavenumber components $\mathbf{F}(k)$ and $\mathbf{T}(k)$ with amplitude spectra given by $|\mathbf{F}(k)|$ and $|(\mathbf{T}k)|$, respectively, and *Re* denotes taking the real parts of the wavenumber components. $CC(k)$ is evaluated from the cosine of the phase difference of $(\Delta\theta k)$ between the two kth wavenumber components.

The gravity effect of the terrain must be effectively modeled in order for its transform to be taken and correlation spectrum to be evaluated. Following von Frese et al. [1981], I use Gauss-Legendre quadrature (GLQ) integration to model with least squares accuracy the gravity effects due to the mass variation that is represented by topographic relief. By the GLQ method, a mass volume is represented by point sources that are positioned so as to account for the quadrature decomposition of the volume. The resulting gravity effect can then be modeled by integrating the point source representations of the mass variation components. The gravity effects (Δg) of topography with a specified density contrast ($\Delta\sigma$) and arbitrary shape in spherical coordinates (φ,θ,r) can be estimated with least squares accuracy by:

$$\Delta g(\varphi,\theta,r)\cong \qquad (2)$$

$$\Delta\varphi'_l\Sigma_l\{\Delta\theta'_j\Sigma_j(\Delta r'_i\Sigma_i[(G/R^2)(\partial R/\partial r)\Delta\sigma]A_i)A_j\}A_l,$$

where G is the gravitational constant, R is the distance or displacement vector between the source points (primed) and observation points (unprimed), r is the radial distance vector between the center of mass of the planetary body and the observation point coordinates, and (A_i,A_j,A_l) are the Gauss-Legrende quadrature weights (Stroud and Secrest, 1966). In addition, $\Delta\varphi'_l = [(\varphi'_{la} - \varphi'_{lb})/2]$, $\Delta\theta'_j = [(\theta'_{ja} - \theta'_{jb})/2]$, and $\Delta r'_i = [(\Delta r'_{ja} - \Delta r'_{jb})/2]$, where $(\varphi'_{la},\varphi'_{lb})$, $(\theta'_{ja},\theta'_{jb})$, and (r'_{ja},r'_{jb}) are the lower a and upper b

volume limits of the body, respectively, in the *l*th coordinate of longitude (φ), the *j*th coordinate of co-latitude (θ), and the *i*th radial coordinate (r).

The gravity effects of the terrain can be modeled in spherical or other coordinates with least squares accuracy by equation *(2)* (von Frese et al., 1981; Mateskon, 1985; Mateskon and von Frese, 1985; von Frese and Mateskon, 1985; Hayden, 1996). The free-air gravity anomalies and the modeled terrain gravity effects can then be transformed by the fast Fourier transform so that their transforms **F** and **T**, respectively, may be compared in the wavenumber domain for their correlation spectrum in equation *(1)*.

Using the correlation spectrum, spectral filters were developed to extract the common features in both the free-air anomalies and terrain gravity effects. In particular, those wavenumber components that show high positive and negative correlation between the free-air anomalies and the terrain gravity effects were identified. These correlated components were inversely transformed to obtain terrain-correlated free-air gravity anomalies that can constrain the local state of isostatic equilibrium within the context of an appropriate crustal compensation model. The terrain-decorrelated free-air gravity anomalies and compensated terrain gravity effects were obtained by subtracting the terrain-correlated free-air gravity anomalies from the free-air anomalies and terrain gravity effects, respectively. Because the compensated terrain gravity effects are not seen in the free-air anomalies, an annihilating anomaly field may be assumed that can be interpreted for possible Moho relief or crustal thickness variations. Reversing the polarities of the compensated terrain gravity effects yields the gravity effects that annihilate the compensated terrain gravity effects. I will herein refer to these effects simply as compensation annihilating effects. Mass imbalances in the subsurface would impose a crustal response and hence the terrain-correlated free-air anomalies may be used to imply local crustal stress fields and the possible tectonic response.

The correlative properties between the free-air gravity anomalies and the terrain gravity effects are revealed in figure 2, where the ratios of output-to-input power are

plotted for the three regions as a function of cutoff values of the correlation coefficient (CC). The cutoff CC's plotted in these spectra correspond to power ratios of the wavenumber k-components for which their correlation $CC(k) \geq CC$ if the cutoff $CC \geq 0$, or $CC(k) <$ if $CC < 0$.

The correlation coefficient power ratio spectra for the three study regions (Figure 2) reflect high positive correlation between free-air gravity and the terrain gravity data. Although the study regions are disparate in tectonic style and location, the correlation coefficient power ratio spectra for the three regions are remarkably similar with most of the power concentrated in wavenumbers that are positively correlated with CC 0.8. Intra crustal density variations related to variations in crustal composition, or temperature, or other factors can add perturbations to the ambient gravity field that are not related to topography. Hence such density contrasts within the crust would tend to minimize correlations between the observed gravity field and the terrain gravity effects in the context of the simple Airy-Heiskanen model for crustal isostacy. However, the correlation power ratio spectra for the various regions are dominated by positively correlated components, which indicates that the crust of Venus may be largely undifferentiated from region to region and within the regions. This finding supports an inferred unimodal crust for Venus (e.g., Weitz and Basilevsky, 1993).

Although correlations between terrain gravity effects and the free-air gravity anomalies are high, the gravity observations are generally of much lower magnitude than the gravity effects of the terrain. Hence the topography may be largely compensated by and closely associated with dynamic support in the mantle related perhaps to thermal convection. Beta Regio is associated with somewhat larger free-air gravity anomalies that may indicate a relatively greater degree of incomplete isostatic equilibrium for the topography of Beta Regio.

Subtracting terrain-correlated free-air gravity anomalies from the free-air gravity anomalies yields terrain-decorrelated free-air gravity components. For the three tectonic

regions of this study, the terrain-decorrelated free-air gravity anomalies are generally minimal in magnitude and bear scant resemblance to either the original gravity observations or the topography. They are inferred to be nonisostatic with the total amplitude ranges for these spectra being less than or equal to 20 milligals. Beta Regio, being associated with relatively large free-air gravity anomalies, yields terrain-decorrelated free-air gravity components that may provide insight on regionally coherent intra-crustal features. However, further analysis of these features is beyond the scope of this study.

To better visualize correlative features between the free-air and the topographic gravity data, local favorability indices may be used (von Frese et al., 1997). To establish positively correlated features between data sets $\boldsymbol{F}$ and $\boldsymbol{T}$, standardized free-air gravity anomalies (f_i) and terrain gravity effects (t_i) can be summed to create the summed local favorability indices (SLFI) by

$$SLFI_i=[f_i-\mu(F)]/\sigma(F) + [t_i-\mu(T)]/\sigma(T) \;\forall\; i=1,2,3,\ldots m,$$

where μ and σ are the respective means and standard deviations of the data sets. Inversely correlated features may be identified by differencing the standardized data sets to create the differenced local favorability Indices (DLFI) according to

$$DLFI_i= [f_i-\mu(F)]/\sigma(F) - [t_i-\mu(T)]/\sigma(T) \;\forall\; i=1,2,3,\ldots m.$$

Plotting only the favorability coefficients above and below their standard deviations enhances the visualization of the most correlative features. Favorability indices facilitate mapping out and interpreting the correlative features between digital data sets. For example, large negative DLFIs enhance areas where free-air gravity minima correspond to terrain gravity effects maxima, while large positive DLFIs enhance areas where free-air gravity maxima correspond to terrain gravity effects minima. Hence, large negative and positive DLFI components can signify regions where the crust is too thick or thin, respectively, relative to Airy-Heiskanen compensation of the topography.

Conversely, large negative SLFIs enhance areas where free-air gravity minima

correspond to minimum terrain gravity effects, while large positive SLFIs target areas where free-air gravity maxima correspond to maximum terrain gravity effects. Hence large positive and negative SLFI components can target regions where crust is anomalously thin and thick, respectively relative to complete Airy-Heiskanen compensation of the topography.

The filtered output of spectral correlation analysis can be no better than the original data and assumptions used to perform the analysis. Interpretations of the analysis can be complicated by serendipitous anomaly correlations due to errors in one or both data sets, the effects of subsurface density variations that are not related to crustal topography, accumulated computational error, and other factors. Hence, care is needed to avoid interpretations based upon feature correlations that may reflect data errors or violate the assumptions of the analysis.

III. Venusian Crustal Analysis

Despite its complex geology, the surface of Venus may be classified geophysically into several broad tectonically related regions that include lowlands, highlands, coronae, and tesserae (e.g., Hansen et al., 1997, Zharkov, 1992). Lowlands or plains known as planitia have elevations at or below the mean planetary radius and constitute about 80% of the surface of Venus. Volcanic rises or dome-volcanic rises, such as Atla, Beta, Eistla Regiones and other areas, are mostly confined to equatorial latitudes (eg., Head et al., 1992). Highlands (Hansen et al., 1997), or crustal plateaus (Zharkov, 1992a), which have also been called plateau-shaped highlands (Bindschadler et al., 1992), are flat-topped high-elevation regions with steep sides (e.g., Alpha, Ovda, Phoebe, Tellus, Thetis, and the unique Ishtar Terra). Complexly ridged areas known as tesserae (from the Greek word meaning tiles) (Bindschadler et al, 1992; Solomon et al., 1992) are often found within highlands (e.g., Alpha Ovda, Thetis). Magellan data suggests that Ishtar Terra has compressional tectonic features and may be a region of thickened crust related to downwelling mantle (e.g., Solomon et al., 1992). Coronae are

often domal and preferentially concurrent with volcanic highlands in lower latitudes (Stofan, et al., 1992).

Previous studies have found that the gravity and topography power spectra for Venus are very similar to those of the Earth. However, the correlation spectrum between Venusian gravity and topography is highly correlated at all wavelengths, indeed, more so than any other planet (Sjogren et al., 1996). This high correlation implies that gravity and topography are strongly related to common interior processes (Sjogren et al., 1980; 1996). Although there is a strong correlation between the topography and the ambient gravity field, significant compensation of the topography may have occurred. The volcanic highlands of Atla and Beta Regiones have large apparent depths of compensation relative to other areas of Venus and smaller Bouguer gravity anomalies, however, suggesting that these regions may not be in complete isostatic adjustment (Sjogren et al., 1983; Smrekar et al., 1997).

Earth-style plate tectonics with rifting and midocean ridges that allow mantle material to breach the planetary surface are not seen on Venus. Hence mantle convection beneath a floating massive crust (50 to 70 km) has been proposed for Venus (Zharkov, 1992a). Long wavelength components of the gravity field that correlate with corresponding harmonics of topography reflect crustal density variations from either temperature (e.g., a hot mantle plume supporting the base of the crust), thickness, or compositional variations. Zharkov [1992a] found that spherical harmonic expansion of the topography correlates well with the corresponding expansion of gravity for degrees greater than 2 even though the topography is largely compensated. For an elastic model of the planet, which would be consistent with evidence regarding rheologies and mantle viscosity from Kaula [1990], Mackwell et al.[1998] and Williams and Pan [1990], Zharkov [1992a] found that crustal thickening compensated highlands of all kinds and crustal thinning--up to the surface--compensated lowlands. Compressional stresses were predicted in lowlands in the Zharkov crustal models. Extensional stresses were predicted

for all highlands including such non-volcanic highlands as Ishtar Terra and Ovda Regio, which Magellan imagery subseqently revealed to have apparently compressionl tectonic features.

Herrick and Phillips [1992] assumed dynamic support of the topography by mantle convection to analyze degree 18 spherical harmonic representations of Venusian gravity and topography. They presented formulas and methodology for inversion of the topography and geoid into surface density anomalies on the crust mantle boundary. Assuming that density anomalies are centered at two particular depths, topography caused by a density anomaly at depth can be found using an appropriate compensation model, such as the Airy-Heiskanen model that they used. Thus near surface density anomalies can be interpreted broadly as being due to crustal variations of composition, temperature, or thickness. Herrick and Phillips [1992] suggested that the crust of Venus appears to be supported by mantle convection where cylindrical regions of hotspots punctuate interconnected regions of downwelling, colder mantle. They found volcanic highlands like Atla and Beta Regio may be supported by mantle upwelling. No strong correlation with crustal thickening is evident in the volcanic highlands, where crustal thickness in these areas appears ambiguous. Thin crust in lowland areas like Atalanta and Lavinia Planitia is inferred to lie over downwelling cold spots. Ovda-like areas and regions of tesserae are regions of maximum crustal thickening with no obvious mantle upwelling or downwelling. No obvious mantle density anomalies were inferred to exist beneath coronae in their findings, however, to support a mantle diapir hypothesis for the origin of coronae. The crustal thickness modeled by Herrick and Phillips [1992] shows a differentiation between highlands--with some highlands, such as Beta Regio, supported dynamically by mantle convections and others, such as Ishtar Terra, supported by deep crustal roots.

These earlier studies illustrate the non-unique nature of interpretations of properties of the Venusian crust from gravity and topography data. For example, both a

thickened crust and a thinned crust beneath volcanic highlands have been proposed. Yet these studies provide important constraints for models of Venusian tectonics and heat loss. New insights on the nature of volcanic highlands, crustal highlands, and lowlands may be revealed by improved quantitative methods for analysis of the crustal properties of Venus. Spectral analysis of correlations between free-air gravity anomalies and terrain gravity effects for the crustal structure of Venus may improve upon and discriminate between hypotheses for Venusian tectonics. I analyze correlations between free-air gravity anomalies and terrain gravity effects for the crustal structure of three distinct tectonic regions, within the context of the geology revealed by the Magellan satellite imagery, for insight into the global tectonics of Venus.

A. Lowland Crust

Lowland volcanic plains make up most of the surface of Venus and they constitute the major tectonic type region on Venus. These lowland plains contain a variety of volcanic features, which include small volcanic domes, coronae, and other features. However, the plains themselves are made up of flood basalts with individual units ranging into thousands of cubic km of material (Guest et al., 1992). Magellan imagery revealed that the otherwise smooth appearing surface of the lowland plains shows a remarkable diversity of features that includes smaller scale fractures and lineations, wrinkle ridges, and polygons as well as the large-scale features such as coronae, ovoids, and ridge belts.

The small-scale polygonal and linear features that occur in lowland plains have been characterized as extensional fractures or tensile cooling cracks (Banerdt, et al., 1992). Small-scale extensional features are locally more abundant in plains areas associated with coronae and small volcanic domes. Wrinkle ridges, troughs, and fracture sets frequently occur in subparallel sets that are hundreds of kilometers in length. The great areal extent and orientation of these ridges and fracture sets provide evidence of regional stress fields that may be associated with mantle tractions on the base of the

lithosphere (Banerdt et al., 1997). These plains ridges and fracture sets closely resemble those associated with Arctic icepack ridges and leads, which develop in response to surface tractions on the base of the ice sheet (Noltimier and Sahagian, 1992).

Although the small-scale polygonal and fracture features often appear to be tensional or extensional, the concentric ridge belts that are commonly located on the periphery of lowland plains have a compressional morphology that may result from global compressional stresses (Solomon et al., 1992; Squyres et al., 1992). It has been hypothesized that the linear to bowl shaped lowland plains are related to downwelling mantle beneath these features because of their depressed, bowl-like shape that is accompanied by negative gravity anomalies, surrounding compressional ridge belts that imply converging crust, and a rarity of volcanic features.

The tectonics of lowland plains impose important constraints on models of interior dynamics and estimates of the thickness of the Venusian crust. Estimates of crustal shortening indicate an 11-18 km thick elastic lithosphere for the north polar plains underthrusting Istar Terra (Solomon and Head, 1990). No more than 100 km of horizontal displacement is required for a 10 to 20 km crust beneath the plains adjacent to ridge belts of 100 km in width with up to 1 km of relief (Solomon et al., 1992). Studies of impact crater relaxation have provided additional corroborating evidence that the crustal thickness of much of the lowland plains of the northern quarter of Venus is between 10 to 20 km (Grimm and Solomon, 1988). The elevated topography of the ridge belts that are associated with lowland plains is consistent with crustal shortening and thickening (Solomon et al., 1992; Squyres et al., 1992).

There are a variety of deformational frequencies and styles seen in the tectonic features associated with the plains of Venus that infer different mechanical, compositional, or rheological layering in the crust and lithosphere of Venus. These rheological layers may range from individual lava flow units to the entire crust or lithosphere (Banerdt et al., 1997). The crust of Venus may have continued to evolve

since the formation of some these tectonic features either by thickening or perhaps thinning. Hence crustal thicknesses estimated by these methods may reflect those of the time of formation of these features (Turcotte, 1993). Although some relative dating can be shown by cross cutting relationships of linear features, partially embayed ridge belts, and deformed lava channel profiles, there remains considerable ambiguity in assigning ages to these deformations (Banerdt et al., 1997).

A prominent example of a Venusian lowland is Atalanta Planitia, which is a high-latitude, low-elevation bowl-shaped lava plain that is centered roughly at (65 °N, 165 °)E. It is approximately 3000 km in diameter, and covers roughly 1.8×10^6 km^2. The related study region encompasses a 64 °-by-64 ° area between (23 ° - 86 °)N and (133 ° - 196 °)E that encompasses an area roughly 5450 km by 6655 km. Figure 3 shows a mosaicked image of Magellan synthetic aperture radar (SAR) data for Atalanta Planitia.

This study area is primarily low-elevation volcanic plains, but it also includes part of easternmost Tethus Regio (Ananke Tessera) and a northern extension of Aphrodite Terra. Prominent ridge belts fan out around Atalanta Planitia (Solomon and Head, 1990). As shown in Figure 5, the mean elevation of the study area is -0.60 km with elevations ranging from -2.13 in central Atalanta Planitia to 1.1 km in Tethus Regio. A portion of Baltis Vallis, the longest lava channel on Venus and the longest channel of any kind yet discovered in the solar system, originates at (44.5 °N, 185 °E) and meanders through the region cutting across various geological units. The variable topographic profile of Baltis Vallis appears to be congruent with ridge belts and wrinkle ridges indicating that some crustal displacement has occurred since formation of the lava channel. Portions of the channel are obscured by more recent lava flows near its origin (Baker et al., 1992). Inspection of high resolution Magellan imagery shows the smooth plains of Atalanta Planitia to be characterized by concentric wrinkle ridges and occasional small volcanic domes with concentric ridge belts dominating the eastern and southern portions of the region.

Figure 4 shows part of central Atalanta Planitia near (65 ° N, 162 ° E) with characteristic wrinkle ridges and a few small volacanic domes. Models by Squyres et al., [1992] considered plausible rheologies to constrain estimates of the thermal gradient, strain rate and crustal thickness. Crustal thicknesses that were considered ranged from 5 to 30 km, with thicknesses in the range of 10 to 15 km being found to best satisfy the inferred rheology. These results indicate that if mantle downwelling continues and compressional tectonic features develop, crustal thickening may occur with a resultant increase in elevation. Hence it was postulated that lowlands may be genetically related to some highland areas, such as Ishtar Terra, which show high relief but lack evidence of hotspot volcanism (Bindschadler et al., 1992, Squyres et l., 1992). If Atalanta Planitia is more than just an incipient region of downwelling mantle, then evidence of crustal thickening associated with Atalanta Planitia would be consistent with this theory.

The study region encompassing Atalanta Planitia is associated with modest free-air gravity anomalies that are well correlated with topography. Equal area azimuthal plots of topography and gravity of Atalanta Planitia are shown in figures 5 and 6. Free-air anomalies amplitudes range from -50 milligals in central Atalanta Planitia to roughly 40 milligals at the periphery. Free-air gravity anomalies are less than a quarter of the amplitude of the terrain gravity effects shown in figure 7, indicating there is significant isostatic compensation of the topography. Figure 8 compares profiles of these data sets along 65 ° N across Atalanta Planitia.

SLFI and DLFI between the free-air gravity anomalies and the terrain gravity effects for Atalanta Planitia are shown in figure 9. These coefficients characterize the data sets as being predominantly positively correlated by the central gravity minima. The terrain-decorrelated components of the free-air gravity anomalies are shown in figure 10. These anomalies are low amplitude features that appear to be related more to computational noise than to broad scale features of the study region. Small amplitude free-air gravity anomalies that are highly correlated with topography and its gravity effect

in combination with small residual terrain-decorrelated free-air gravity components are consistent with a crust that is largely compensated by mantle processes.

The compensated terrain gravity effects are shown in figure 11, whereas Figure 12 gives the compensation annihilating gravity effects that were used to model the Moho and crustal thickness for Atalanta Planitia by inversion. For the inversion, a crust/mantle density contrast of 0.5 g/cm^3 and a mean crustal thickness of 15 km were assumed. The Moho was modeled and its gravity effects are shown in Figure 13. These modeled effects show 99% correlation to the original compensation annihilating with a mean error of zero mgals and a standard error that is less than 0.04 mgals. The resulting Moho and crustal thicknesses are shown in figures 14 and 15, respectively. Crustal thicknesses for the region range between about 6 km in central Atalanta Planitia to roughly 25 km beneath adjacent tessera terrain in the western portion of the study area. The crustal thickness contour map in Figure 15 and corresponding profiles shown in figure16 indicate a thinned crust in the central, bowl-shaped basin of Atalanta Planitia that is surrounded by relatively thickened crust of the concentric ridge belts and isolated tessera terrain. Crustal thicknesses can increase dramatically from the central Atalanta depression towards the ridge belts to the south (e.g., 45 °N,165 °E) and east, which includes Vedma Dorsa (e.g., 50 °N,170 °E). Crustal thicknesses appear to increase more gradually from the central depression to Tethus Regio in the west-central part of the study area.

Atalanta Planitia may represent a slowly evolving tectonic region since emplacement of extensive regional flood lavas and the longest lava channel Baltis Vallis. However, absolute dating of the formation of the ridge belts, the lava channel deformation, and the individual stratigraphic lava units remains ambiguous. Crater densities for regional plains indicate that the average age for most of these regions is near the global average for the planet, which corresponds to a reference age of approximately 300 Ma (Basilevsky et al., 1997). Ridge belts disrupt the smooth plains surface, while tesserae appear partially embayed by flood lavas, indicating that ridge belt formation

occurred subsequent to tesserae and flood volcanics formation and may continue at present. The crustal thickness profiles (fig. 16), indicate abrupt crustal thickness increases associated with the compressional ridge belts surrounding Atalanta Planitia and hence suggest crustal shortening and thickening associated with the convergence of the underlying mantle in the vicinity of the central depression. The cross-cutting relationship of ridge belts superposed upon plains units indicates that tectonic processes subsequent to plains formation may be responsible for the crustal shortening and thickening associated with the concentric ridge belts around Atalanta Planitia. These findings are consistent with crustal compression and shortening associated with a region of downwelling mantle.

B. Volcanic Highlands Crust

Volcanic rises are concentrated in the equatorial latitudes in a region extending from 180 ° to 310 ° E and 45 ° N to 45 ° S over roughly one third of the Venusian equatorial circumference. These rises are volcanically constructed regions characterized by broad domal topography with diameters from 1000 to 2500 km and heights from 1 to 2.5 km. These regions have large positive gravity anomalies and have comparatively deep apparent depths of compensation. They exhibit large volcanic edifices and often have coronae and extensive rifting (Bindschadler et al., 1992).

Hansen et al. [1996] identify nine volcanic highlands including Atla, Bell, Beta, Dione, Imdir, Themis, Regiones and eastern, central, and western Eistla Regio. Volcanic highlands and intervening highland terrain cover about 20% of the planet's surface. It appears that the most recent volcanic activity was within the Beta/Atla/Themis area and south of Alpha Regio (Head et al., 1992; Crumpler et al., 1996). The entire crust of Venus appears to be volcanic in nature and mostly basaltic in composition (eg. Saunders et al., 1991; Weitz and Basilevsky, 1993). Volcanism may have subsided considerably subsequent to a major resurfacing of Venus 300 to 500 Ma ago, however, during which the regional plains material was emplaced. A shift to rift and shield basaltic volcanism may have occurred subsequent to formation of the plains (Basilevsky et al., 1997). Based

on stratigraphic relationships, many large volcanoes, rifts, coronae, and lava flows appear to be much younger than the age of global resurfacing and ongoing volcanic activity is likely (Price et al., 1996).

Venusian volcanoes are not confined to linear zones as they are on Earth where volcanic features are concentrated along divergent and convergent plate boundaries (Head et al., 1992) and plate tectonics do not appear to be important on Venus (e.g. Hansen and Phillips 1993). While shield, intermediate, and large volcanoes look much like the shield volcanoes on Earth such as in Iceland (Garvin and Williams, 1990), the calderas resemble hot spot areas such as Yellowstone. The lack of coherent lineation in volcanic features that resemble terrestrial hotspots and evidence from the distribution of impact craters indicates that Earth-style tectonic activity has not occurred on Venus within the past few hundred million years (Schaber et al., 1992).

The radial and axial fracture systems associated with volcanic rises are evidence of regional uplift and deformation that proceeded during formation of the volcanic constructs (Grimm and Phillips, 1992). While tensional tectonic features in volcanic rises are incompatible with conventional flexural models, they are consistent with upwelling mantle support within a hot spot model (Banerdt, 1986).

Since volcanic rises are associated with large positive free-air gravity anomalies that correlate well with the topography, any explanation of the topography of these rises must also be consistent with these anomalies. Volcanic rises are inferred by these large gravity anomalies to be supported dynamically by an upwelling mantle in the subsurface since a simple Airy-Heiskenen type root to the topography would result in a much smaller anomalies (Turcotte, 1993). The concentration of volcanic features, the presence of regional highlands with extensional tectonic features and rifting indicating crustal uplift, and large positive gravity anomalies, all point to a hot mantle upwelling origin for volcanic highlands (Crumpler, et al 1993; Phillps at al., 1991; Smrekar et al., 1996).

Grimm and Phillips [1992] analyzed the geology and gravity anomalies of hot

spots located in western and central Eistla Regio to infer regional dynamic mantle support, regional stress and strain fields, and variations in lithospheric thickness. Using an inversion of topography and gravity data to solve for mass variations on the crust/mantle boundary, crustal thicknesses were inferred. If volcanism and crustal thickening were entirely responsible for the volcanic edifice, gravity anomalies would be minimal, and thus at least part of the topography may be supported dynamically by thermal convection in the mantle. Grimm and Phillips [1992] find regional dynamic uplift with crustal thinning beneath the rift zone of Guor Linea and the large volcanic edifice of Guor Mons. Central Eistla Regio was interpreted to be a waning mantle plume with mature volcanic structures and a larger crustal component implying crustal thickening.

Debate continues on whether mantle convection is confined beneath a thickened lithosphere or results in crustal thinning and extension beneath volcanic rises and rift zones. Although a thickened lithosphere is consistent with the overall apparent low levels of volcanism, lithospheric thinning beneath volcanic rises is consistent with apparent recent volcanism (Smrekar, 1994), rifting, and the topographic loads that may be supported dynamically by upwelling mantle (Semrekar et al., 1996). Evolution from active hot spot to mature hotspot may also result in thickened crust composed of cooled and relatively evolved source magma. Eventually hot spots may become extinct, collapse, and gravitationally spread, which may indicate a genetic relationship between volcanic rises and crustal highlands (Phillips et al., 1991).

A prominent example of a volcanic highland that may be considered a "type" hot-spot volcanic highland on Venus (Phillips et al., 1991) is Beta Regio, which is shown in Figure 17. Beta Regio is an approximately 1800 km diameter broad, roughly circular, domal volcanic highland region that intersects a triple junction of rift zones and extensional linea that is centered at approximately 30 °N, 285 °E. Magellan imagery shows that Beta Regio is dominated by the volcanic edifice of Theia Mons, which is in

excess of 2 km in height, the topographic peak of Rhea Mons, and the north-south rifting of Devana Chasma. Topography for Beta Regio is plotted in an equal area azimuthal projection in figure 18. Beta Regio is associated with large positive free-air gravity anomalies with maximum amplitudes exceeding 130 milligals as shown in figure 19. Free-air gravity anomalies are highly correlated with topography and its related terrain gravity effects that are shown in figure 20.

Comparisons of topography, terrain gravity effects, and free-air gravity anomalies along 30 $^{\circ}$ N latitude across Beta Regio are shown in figure 21. The terrain-decorrelated free-air gravity anomalies shown in figure 22 appear to be mostly related to the structure of central Beta Regio, thereby indicating only partial isostatic compensation of the Beta Regio dome.

Theia Mons is a large volcanic edifice located within the center of Beta Regio. It is superposed on the Devana Chasma rift zone, but is cut by subsequent rifting indicating that volcanism and rifting have been concurrent. The Theia Mons caldera with volcanics superposed upon rifting is seen in figure 23. The occurrence of rifting, volcanism superposed upon rifting, and a rifted impact crater imply that Beta Regio is a site of extensive recent volcanism and tectonic activity (Solomon et al., 1992). Magellan imagery shows that Rhea Mons is within a region of rifted, complexly ridged terrain or tessera that is composed of primarily NE trending ridges and volcanically embayed valleys. Rhea Mons is not associated with volcanic flows and does not appear to be a volcanic edifice (Solomon, et al., 1992). The central bifurcating rift zone of Devana Chasma, which is overlain by the volcanic edifice of Theia Mons and its associated volcanics, has a total vertical relief of over 6 km south of Theia Mons. Coronae are noted on the flanks of Beta Regio and a string of coronae are associated with extensional linea to the north of Beta Regio.

Although a variety of compensation mechanisms may contribute to the total compensation of volcanic highlands, involving temperature, density, or crustal thickness

variations, it is impossible to separate unambiguously the relative contributions of these mechanisms from gravity and topography observations alone (Smrekar et al., 1994). However, despite this ambiguity, some constraints may still be implied for the contributions of topography and mantle upwelling. The effects of flexural compensation of topographic loads, such as due to volcanic edifices, that are not recognized in the long wavelength gravity and topography data may be apparent in the short wavelength observations and hence distinguished from other compensation mechanisms (Smrekar et al., 1994).

The SLFI and DLFI for Beta Regio shown in figure 24, for example, can provide indications of the topographic load associated with its volcanic dome. Large positive SLFI target the distribution of highly correlated free-air gravity and the terrain gravity maxima that infer strong topographic components to the gravity field. Large positive SLFI components are associated with central Beta Regio to indicate that crustal thickness may be enhanced here. While large positive SLFI components dominate the central Beta massif, large negative DLFI components, which highlight negative free-air gravity components that correspond to positive terrain gravity effects, effectively encircle the positive SLFI feature. This feature coincidence is compatible with the central volcanic massif being associated with thickened crust, but which also is loading the surface and surrounding relatively thinner crust. The topographic and free-air gravity anomaly profiles (see fig. 21) are broadly comparable to topographic and free-air gravity anomalies of an Hawaiian isle, which represents a topographic load that flexurally bends the oceanic crust (Fowler, 1996). In general, Beta Regio topography, free-air gravity, and local favorability indices are consistent with the presence of a large volcanic edifice with relatively thickened crust that is exerting a short wavelength topographic load on the adjacent thinner crust

Compensated terrain gravity effects are shown in figure 25 and their related annihilating effects are shown in figure 26. Inversion of the compensation annihilating

effects for the Moho was developed for the 64°-by-64° area encompassing Beta Regio using a crust/mantle density contrast of 0.5g/cm^3 and a mean crustal thickness of 15 km. The gravity effects of the modeled Moho as shown in figure 27 match more than 99% of the compensation annihilating effects with mean error of 0 mgals and standard error that is less than 0.02 mgals. The resulting Moho and crustal thicknesses are shown in figures 28 and 29, respectively, with corresponding crustal thickness profiles are shown in figures 30 and 31. The modeled crustal thicknesses varied roughly between 7 km to 42 km and are well within plausible thicknesses for the region. The model produced a thickened crust for Beta Regio ranging generally between 25 and 30 km. Crustal thicknesses for Beta Regio may be ambiguous due to difficulties in separating density variations due to crustal thickness or temperature variations. However, evidence of topographic loading support a thickened crust for Beta Regio as shown in the crustal thickness maps and profiles. This finding is consistent with predictions of a thickened crust associated with this volcanic highland and may be compatible with theories predicting limited levels of Venusian volcanism currently.

C. Plateau Crust

Venusian highlands, which are classified as crustal plateaus based on their gravity and tectonic characteristics, constitute a major and enigmatic type of tectonic province (Bindschadler et al., 1992; Hansen et al., 1996). Steep outer rises outline crustal plateau regions that range from 1000 to 3000 km in diameter and may reach elevations up to 4 km. Crustal plateaus are dominated by complex ridge and trough terrain that is frequently indicative of multiple deformation episodes and complex developmental histories. Compressional ridge belts are common at the periphery of crustal plateaus and may occur locally in the interior of the highland. These regions have small gravity anomalies and geoid-to-topography ratios and small apparent depths of compensation compared to volcanic highlands. The surfaces of crustal highlands are dominated by complexly ridged terrain with fewer volcanic flow features than in the plains, and few of

the large volcanic shields that are associated with the volcanic highlands.

Topography and gravity data provide a basis for distinguishing crustal plateaus from other highlands. Gravity anomalies, geoid-to-topography ratios and apparent depths of compensation for crustal plateaus are depressed relative to volcanic highlands (e.g., Phillips et al., 1991). Crustal plateaus may be isostatically compensated regions of thickened crust with low correlation between long wavelength topography and gravity anomalies (Hansen et al., 1996).

Hansen et al. [1996] included Ovda, Thetis, Tellus, Alpha, and Phoebe Regiones as crustal plateaus. Magellan imagery has shown that Ishtar Terra has tectonic features that are considered compressional and actually appear to be associated with a downwelling mantle region (e.g., Solomon et al., 1992). Highlands of Ishtar Terra exhibit a set of rather unique characteristics with regard to its massive Maxwell Montes mountain range, compressional deformation, and gravity signature.

Formation of crustal plateaus remains a controversial subject for Venus investigators who have identified two end model hypotheses for their formation. One theory relates evolution of crustal plateaus to mantle downwelling with formation of compressional ridge belts and complex terrain developing as crustal units are brought together by downwelling mantle (Bindschadler et al., 1992). Compressional tectonic features often are found on the periphery of crustal highlands while transform faults, graben, and other features indicative of spreading are not seen in these regions. Bindschadler et al. [1992] also do not find evidence of major volcanic structures as evidence of an evolutionary sequence within crustal highlands to support a genetic relationship to hot spots or volcanic highlands. A competing hypothesis relates these highlands to the extinction of the hot spot associated with a volcanic rise followed by crustal thickening and subsequent relaxation of the topography by gravity spreading and crustal deformation as the region evolved finally into the crustal plateau (Phillips et al., 1991).

A sequence of events is invoked in the cold-spot theory for highland formation as a result of cold, downwelling flow that is nucleated at the unstable upper thermal boundary layer of a convecting mantle. First, surface topography is deflected downward in response to downwelling mantle. As inward flow continues, crustal shortening and thickening occurs next with development of a highland on the scale of hundreds of millions to a billion years. The crustal plateau then rebounds as mantle flow wanes with a resulting increase in elevation. Finally, the region collapses and crustal gravity spreading occurs. Apparent depths of compensation should increase through this sequence, passing asymptotically through zero and becoming negative, and finally resolving to a small positive value. This prediction has not been observed in calculating apparent depths of compensation from Venus topography and gravity data, which mitigates against the cold spot hypothesis (Solomon et al., 1992).

Volcanic highlands could also evolve into crustal plateaus by a hot, rising mantle plume that creates a broad domal uplift. Partial melting at the plume head may eventually create a thickened crustal unit by magmatism and volcanic intrusion. Topography then might subside as the mantle plume wanes and topography collapses by gravity spreading. An explanation of the complex deformation of crustal plateaus within the hot spot evolutionary sequence remains problematic, because remnants of large volcanic shields are not seen in crustal plateaus (Solomon et al., 1992). Hence, crustal deformation would have to be severe enough to obliterate evidence of the earlier volcanic features.

Hansen et al. [1996] noted that if crustal plateaus were evolved from volcanic highlands, then the lack of transitional forms as evidence of earlier volcanic constructs within crustal plateaus becomes problematic. However, the significance of the lack of these forms also remains unclear. An alternative explanation relates the formation of crustal plateaus to mantle plume magmatism interacting with relatively thinner crust, where volcanic highlands result from the interaction of such plumes with relatively

thicker crust. Conditions extant at the time of crustal highland formation may have inhibited production of early stage volcanic constructs with crustal thickening being dominated by subsurface magmatism rather than surface volcanism. In this construct, plateaus and volcanic rises may both have formed in response to hot mantle plumes.

Recent progress in deciphering stratigraphic relationships and determining relative ages from impact crater densities suggest that complexly ridged terrain and crustal highlands represent some of the oldest crust on the planet (e.g., Basilevsky et al., 1997; Price et al., 1996). This age difference imposes serious problems for both hot spot and cold spot theories of crustal highland formation. It alludes that these regions may be related to an earlier phase in Venusian tectonic history where they remained as relicts of that earlier epoch.

Estimates of crustal thickness from gravity data for crustal highlands infers a thickened crust relative to plains and volcanic highlands, with thicknesses reaching the upper limit of 50 km for Venus (Grimm and Hess, 1996). Soloman and Head [1991] noted that the crust of Venus in the plains regions is typically 10 to 30 km thick, but correlations of tectonic style with elevation suggest crustal thicknesses in the tessera regions may be tens of kilometers thicker than in the plains regions. Such areas of thickened crust may be areas where crustal recycling by basal melting occurs or where an eclogite assemblage capable of sinking into the mantle may be forming.

A prime example of a crustal plateau is Thetis Regio, which is a roughly oblate plateau highland region centered at about 12 ° S, 129 ° E that is approximately 1500 km in diameter. The area of interest is the radar bright area below the label in figure 32. The case study area described herein is encompassed by the 64 ° -by-64 ° region from 36 ° S to 27 ° N, 99 to 162 ° E and is roughly 3900km by 6750 km. Thetis Regio is characterized by peripheral fracture sets and interior complexly ridged terrain with generally NE trending linear ridges and troughs. Figure 33 shows an equal area azimuthal projection of the topography of Thetis Regio. The highest elevations are

located on the margins of the region with peaks in excess of 4 km.

Free-air gravity anomalies for the Thetis Regio study area are shown in figure 34. Free-air gravity anomalies are modest with positive and negative anomalies that have magnitudes which are generally less than 50 mgals. In this complicated, highly tectonized region, free-air gravity anomalies do not correlate as strongly with topography and the terrain gravity effects as was found for the other study areas. The terrain gravity effects are shown in figure 35. Profiles of topography, terrain gravity effects, and free-air gravity anomalies along 8 ° S latitude across Thetis Regio are shown in figure 36. The limited magnitudes of the free-air gravity anomalies relative to the terrain gravity effects and their lowered correlation may reflect a fairly complete state of isostatic compensation for this region.

Local favorability indices for Thetis Regio are shown in figure 37. These coefficients are notable for the high correlation between these data sets within the central highland indicating crustal thicknesses may be greater yet in this region. NE trending positive DLFI components appear to be commensurate with possible rifting and thinned crust that is seen transecting southeastern Thetis Regio.

The terrain-decorrelated components of the free-air gravity anomalies are shown in figure 38. The terrain-decorrelated free-air gravity anomalies are of low magnitude and appear to be related more to computational noise than to the structure of Thetis Regio. The low magnitude of these components, and their lack of structural relationship to the region may indicate that the crust of Thetis Regio is largely compensated.

The dryness and relative lack of recycling of the Venusian crust and mantle do not necessarily preclude differentiation of crustal materials beyond basalt (Kaula, 1990). Notwithstanding the similarity of Thetis Regio's correlated coefficient power ratio spectrum to those of the other areas under consideration, a significantly larger percent (2%) of wavenumber power is in inversely correlated (see fig. 2). The relatively lower correlation between free-air gravity anomalies and terrain gravity effects may result from

either density variations or uncompensated crustal thickness contrasts within the region. Hence, the crust of Thetis Regio may contain relatively differentiated crustal material.

Generally NE trending ridges and valleys dominate the complex terrain in the northwestern half of the region. The topography of Thetis Regio transitions gradually into northern plains units, which embay its complexly ridged terrain. Outliers of tessera terrain protrude above the plains volcanism as islands and appear to be of similar deformation style and trend as the highland itself. Plains units to the north of Thetis Regio, which embay this complex terrain at lower elevations, are crosscut by fracture systems and coronae.

Relief from Thetis Regio into the ridge and valley terrain in the southeast and into areas east of the Thetis highlands can be abrupt. Portions of the NE trending valleys in the southeastern part of Thetis Regio are embayed by plains forming lavas. The area to the southeast shown in figure 39 is divided by chasma with radial to NE trending fractures, which are superposed on and extend into the surrounding plains. Again, plains units embay the lower elevations of the highland area and have fractures and rifting superposed upon plains units. Artemis Corona and Chasma with its associated flood volcanics appear to crosscut all other units to the south of this study area.

The compensated terrain gravity effects are shown in figure 40 and their related compensation annihilating effects are shown in figure 41. Inversion of the compensation annihilating effects for the Moho was developed for the 64 ° -by-64 ° area encompassing Thetis Regio using a crust/mantle density contrast of 0.5g/cm^3 and a mean crustal thickness of 15 km. The gravity effects of the modeled Moho in figure 42 match more than 71% of the annihilating effects with a standard error of less than 0.02 mgal and mean error of zero mgal in this complex region.

The resulting Moho and crustal thicknesses are plotted in figures 43 and 44, respectively. Crustal thicknesses varied roughly between 6 and 47 km, where the local favorability indices may indicate that the crust in central Thetis Regio may be even

thicker. Crustal thicknesses transition gradually into the plains north of Thetis Regio. Crustal thickness profiles shown in figure 45 indicate that the transition from central Thetis Regio to areas east of the highland can be abrupt. Significant crustal thinning appears concurrent with chasma to the east and south of Thetis Regio. It is associated with the embayed valley that divides southeastern Thetis Regio, giving the impression that this feature is also a rift or chasma that may also postdate formation of the highland. These crustal thicknesses are compatible with predictions that crustal plateaus represent some of the thickest crust on Venus. Stratigraphic relationships and crustal thickness profiles indicate that crustal plateaus may also represent some of the oldest crust on Venus.

IV. Discussion

Crustal modeling of Venus utilizing spectral correlation analysis of free-air gravity anomalies and terrain gravity effects produced crustal thicknesses for a lowland plain, volcanic highland, and crustal plateau that are within ranges predicted from other geophysical evidence. Given appropriate *a priori* constraints, this approach offers comprehensive, quantitative models of the structure of the Venusian crust. This approach can improve the utility of the high-resolution gravity and topography data from Magellan and earlier satellite missions for interpreting the crustal properties of Venus. Discrete crustal models, when interpreted within the context of the geology revealed by the high resolution imagery provided by Magellan, can yield new insight regarding the complex tectonic history of Venus.

The crustal model for Atalanta Planitia infers that the region is underlain by thinned crust with crustal thickness increasing, sometimes dramatically, towards the concentric ridge belts and tessera terrain. The gradual crustal thickening seen between the volcanically embayed Ananke Tessera and the central Atalanta depression contrasts with the rapid crustal thickening seen beneath concentric ridge belts to the south and east of central Atalanta Planitia. The gradual change in crustal profile for Ananke Tessera

might infer that the tessera unit predates the plains, was embayed by plains forming volcanism, and remains as a relic crustal terrain that survived plains formation, or was formed in-situ concurrently with plains formation. The dramatic "wall of crust" associated with ridge belts south and east of Atalanta Planitia may imply crustal shortening and thickening after plains formation and is consistent with predictions of crustal thickening associated with a downwelling mantle cold spot.

For Beta Regio the model produced 25 - 30 km crustal thicknesses with indications from the topographic and gravity profiles and local favorability indices that there is significant topographic loading by the central Beta massif. Stratigraphic and crater density statistics indicate that rifted volcanic highlands represent some of the youngest crustal units on Venus as described by Basilevsky et al. [1997]. Beta Regio appears to be thermodynamically supported by mantle upwelling and have a thickened crust that is not yet completely compensated. If volcanism is not occurring at present in Beta Regio, then it is likely that volcanism ceased in geologically recent times.

Thetis Regio has a thickened well-compensated crust that approaches 50 km in maximum relief. This finding generally agrees with predictions for such regions from earlier geophysical studies. The gradual decrease in crustal thickness towards the plains north of Thetis Regio, the presence of outliers of similar terrain within the plains, and the fact that plains lavas embay tessera at lower elevations strongly suggest that Thetis Regio is a relict crustal unit that predates plains formation. The presence of rifting and coronae superposed upon Thetis Regio and their associated shallow Moho relief that approaches surface elevations and appears to cut through the highland crust strongly suggest that these features predate highland formation and possibly plains formation.

The average age of the Venusian crust is probably Paleozoic in the geologic time frame of Earth. However, significant progress was made recently in assigning relative ages to individual units within plains, volcanic highlands, and tesserae (Basilevsky et al., 1997). Evidence is strong from stratigraphic relationships and crater density statistics that

tesserae and complexly ridged terrain represent the oldest crustal units on the planet. The possibility exists that such preexisting tesserae were inundated by lavas associated with plains formation. The partially embayed tessera west of Atalanta Planitia is associated with thickened crust as are the ridge belts that are concentric about the central Atalanta depression. However, crustal thickening is relatively gradual in the profiles going from plains to tessera in contrast to the abrupt thickness changes in the profiles across the younger ridge belts. It is possible that plains formation largely obliterated the pre-existing landscape, except for the higher elevation blocks of tessera which remained above the reach of the plains forming lavas.

Stratigraphic relationships and crater density statistics infer that tessera and complexly ridged highlands are older than the plains that cover and embay them. Evidence from free-air gravity anomalies further indicates that these areas may be relatively old since they have achieved a fairly complete state of isostatic equilibrium. Volcanic highlands are superposed on older plains and tessera units, which strongly infers that they are younger than either of these other features. The large free-air gravity anomalies associated with Beta Regio provide strong evidence that this region is not yet in a state of complete isostatic adjustment and, hence, may be younger than areas that have achieved such adjustment.

The crustal analysis and thickness profiles derived herein provide strong indications that plains units embay and cover preexisting complexly ridged terrain and tessera except where these regions have achieved sufficient relief that they survive as relict crustal units, which we now recognize as crustal plateaus or crustal highlands. Based on stratigraphic relationships and this crustal analysis, it is highly unlikely that a direct relationship to either downwelling cold mantle or upwelling hot mantle can adequately explain the evolution of crustal plateaus or tessera. Additional analysis may be needed to determine if these cross cutting relationships and crustal structures hold for the entire planet. If so, then crustal plateaus are likely remnants of some tectonic process

in effect prior to formation of the Venusian plains and volcanic highlands.

V. Conclusions and Recommendations

High resolution radar imagery, altimetry, and gravity observations from the Magellan mission have substantially increased our understanding of the geologic history of Venus. Models of mantle convection patterns for Venus derived from gravity and topography data have improved substantially our understanding of the internal dynamics of the planet. Crustal structures inferred from gravity and topography observations provide constraints for the tectonic and resurfacing history of Venus. The crustal properties and thickness of Venus remains a fundamental problem for planetary geologists and scientists in constraining theories of the planet's geologic history. Crustal modeling by spectral correlation analysis of free-air gravity and terrain gravity effects provides a new quantitative approach for obtaining new insight on this critical problem. Implementation of this approach on three tectonically disparate features of the Venusian crust yielded the following:

1. This new quantitative approach is effective for modeling the crustal properties of Venus from correlations between free-air gravity anomalies and terrain gravity effects. These correlations may be used to model the Venusian Moho and local state of isostatic compensation within the context of an appropriate isostatic model of the crust. Hence, the geologic utility of topographic and gravity observations from Magellan and earlier satellite missions may be enhanced by the application of this procedure.
2. Moho estimates for three disparate Venusian regions from the inversion of the gravity effects that annihilate the compensated gravity effects varied between roughly 5 km beneath plains units and chasmata to roughly 50 km beneath the crustal highland of Thetis Regio. My results support a relatively thin crust for Venus that is compatible to the 10 – 15 km thick oceanic crust of Earth.
3. The correlated output-to-input power ratio spectra are very similar between three

disparate tectonic regions of Venus. More than 80% of the power in the free-air gravity anomalies and the terrain gravity effects is preserved in wavenumber components that correlate at CC > 0.8. The lack of power in low and inversely correlated wavenumbers provides evidence for a largely undifferentiated, unimodal Venusian crust.

7. Correlation between free-air gravity anomalies, topography and its related gravity effects is strongly positive for all three study regions. However, free-air gravity anomaly amplitudes are small compared to the terrain gravity effects for Atalanta Planitia and Thetis Regio implying that the crust of these regions may be largely compensated. On the other hand, Beta Regio has large free-air gravity anomalies that infer a lower level of crustal compensation for this region.
5. Crustal thicknesses increase from roughly 6 km in central Atalanta Planitia to roughly 25 km on the periphery of the lowland. Crustal thicknesses appear to increase abruptly between the central lowland and concentric ridge belts, and more gradually from the lowland to the peripheral tesserae.
6. Beta Regio is a region of relatively thickened crust that decreases from roughly 40 km to roughly 6 km beneath adjacent lowlands. Significant crustal thinning is associated with the chasmata that cut across Beta Regio.
7. Thetis Regio also is a region of thickened crust that decreases from almost 50 km to roughly 6 km beneath adjacent lowlands. Crustal thicknesses decrease gradually towards the lowlands north of Thetis Regio. Chasmata that cut across the study area are associated with thinned crust. Both chasmata and their associated crustal thickness variations appear to disrupt the crust, and hence postdate the formation of Thetis Regio.
8. Cross-cutting relationships revealed in Magellan satellite imagery and details regarding crustal structure derived herein strongly imply that Thetis Regio may be a relict tectonic terrain which is older than the plains that partially embay it.

9. Atalanta Planitia is disrupted by ridge and fracture sets that are concentric about the central lowland. These features and their associated crustal thicknesses strongly imply that deformation followed emplacement of the plains units and may continue at present.
10. Plains volcanics of Atalanta Planitia embay tesserae on the periphery of the study region. Cross cutting relationships and crustal thicknesses associated with the embayed tesserae strongly imply that the tesserae are older than the plains units and remain as relict crustal units.
11. If further analysis of stratigraphic relationships and crustal structure establish crustal highlands and tesserae remain only as relict crustal units over the entire planet, then new models for the origin of crustal highlands may need to be proposed.

Several recommendations can be made for extending the results of this study. For example, additional analysis of crustal transitions between tessera and plains units or volcanic areas and ridge belts and plains units could provide new insights on their origin and evolution. Additional analysis and interpretation of specific features of interest identified within the data sets obtained by this initial study, which may include but are not limited to:

(a) A search for additional possible isolated tesserae located within the initial study regions to determine if they appear to predate other crustal units.
(b) Further analysis of chasmata and coronae located within the initial study regions to gain insight on their formation and history.

The impact of other crustal sources of density changes (i.e., temperature, compositional) to the gravity field and derived crustal thicknesses should be investigated. Crustal models for other important tectonic regions such as Artemis Corona and Chasma and Ishtar Terra should be developed for a more comprehensive view of the crust of Venus. In addition, a global model for the Venusian crust should be constructed by this approach to help resolve the subcrustal distribution of density variations.

VI. Acknowledgements

I owe gratitude to many for the opportunity to experience this Honors Research Project. I wish to express my gratitude and appreciation to Dr R. R. B. von Frese for his great effort and tolerance in guiding me though this research project. Members of the geophysics computing research group were invaluable to me and I would especially like to acknowledge the efforts of Dr. Li Tan, as well as Dan Roman, Laramie Potts, and H. R. Kim without who's efforts I would have been lost. Thanks to Dr. Hallan Noltimier for his knowledge, wisdom, and inspiration.

This thesis was supported by grants from the Honors Program of the Colleges of Arts and Sciences at The Ohio State University. Computing support was provided by the geophysics computing facilities and the Kresgie-Shell computing lab in the Department of Geological Sciences and by a research grant from the Ohio Super Computer Center. Data for this research were provided by the Planetary Data System archive at Washington University, St. Louis, Missouri.

37

VII. References Cited

Baker, V. R. and Komatsu, G., Parker, T. J., Gulick, V. C., Kargel, J., S. and Lewis, J. S., Channels and Valleys on Venus: Preliminary Analysis of Magellan Data, *J Geophys. Res.* 97, 13421-13444, 1992.

Banerdt, W. B., Support of Long-Wavelength Loads on Venus and Implications for Internal Structure, *J Geophys. Res.* 91, 403 - 419, 1986.

Banerdt, W. B., and Sammis, C. G., Small-Scale Fracture Patterns on the Volcanic Plains of Venus, *J Geophys. Res.* 97, 16194-16166, 1992.

Banerdt, W. B., McGill, G. E., and Zuber, M. T., Plains Tectonics on Venus, *Venus II: Geology, Geophysics, Atmosphere, and Solar Wind Environment.* Ed. S. W. Bougher, D. M. Hunten, and R. J. Phillips, Tucson: UAP, pp 901 - 930, 1997.

Basilevsky, A. T., Head, J. W., Schaber, G. G., and Strom, R. G., The Resurfacing History of Venus, *Venus II: Geology, Geophysics, Atmosphere, and Solar Wind Environment.* Ed. S. W. Bougher, D. M. Hunten, and R. J. Phillips, Tucson: UAP, pp 1047 - 1084, 1997.

Bindschadler D., G. Schubert, and W. Kaula, Coldspots and Hotspots: Global Tectonics and Mantle dynamics of Venus, *J Geophys. Res.* 97, 13395-13432, 1992.

Crumpler, L. S., Head, J. W., and Auble, J. C., Relation of Volcanic Center Concentration on Venus to Global Tectonic Patterns, *Science*, 261, No. 5121, 591 - 596, 1993.

Crumpler, L. S. and Auble, J. C., Senske, D. A., Keddie, S. T., Magee, K. P., and Head, J. W., Volcanoes and Centers of Volcanism on Venus, *Venus II: Geology, Geophysics, Atmosphere, and Solar Wind Environment.* Ed. S. W. Bougher, D. M. Hunten, and R. J. Phillips, Tucson: UAP, pp 697 - 756, 1997.

Fowler, C. M. F., *The Solid Earth: An Introduction to Global Geophysics*, Cambridge UP, 1996.

Garvin, J. B., and Williams Jr., R. S., Small Domes on Venus: Probable Analogs of Icelandic Lava Shields, *Geophys. Res. Lett.* 17, No. 9, 1381 - 1384, 1990.

Grimm, R. E., and Phillips, R. J., Anatomy of a Venusian Hot Spot: Geology, Gravity, and Mantle Dynamics of Eistla Regio, *J. Geophys. Res.* 97, 16035 - 16054, 1992.

Grimm, R. E., and Hess, P. C., The Crust of Venus, *Venus II: Geology, Geophysics, Atmosphere, and Solar Wind Environment*. Ed. S. W. Bougher, D. M. Hunten, and R. J. Phillips, Tucson: UAP, 1205 - 1244, 1997.

Guest, J. E., Bulmer, M. H., Auble, J., Beratan, K., Greeley, R., Head, J. W., Michaels, G., Weitz, C., and Wiles, C., Small Volcanic Edifices in the Plains of Venus, *J. Geophys. Res.* 97, 15947 - 15966, 1992.

Hansen, V. L., Willis, J. J., and Banerdt, W. B., Tectonic Overview and Synthesis, *Venus II: Geology, Geophysics, Atmosphere, and Solar Wind Environment*. Ed. S. W. Bougher, D. M. Hunten, and R. J. Phillips, Tucson: UAP, 1997.

Hansen, V. L. and Phillips, R. J., Tectonics and Volcanism of Eastern Aphrodite Terra, Venus: No Subduction, No Spreading, *Science*, 260, No.5170, 526 - 531, 1993.

Hayden, K., Airborne Gravity and Magnetic Surveys Over Rugged Topography: A Case Study for The apalacians, *M.Sc. Thesis (unpubl.),* Dept. of Geological Sciences, The Ohio State University, Columbus, Ohio, 1996.

Head J., Campbell, D. B., Elachi, C., and Guest, J. E., Venus Volcanism: Initial Analysis from Magellan Data, *Science*, 252 No. 5003, 276 - 289 1991.

Head J., Crumpler L., Aubele J., Guest J., and Saunders R., Venus Volcanism: Classification of Volcanic Features and Structures, Associations, and Global Distribution from Magellan Data *J. Geophys. Res.* 97, 13153-13197, 1992.

Herrick, R. R., and Phillips, R. J., Geological Correlations with the Interior Density Structure of Venus, *J. Geophys. Res.* 97, 16017 - 16034, 1992.

Kaula, W. M., Mantle Convection and Crustal Evolution on Venus, *Geophy. Res. Lett.*, 17, 1401 - 1403, 1990.

Kim, J. W., and von Frese, R. R. B., Crustal Structure of Ohio from Topographic and Gravity Correlations, *Geophysics*, ????

Konopliv, A. S., Personal communication, 1998.

Mackwell, S. J., Zimmerman, M. E., and Kohlstedt, D. L.. High-temperature deformation of dry diabase with application to tectonics on Venus, *J Geophys.*

Res., 103, No. B1, 975-984, 1998.

Mateskon, S.R., Gravity and Magnetic Terrain Effects Computed by Gaussian Quadrature Integration, *M.Sc. Thesis (unpubl.),* The Ohio State University, Columbus, Ohio, 1985.

Mateskon, S.R., and vonFrese, R.R.B., Gravity and Magnetic Terrain Modeling by Gaussian Quadrature Integration, International meeting on potential fields in rugged topography, (Institute de Geophysique, Universite de Lusanne, CH*), IGL-Bulletin*, #7, 30-33, 1985.

Noltimier H. and Sahagian D., Tectonic Style of Venus: An Analog to Polar "Icepack Tectonics" *J. Geodynamics* 16, No 1/2, 65-79, 1992.

Pettengill, G. H., Ford, P. G., Johnson, W. T. K., Raney, R. K., and Soderblom, Magellan: Radar Performance and Data Products, *Science*, 252, No.5006, 260 - 265, 1991.

Phillips R. J., Grimm, R. E., and Malin, M. C., Hot-spot Evolution and the Global Tectonics of Venus, *Science*, 252, 651 - 659, 1991.

Phillips R., Raubertas R., Arvidson R., Sarkar I., Herrick R., Izenberg N., and Grimm R., Impact Craters and Venus Resurfacing History *J. Geophys. Res.* 97 15923-15948, 1992.

Price, M. H., Watson, G., Suppe, J., and Brankman, C., Dating Volcanism and Rifting Using Impact Crater Densities, *J. Geophys. Res.* 101, 4657 - 4671, 1996.

Rappaport, N. J. and Plaut, J. J., 360 Degree and Order Model of Venus Topography, *Icarus*, 112, 27 - 33, 1994.

Saunders, R. S., Arvidson, R. E., Head, J. W., Schaber, G. G., Stofan, E. R., and Solomon, S. C., An Overview of Venus Geology, *Science*, 252, No. 5003, 249 - 253, 1991.

Schaber G., Strom, R., Moore, H., Soderblom L., Kirk R., Chadwick D., Dawson D., Gaddis L., Boyce J., and Russell J. Geology and Distribution of Impact Craters on Venus: What Are They Telling Us? *J. Geophys. Res.* 97, 13,257-13,301, 1992.

Sjorgren, W. L., Phllips, R. J., Birkeland, P. W., and Wimberly, R. N., Gravity Anomalies on Venus, *J. Geophys. Res* 85 No. A13, 8295 - 8302, 1980.

Sjogren, W. L., Bills, B. G., Birkeland, P. W., Esposito, P. B., Konopliv, A. R., Mottinger, N. A., and Ritke, S. J. with Phillips, R. J., Venus Gravity Anomalies and Their Correlations With Topography, *J. Geophys. Res* 88 No. B2, 1119 - 1128, 1983.

Sjogren, W. L., Banerdt., W. B., Chodas, P. W., Konopliv, A. W., Balmino, G., Barriot, J. P., Arkani-Hamed, J., Colvin, T. R., and Davis, M. E., The Venus Gravity Field and Other Geodetic Parameters, *Venus II: Geology, Geophysics, Atmosphere, and Solar Wind Environment.* Ed. S. W. Bougher, D. M. Hunten, and R. J. Phillips, Tucson: UAP, pp. 1125 - 1161, 1997.

Smrekar, S. E., Evidence for Active Hotspots on Venus from Analysis of Magellan Gravity Data, *Icarus*, 112, 2 - 26, 1994.

Smrekar, S. E., Keifer, W. S., and Stofan, E. R., Large Volcanic Rises on Venus, *Venus II: Geology, Geophysics, Atmosphere, and Solar Wind Environment.* Ed. S. W. Bougher, D. M. Hunten, and R. J. Phillips, Tucson: UAP, pp. 845 - 878, 1997.

Solomon, S. C., and Head, J. W., Lithopheric Flexure Beneath the Freyja Montes Foredeep, Venus: Constraints on Lithopheric Thermal Gradient and Heat Flow, *Geophys. Res. Lett.* 17, No. 9, 1393 - 1396, 1990.

Solomon, S. C., Smrekar, S. E., Bindschadler, D. L., Grimm, R. E., Kaula, W. M., McGill, G. E., Phillips, R. J., Saunders, S. S., Schubert, G., Squyres, S. W., and Stofan, E. R., Venus Tectonics: An Overview of Magellan Observations, *J. Geophys. Res.* 97, 13199-13255, 1992.

Squyres, S. W. and Jankowski, D. G., Simmons, M., Solomon, S. C., Hager, B. H., McGill, G. E., Plains Tectonism on Venus: The Deformation Belts of Lavinia Planitia, *J. Geophys. Res.* 97, 13579 - 13599, 1992.

Stefanick, M. and Jurdy, D. M., Venus Coronae, Craters, and Chasmata, *J. Geophys. Res.* 101. No. E2, 4637 - 4643, 1996.

Stofan, E. R., Sharpton, V. L., Schubert, G., Baer, G., Bindschadler, D. L., Janes, D. M., and Squyres, S. W., Global Distribution of Coronae and Related Features on Venus: Implications for Origin and Relation to Mantle Processes, *J. Geophys. Res.* 97, 13347-13378, 1992.

Tan, L. and von Frese, R. R. B., Satellite Geopotential Models of the East Asian

Lithosphere, *EOS (Am. Geophys. Union Trans.),* 78, No. 17, 114, 1997.

Turcotte, D. L., An Episodic Hypothesis for Venusian Tectonics, *J. Geopyhys.Res*, 98, 17061 - 17068, 1993.

von Frese, R. R. B., W. J. Hinze, L. W. Braile, and A.J. Luca, Spherical Earth Gravity and Magnetic anomaly Modeling by Gauss-Legendre quadrature integration, *J. Geopyhys.*, 49, 234-242, 1981.

von Frese, R. R. B., and Mateskon, S. R., Modeling Magnetic and Gravit Effects of the Transantarctic Mountains, *Ant. J. U.S., XX*, 1-3, 1985.

von Frese, R. R. B, L. Tan, L.V Potts, J.W. Kim, C. J. Merry, and J. D. Bossler, Lunar Crustal analysis of Mare Oriental from Topographic and Gravity Correlations, *Geophysics*, 62, 365 - 380 1997a

von Frese, R.R.B, L. Tan, J.W.Kim, and Bentley, C. R., Antarctic Crustal Modeling from Spectral Correlation of Free-Air Gravity Anomalies with Terrain, *J. Geopys. Res* 1997b (in review).

von Frese, R. R. B., Potts, L. V., Tan L., Kim, J. W., Leftwich, T. E., Merry, C. J., and Bossler, J. D., Comparative Crustal Modeling of the Moon and Earth from Topographic and Gravity Correlations: in Lunar and Planetary Science XXIX Abstract #1870, Lunar and Planetary Science Institute, Houston (CD-ROM), 1998.

Weitz, C. M. and Basilevsky, A. T., Magellan Observations of the Venera and Vega Landing Site Regions, *J. Geopys. Res.*, 98, No. E9, 17069 - 17097, 1993.

Williams, D. R., and Pan, V., Consequences of a Hydrous Mantle for Venus Tectonics:Predictions for Magellan, *Geophys. Res. Lett.* 17, No. 9, 1397 - 1400, 1990.

Zharkov V. N., and Marchenko, K. I., The Stress State of the Venusian Crust and Variations of its Thickness: Implications for Tectonics and Geodynamics. *Venus Geology, Geochemistry, and Geophysics: Research Results from the USSR.* Ed. V.L. Barsukov et al. Tucson: UAP, 1992a.

Zharkov V. N., Gravity Field Coefficients, Anomalous Density Waves, and the Case of Long Wave, *Venus Geology, Geochemistry, and Geophysics: Research Results from the USSR.* Ed. V. L. Barsukov et al., Tucson: UAP, 1992b.

Zharkov V. N., Model of the Interior Structure: Earth-Like Models. *Venus Geology, Geochemistry, and Geophysics: Research Results from the USSR.* Ed. V.L Barsukov et al., Tucson: UAP, 1992c.

VIII. Figure Captions and Figures

Figure 1: Shaded relief cylindrical projection of Venus topography with the study areas Atalanta Planitia, Beta Regio, and Thetis Regio labeled.

Figure 2: Correlated coefficient power ratio spectra where the ratios of output-to-input power are plotted as a function of cutoff values of the correlation coefficient (CC) between the free-air gravity anomalies and the terrain gravity effects. The spectra for all three regions are quite similar with more that 80% of the energy of both data sets preserved at a correlation coefficient cutoff of 0.8.

Figure 3: C3-MIDR (compressed, thrice mosaicked image data record) of the region encompassing Atalanta Planitia. Compressional ridge belts are prominent in the NW to south central portions of the image. Part of Tethus Regio is seen in the west-center portion of the image to the west of central Atalanta Planitia.

Figure 4: Portion of full-resolution mosaicked image data record F-MIDR65n162 for central Atalanta Planitia showing wrinkle ridges and a few small volcanic domes.

Figure 5: Equal area azimuthal projection of Atalanta Planitia topography with shaded relief. Lighting effect is used with lighting origin azimuth of 90 ° and height 45 °.

Figure 6: Equal area azimuthal projection of free-air gravity anomalies (FAGA) for Atalanta Planitia.

Figure 7: Equal area azimuthal projection of terrain gravity effects (TGE) for Atalanta Planitia.

Figure 8: Comparison of topography, free-air gravity anomalies, and terrain gravity effects along 65 ° N across Atalanta Planitia. The high correlation between these data sets is apparent.

Figure 9: Summed local favorability indices (left) and differenced local favorability indices (right) between the free-air gravity anomalies and the terrain gravity effects for Atalanta Planitia. The strongly correlated negative values of the two data sets associated with the central Atalanta depression are evident in SLFI's in figure 6 plotted below 1 ASD.

Figure 10: Terrain-decorrelated free-air gravity anomalies for Atalanta Planitia are of low magnitude and apparently structurally unrelated to topography or FAGA. Since these components are inferred to be nonisostatic, their lack of coherence and low magnitude imply that the topography of Atalanta Planitia is largely compensated.

Figure 11: Atalanta Planitia compensated terrain gravity effects (CTGE). An annihilating field can be assumed for these effects, which is inverted for Moho relief.

Figure 12: Atalanta Planitia compensated terrain gravity effects annihilating anomalies, or simply compensation annihilating effects, that are used to obtain a least squares model of Moho variations.

Figure 13: The gravity effects of the Moho model compensation annihilating effects and show high correlation when compared to the original compensation annihilating effects.

Figure 14: Moho undulations modeled from the inversion of the compensation annihilating effects for Atalanta Planitia.

Figure 15: Atalanta Planitia crustal thickness variations.

Figure 16: Atalanta Planitia crustal thickness profiles along selected latitudes and longitudes. Latitudinal profiles show a generally gradual increase in crustal thickness from the central Atalanta depression to tessera terrain to the west. Crustal thickness can increase abruptly from the central Atalanta depression to the ridge belts to the south and east.

Figure 17: Part of twice-compressed mosaicked image data record C2-MIDR c230n284 of Beta Regio.

Figure 18: Shaded relief equal area azimuthal projection of Beta Regio topography. Lighting effect is used with lighting origin azimuth of 90 ° and height 45 °.

Figure 19: Equal area azimuthal projection of Beta Regio free-air gravity anomalies (FAGA).

Figure 20: Equal area azimuthal projection of Beta Regio terrain gravity effects (TGE).

Figure 21: Comparison of topography, free-air gravity anomalies, and terrain gravity effects along 30 ° N across Beta Regio. The high correlation between these data sets is apparent. Free-air gravity anomalies are roughly half the amplitude of the terrain gravity effects indicating dynamic mantle support by thermal convection or partial isostatic compensation of the topography.

Figure 22: Terrain-decorrelated free-air gravity anomalies for Beta Regio show components that appear structurally related to topography and free-air gravity anomalies. Since these components are inferred to be nonisostatic, their coherence implies that the topography of Beta Regio may not be isostatically compensated.

Figure 23: Part of F-MIDR (full-resolution MIDR) 125n278 showing the Thiea Mons

caldera with volcanics superposed on rifting. Some fracturing of the caldera volcanics is also apparent indicating fracturing and volcanism were concurrent. Blackened area is missing data coverage.

Figure 24: Summed local favorability indices (left) and difference local favorability indices (right) between the free-air gravity anomalies and the terrain gravity effects for Beta Regio. The positive SLFI components are prominent in the central Beta massif while negative DLFI components encircle the volcanic edifice highlighting the apparent topographic loading of this feature. The crustal thickness of central Beta Regio may actually be thicker and its encircling crust thinner than the model suggests.

Figure 25: Beta Regio compensated terrain gravity effects (CTGE). An annihilating field can be assumed for these effects, which is inverted for Moho relief.

Figure 26: Compensation annihilating effects that were used to obtain a least squares model of Moho variations for Beta Regio.

Figure 27: The gravity effects of Moho relief model the compensation annihilating effects and show high correlation when compared to the original compensation annihilating effects providing a quantitative control of model accuracy.

Figure 28: Moho relief for Beta Regio.

Figure 29: Beta Regio crustal thickness variations.

Figure 30: Beta Regio crustal thickness profiles.

Figure 31: Topography and Moho profiles along 30 ° N across Beta Regio.

Figure 32: C3-MIDR c314s180 with the crustal highland of Thetis Regio labeled. The southeastern portion of Thetis Regio is cut by chasma. The circular Artemis Corona and Chasmata are clearly seen to the south of Thetis Regio. The northern portion of Artemis Corona is included in the study area.

Figure 33: Shaded relief equal area azimuthal projection of Thetis Regio topography. Lighting effect is used with lighting origin azimuth of 90 ° and height 45 ° .

Figure 34: Equal area azimuthal projection of Thetis Regio free-air gravity anomalies (FAGA).

Figure 35: Equal area azimuthal projection of Thetis Regio terrain gravity effects (TGE).

Figure 36: Profiles of topography, terrain gravity effects, and free-air gravity anomalies along 8 ° S latitude across Thetis Regio. Somewhat less correlation between

topography and its gravity effects and the free-air gravity anomalies is seen.

Figure 37: Summed local favorability indices (left) and difference local favorability indices (right) between the free-air gravity anomalies and the terrain gravity effects for Thetis Regio. High positive correlation between the free-air gravity anomalies and the terrain gravity effects for central Thetis Regio are seen in the SLFI's.

Figure 38: Terrain-decorrelated free-air gravity anomalies for Thetis Regio are of low magnitude and apparently structurally unrelated to topography or FAGA. These components appear to be related more to computational noise than to broad scale features of the study region. Since these components are inferred to be nonisostatic, their lack of coherence and low magnitude imply that the topography of Thetis Regio is largely compensated.

Figure 39: The southeastern portion of Thetis Regio showing volcanically embayed complexly-ridged terrain. A broad chasm divides this area, which appears to have been resurfaced by plains forming lavas. These plains forming lavas are superposed by fracture sets that extend into the surrounding plains.

Figure 40: Thetis Regio compensated terrain gravity effects (CTGE). An annihilating field can be assumed for these effects, which is used to Moho relief.

Figure 41: Thetis Regio compensation annihilating effects that are used to obtain a least squares model of Moho variations.

Figure 42: The gravity effects of Moho relief model the compensation annihilating effects and show high correlation when compared to the original data set.

Figure 43: Moho undulations modeled from the compensation annihilating effects for Thetis Regio.

Figure 44: Thetis Regio crustal thickness variations.

Figure 45: Thetis Regio crustal thickness profiles.

SHADED RELIEF VENUS GLOBAL TOPOGRAPHY

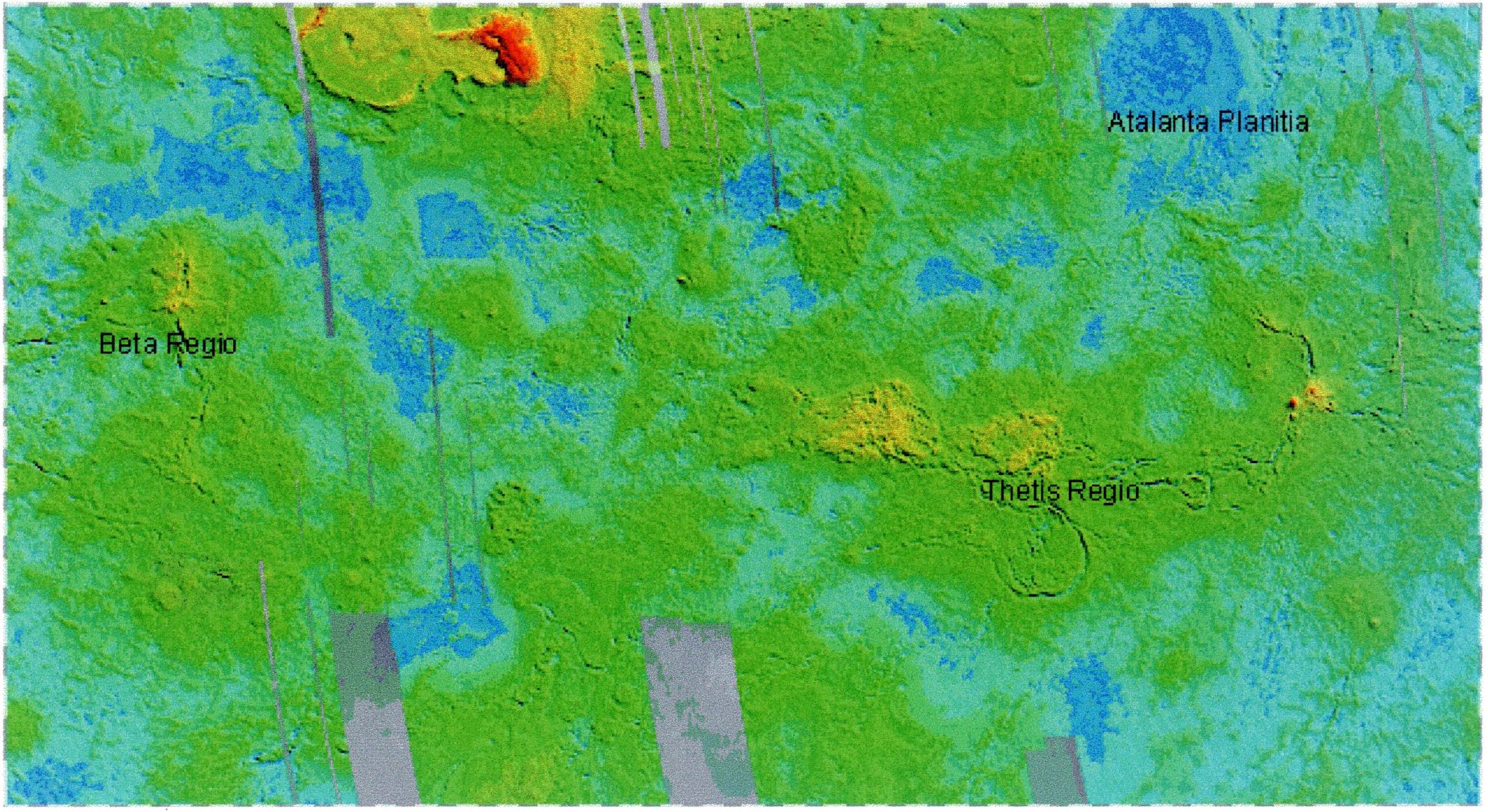

Figure 1.

Correlation Coefficient output–to–input Power Ratio Spectra

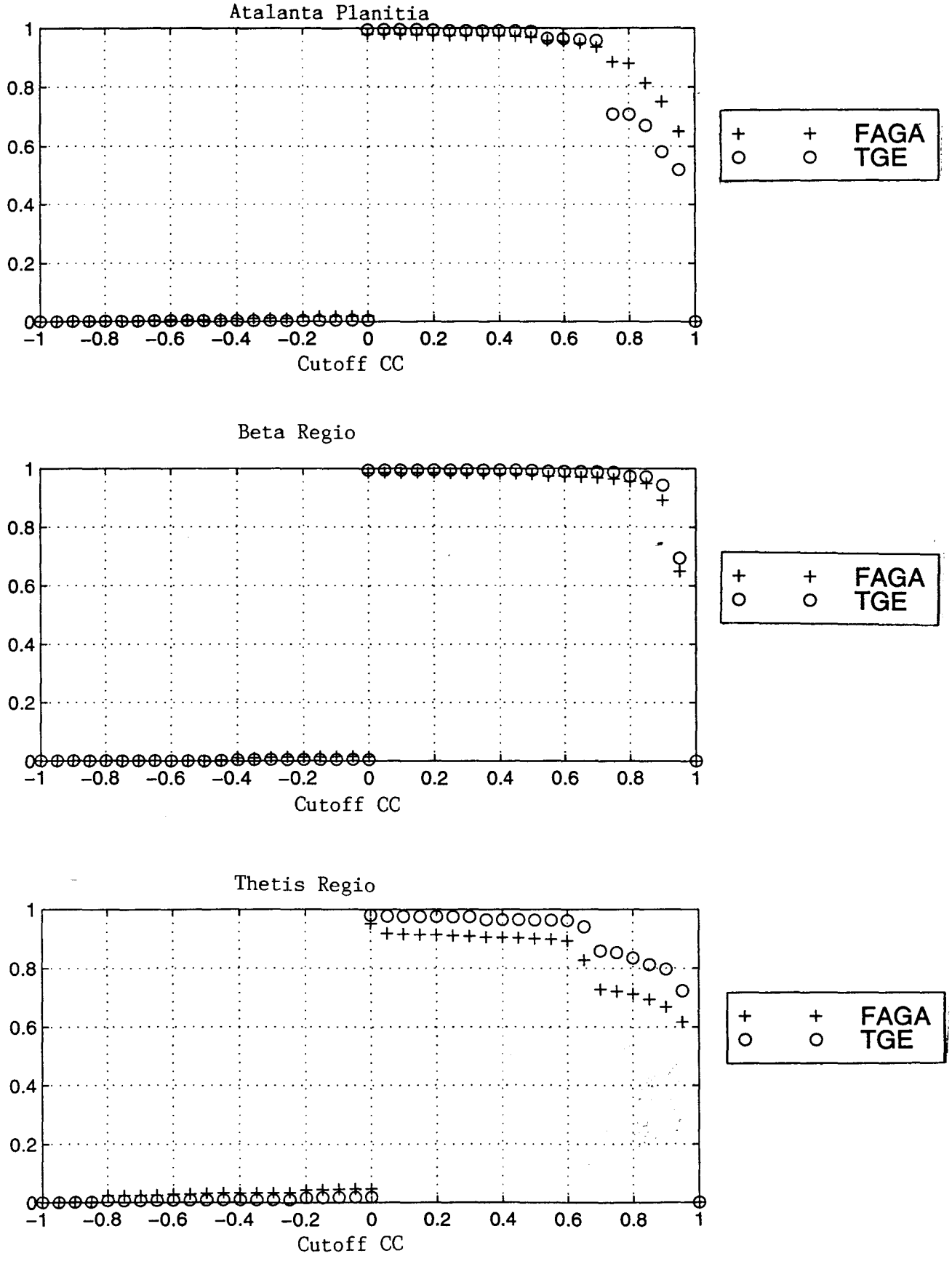

Figure 2.

Northern Plains Encompassing Atalanta Planitia

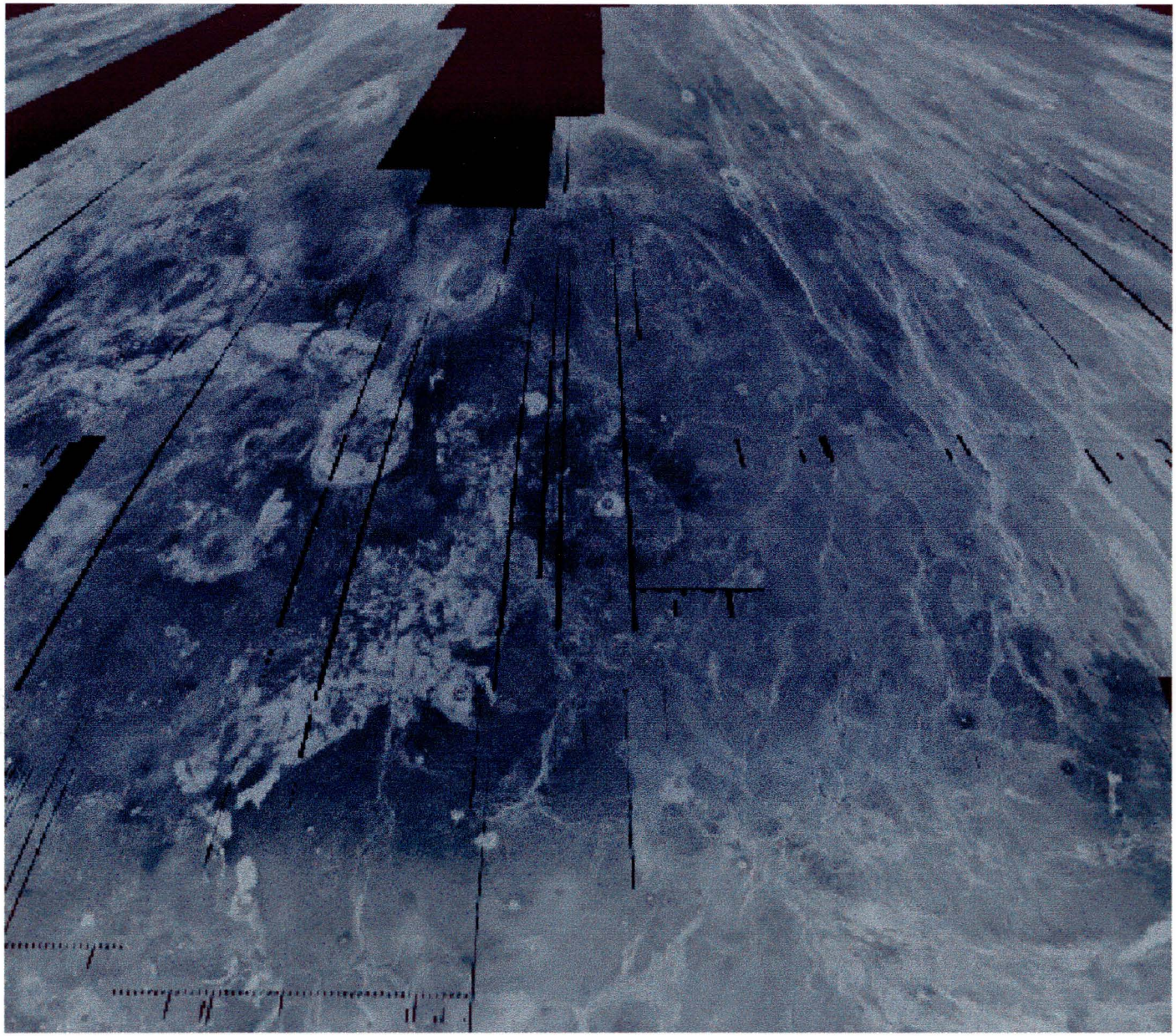

Figure 3.

Central Atalanta Planitia (F-MIDR65n162)

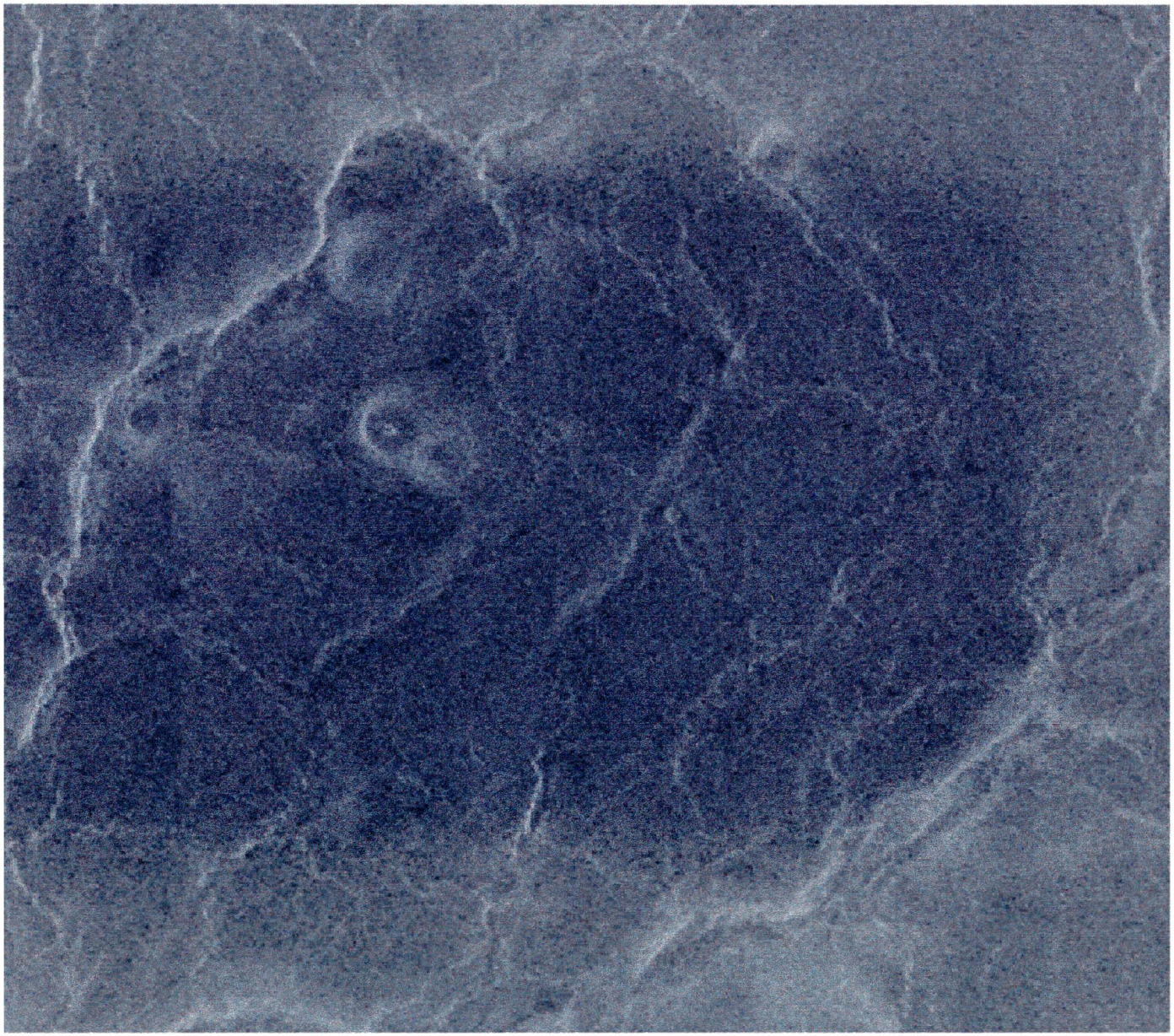

Figure 4.

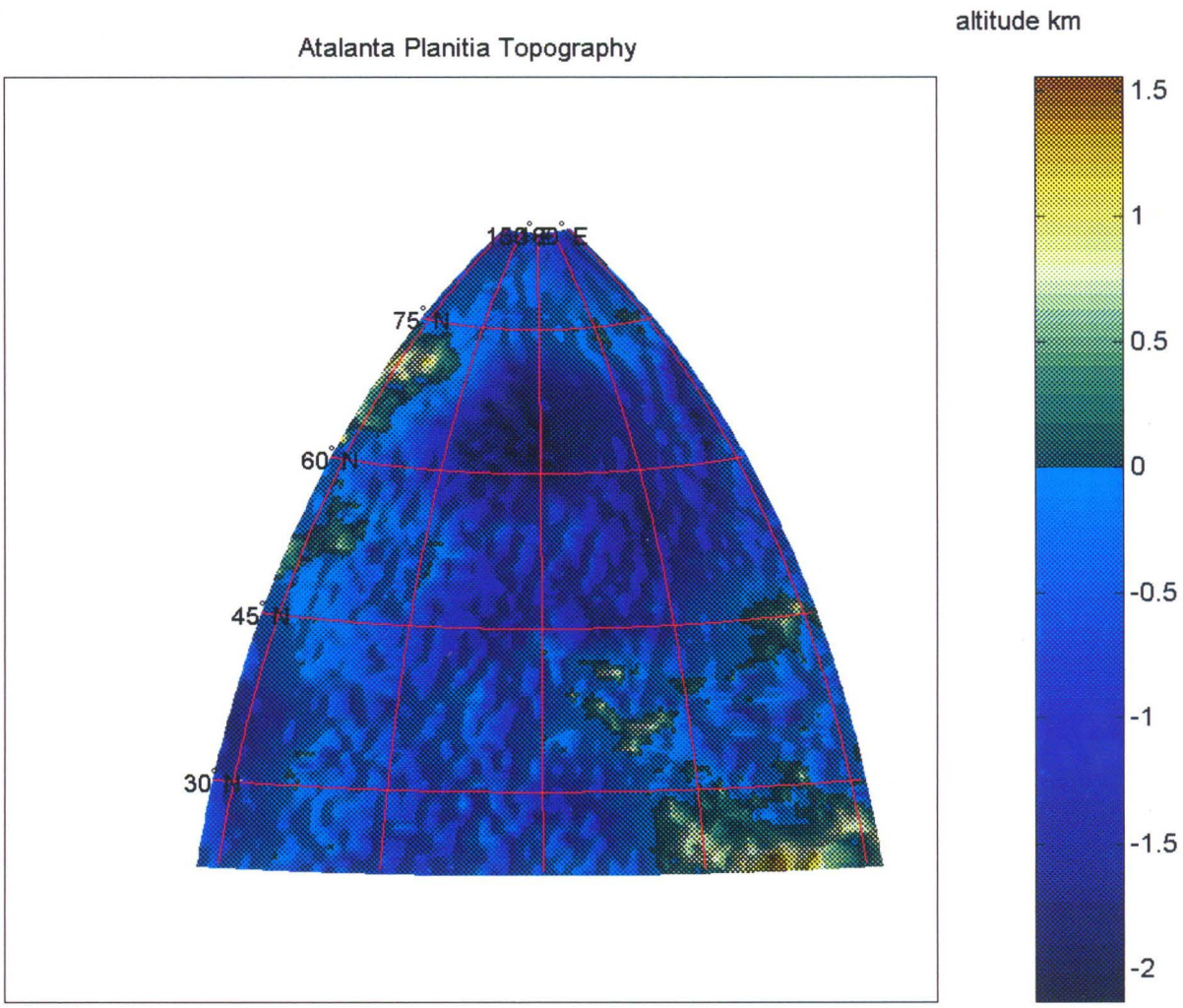

AR=-2.13; 1.1, AM=-0.6006, ASD=0.5187, AU=km, Z=6052km, GI=1deg (lat/lon)

Figure 5.

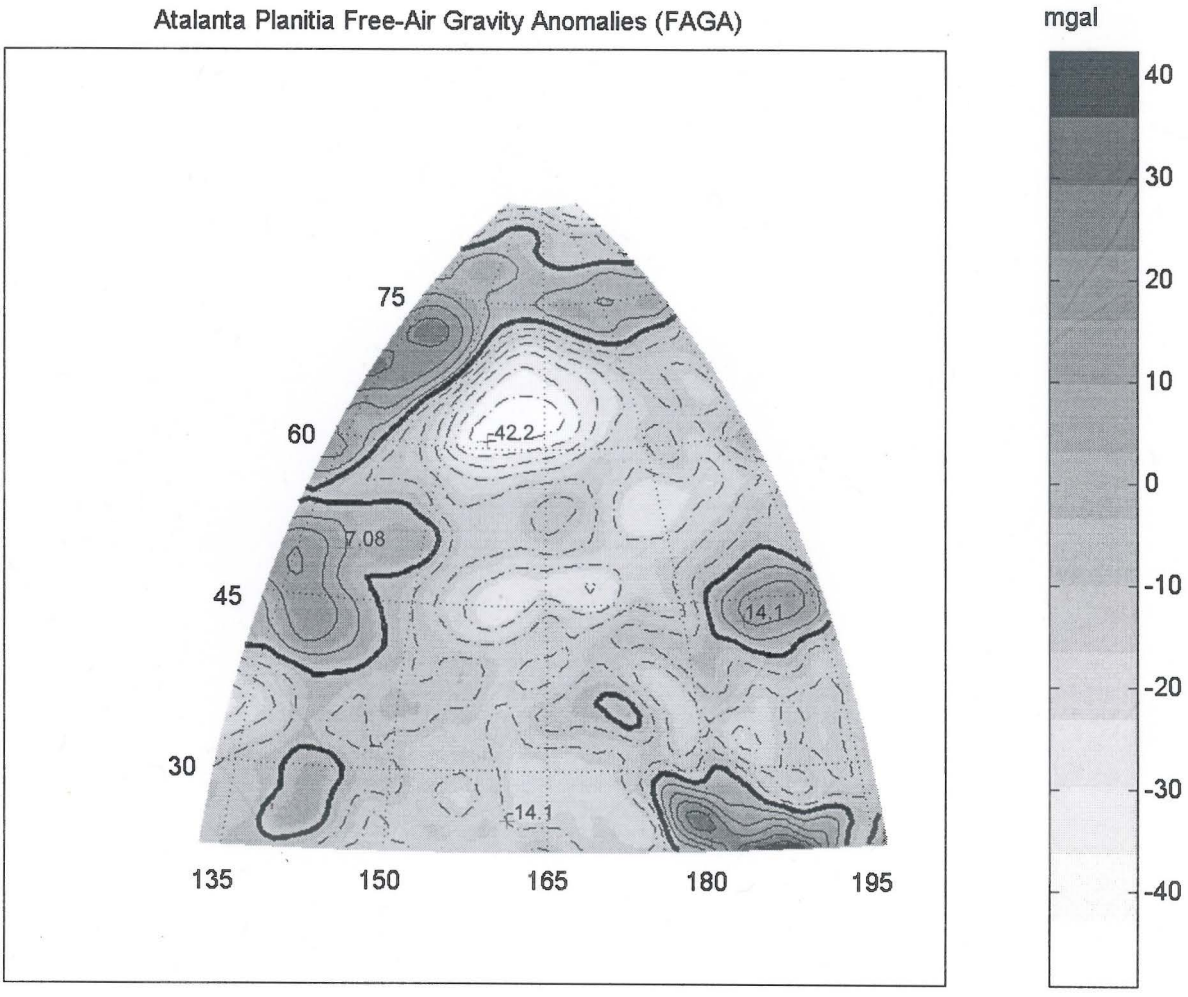

AR=-49.28; 42.31, AM=-6.6943, ASD=14.0656, AU=mgal, Z=100km, GI=1x1deg (lat/long)

Figure 6.

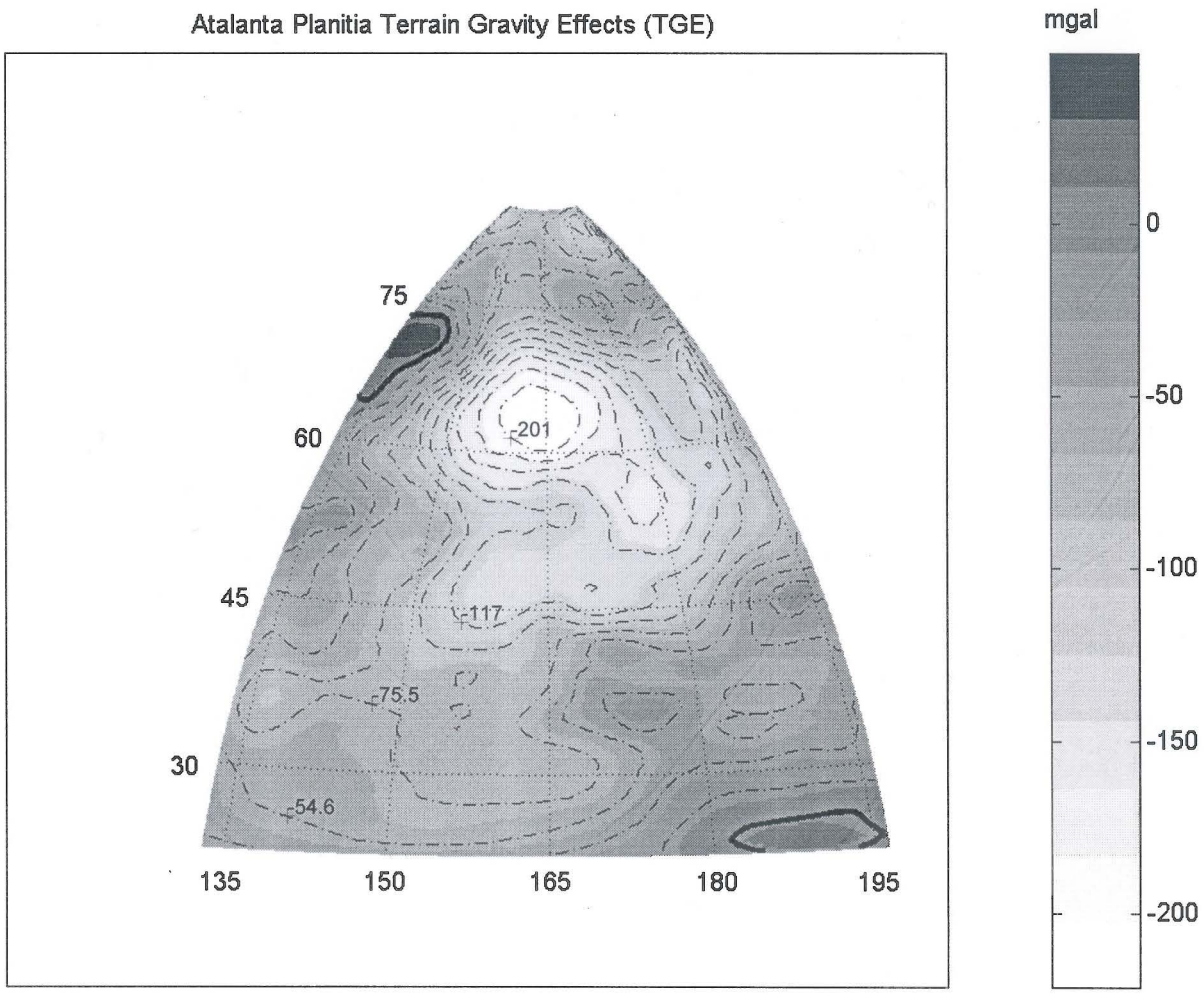

AR=-200.63; 49.75, AM=-76.2636, ASD=47.4861, AU=mgal, Z=100km, GI=1x1deg (lat/long)

Figure 7.

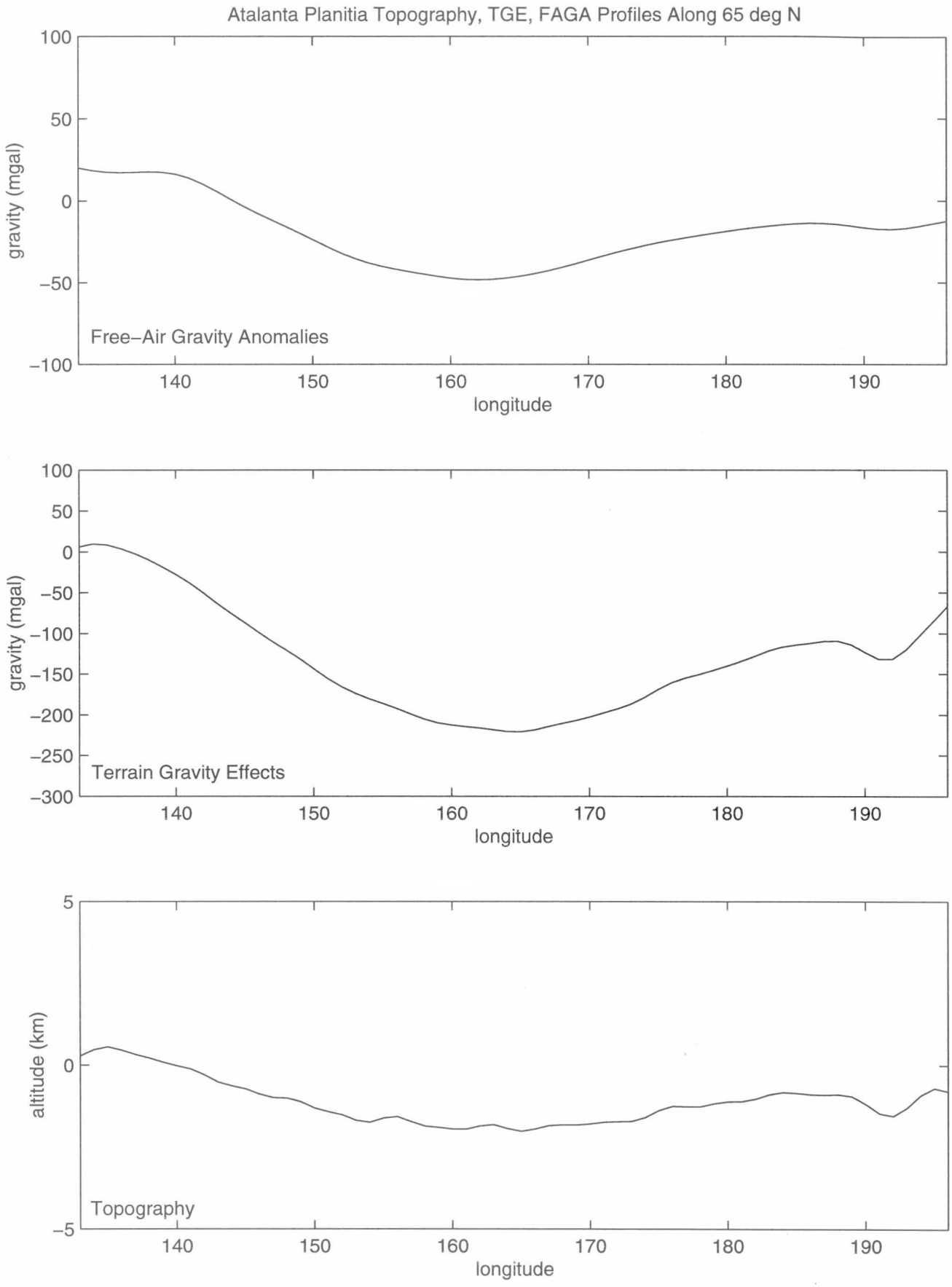
Atalanta Planitia Topography, TGE, FAGA Profiles Along 65 deg N
gravity (mgal)
Free–Air Gravity Anomalies
longitude
Terrain Gravity Effects
Topography
altitude (km)

Figure 8.

Atalanta Planitia Local Favorability Indices

Summed Local Favorability Indices

Differenced Local Favorability Indices

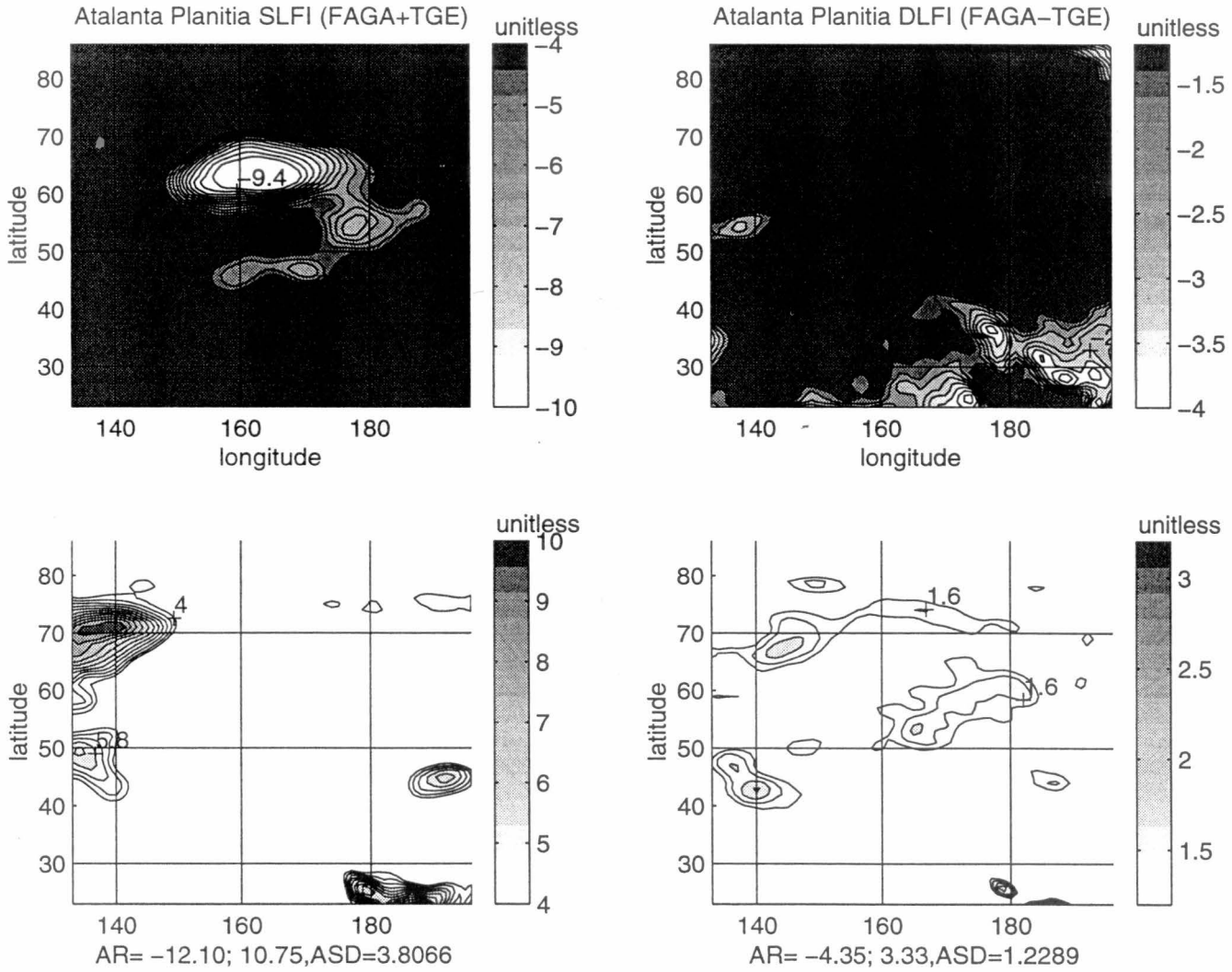

Figure 9.

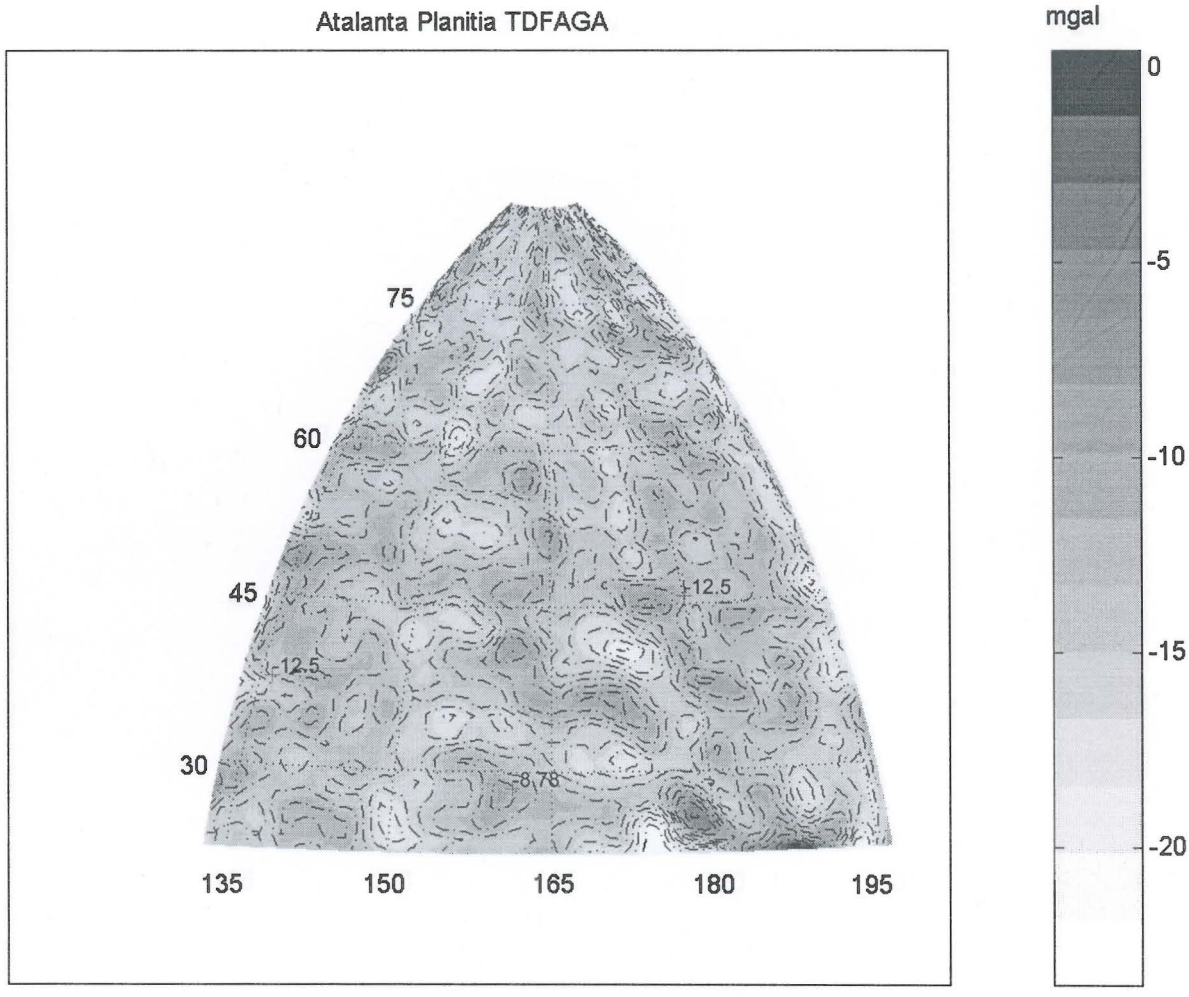

AR=-16.85; 7.14, AM=(-6.6943), ASD=2.4863, AU=mgal, Z=100km, GI=1x1deg (lat/long)

Figure 10

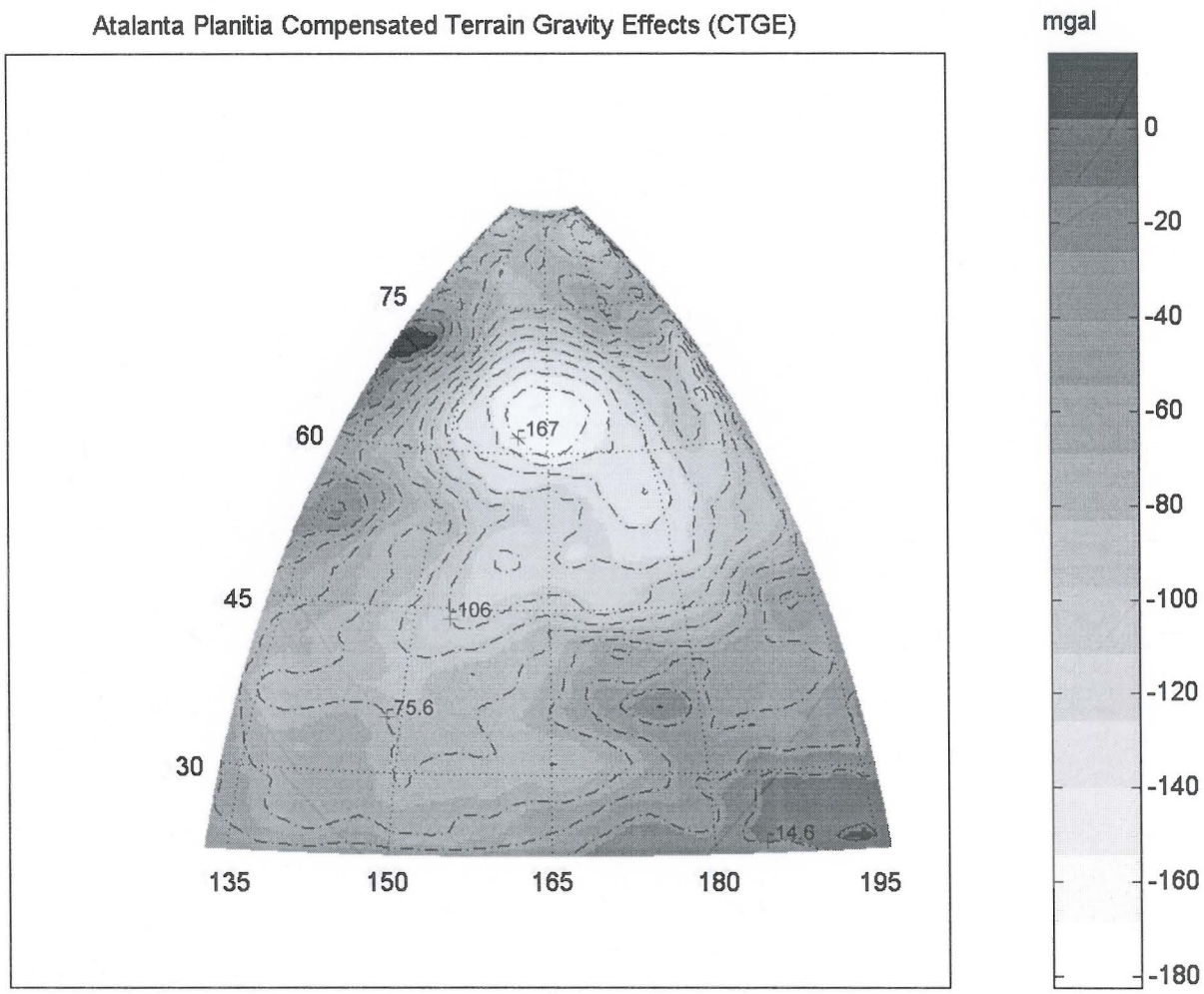

AR=-182.37; 15.93, AM=76.2636, ASD=36.8914, AU=mgal, Z=100km, GI=1x1deg (lat/long)

Figure 11.

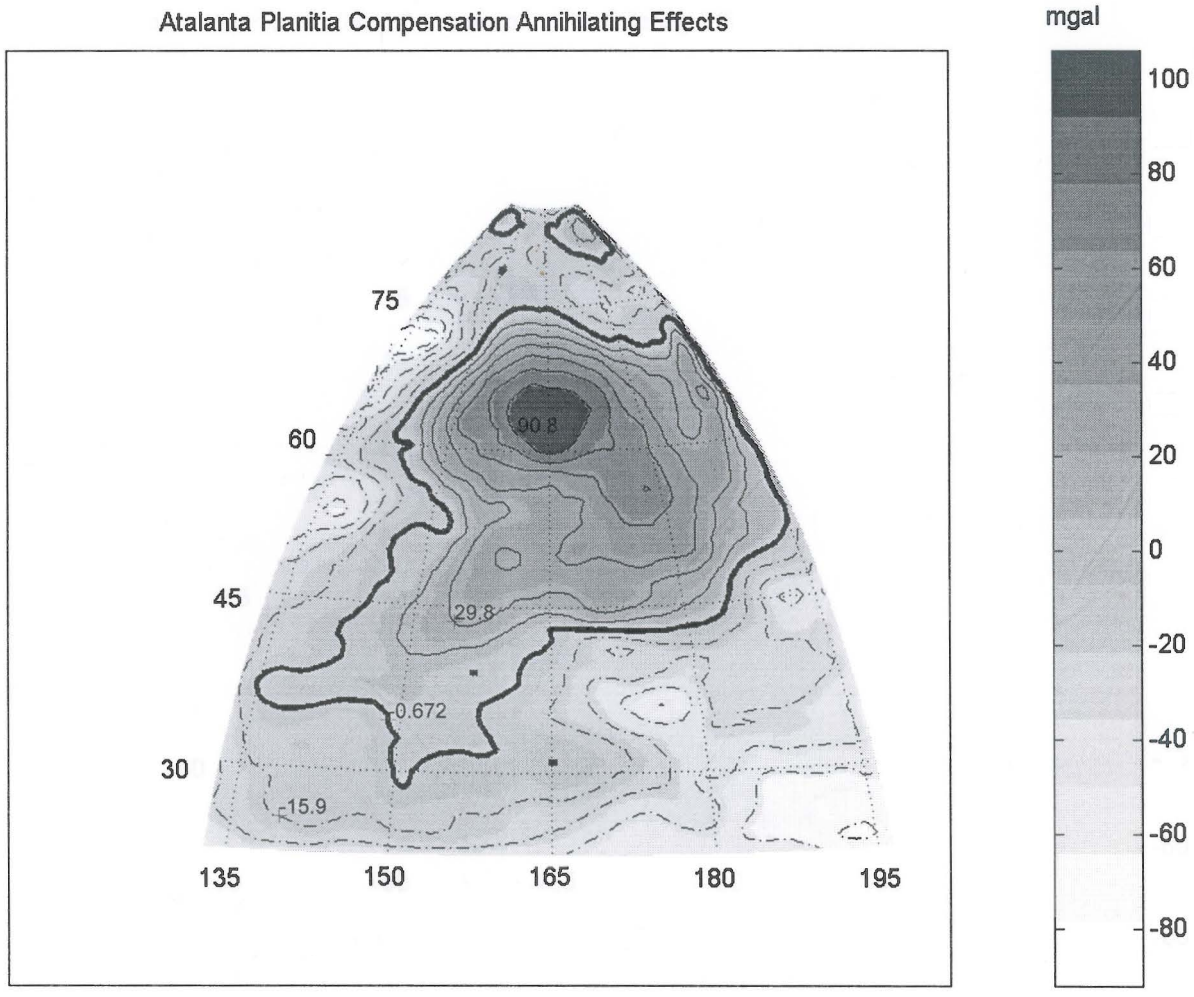

AR=-92.19; 106.10, AM=4.9121e-05, ASD=36.8914, AU=mgal, Z=100km, GI=1x1deg (lat/long)

Figure 12.

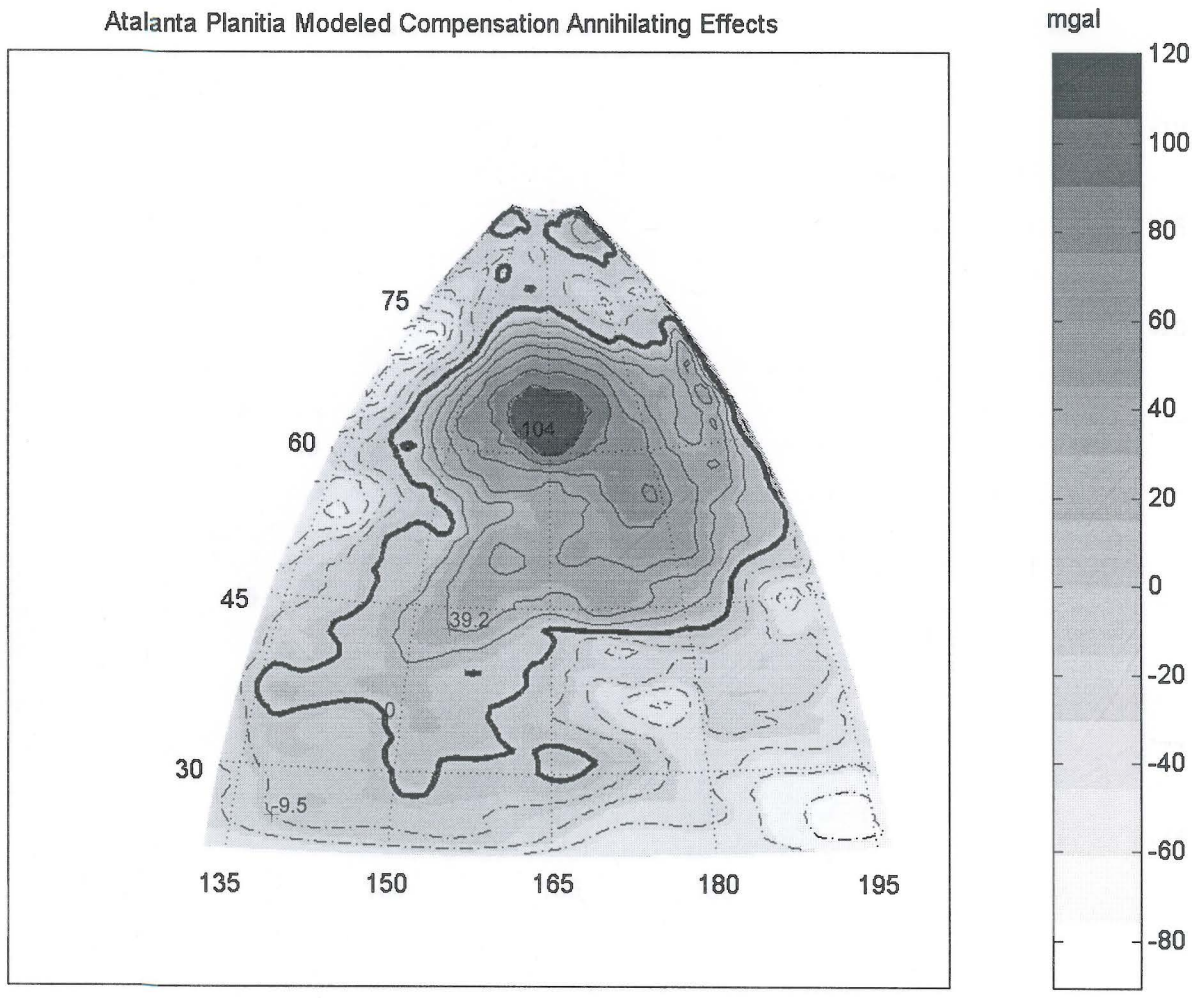

AR=-85.68; 120.38, AM=(15.8594), ASD=38.2301, AU=mgal, Z=100km, GI=1x1deg (lat/long)

Figure 13.

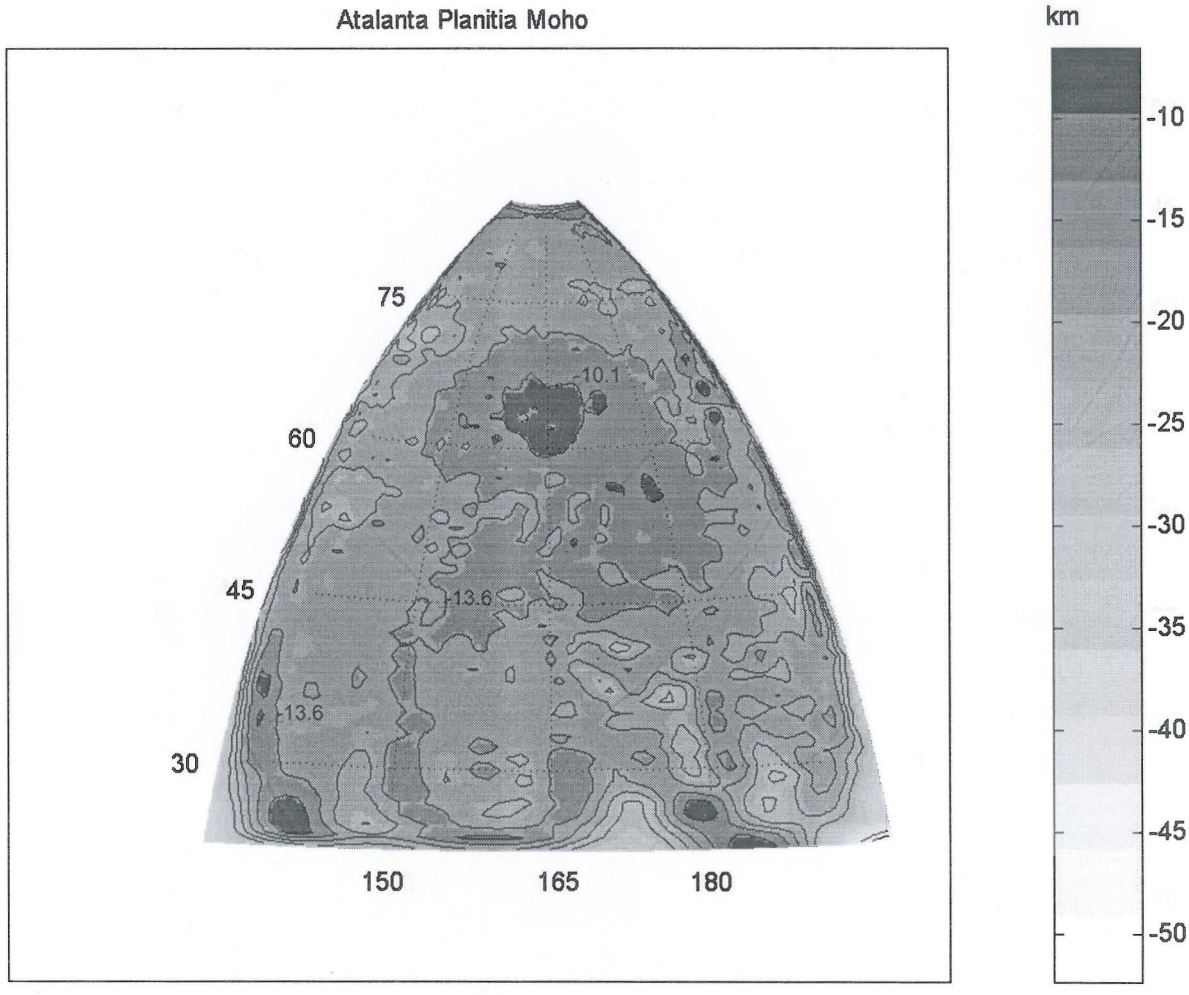

AR=-25.13; -6.56, AM=-14.6228, ASD=2.5335, AU=km, Z=6052km, GI=1x1deg (lat/long)

Figure 14.

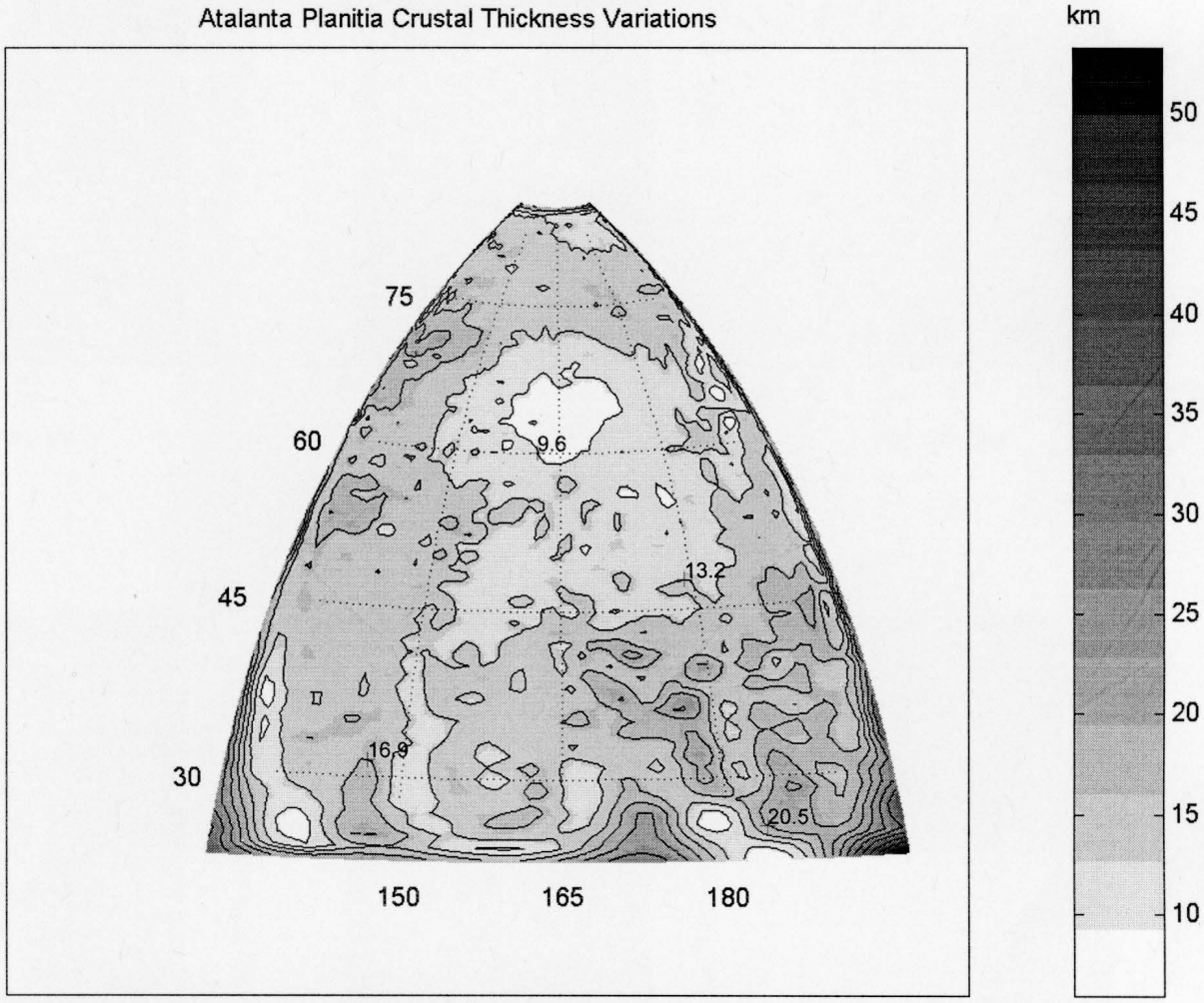

AR=5.96; 24.85, AM=14.0509, ASD=2.6705, AU=km, Z=6052km, GI=1x1deg (lat/long)

Figure 15.

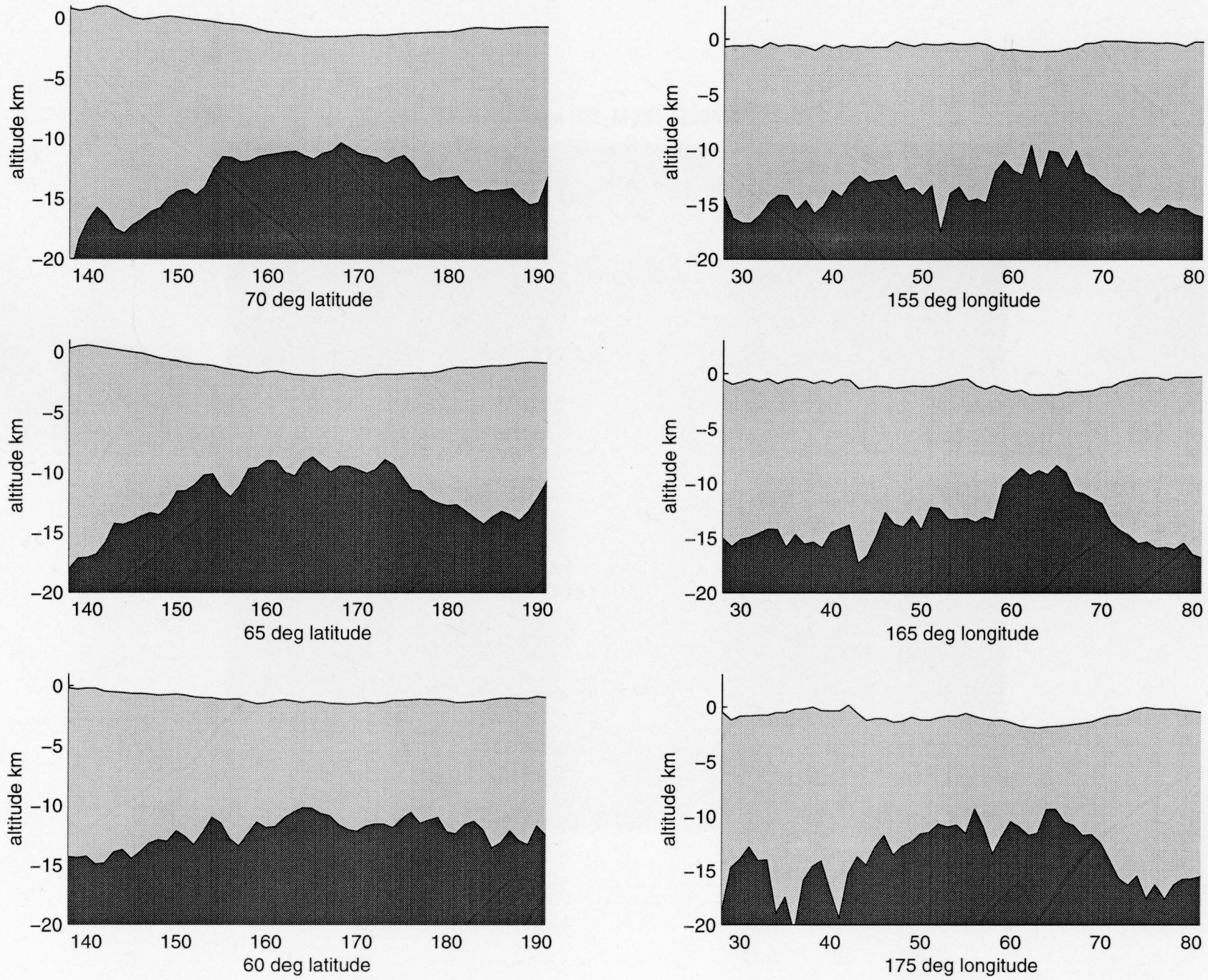
Crustal Thickness Profiles Across Selected Latitudes and Longitudes Through Atalanta Planitia
altitude km
0
−5
−10
−15
−20
140
150
160
170
180
190
70 deg latitude
65 deg latitude
60 deg latitude
30
40
50
60
70
80
155 deg longitude
165 deg longitude
175 deg longitude

Figure 16.

Beta Regio (C2-MIDR c230n284)

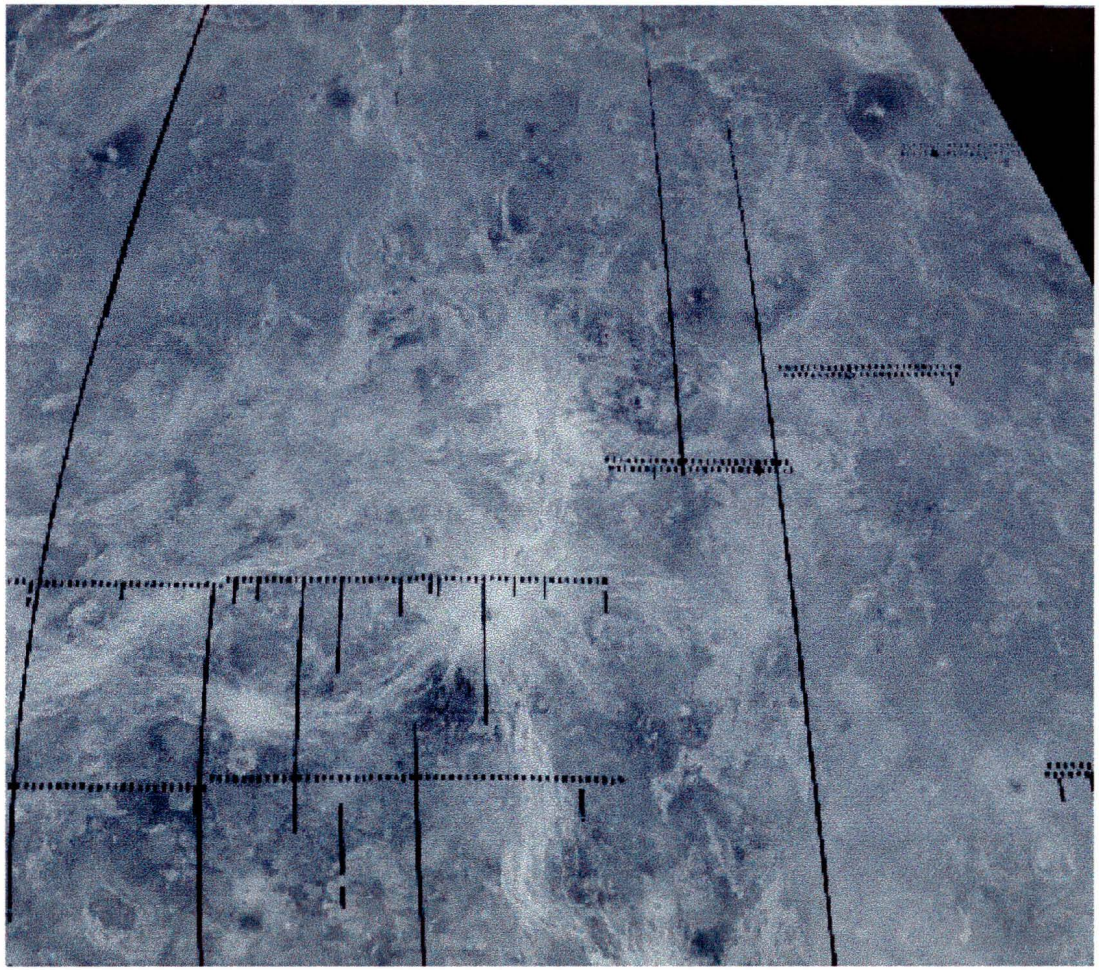

Figure 17

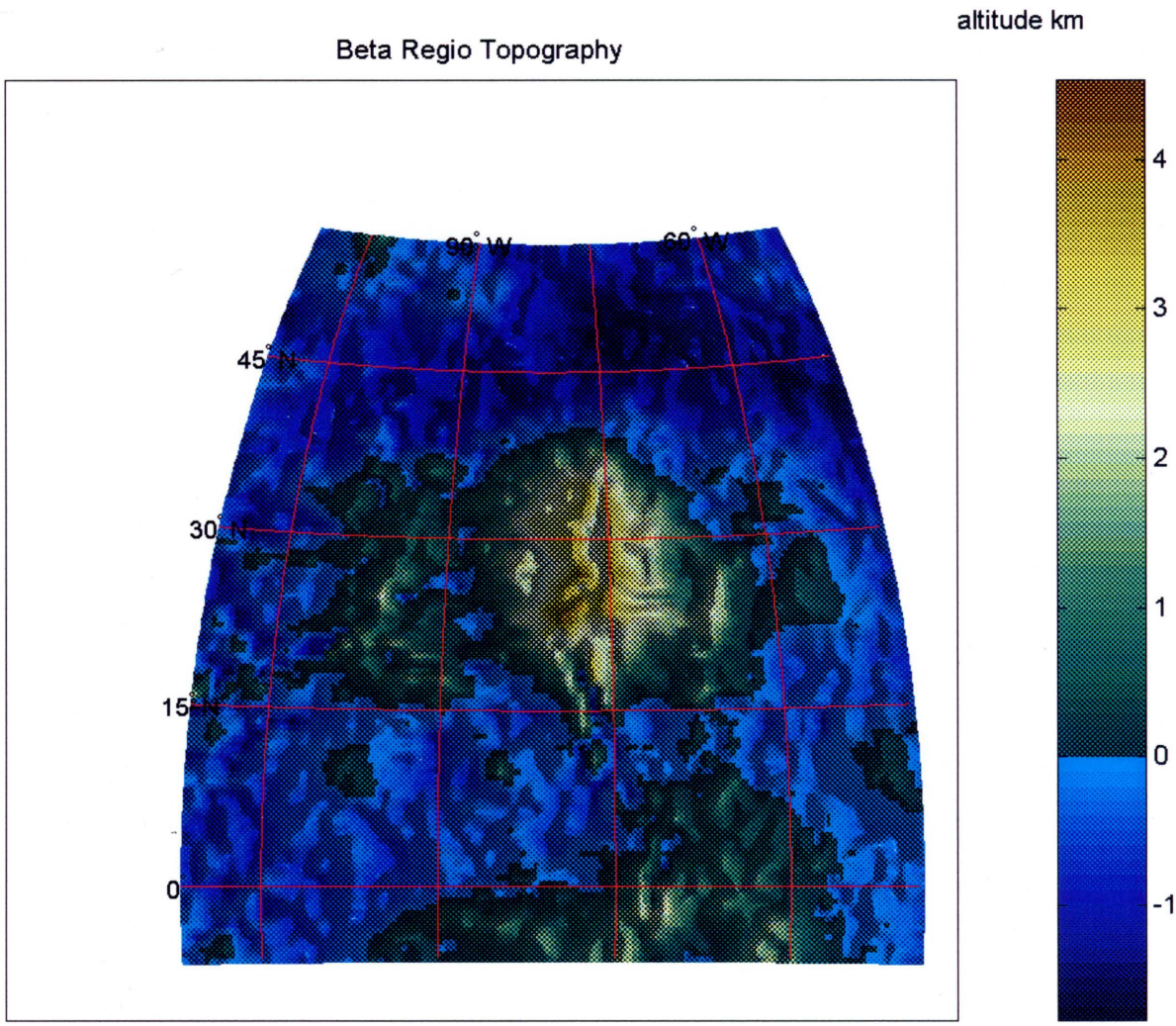

AR=-1.72; 4.53, AM=-1.1177, ASD=0.0961, AU=km, Z=6052km, GI=1deg (lat/lon)

Figure 18.

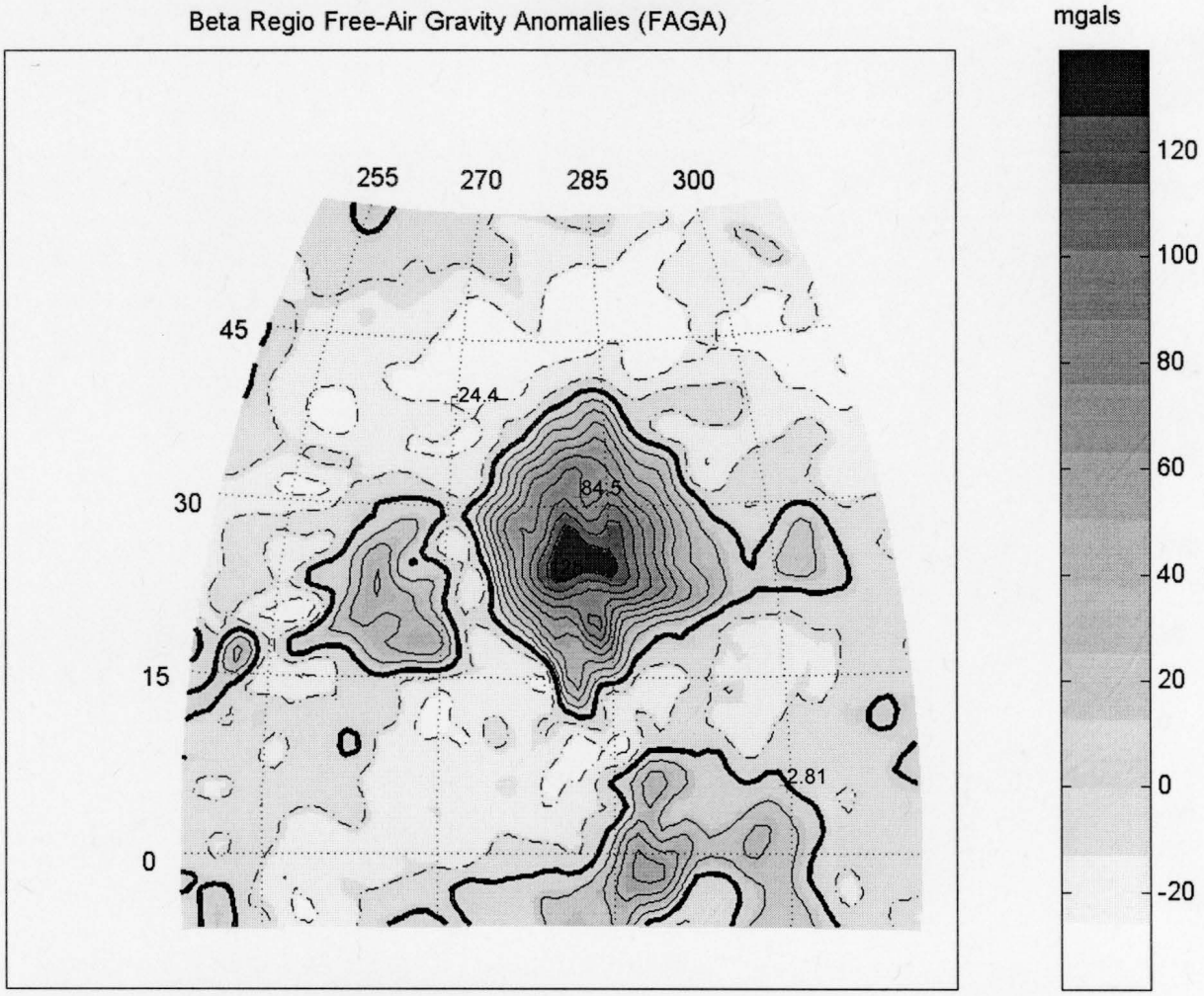

AR=-38.05; 138.99, AM=-2.2786, ASD=27.3069, AU=mgal, Z=100km, GI=1x1deg (lat/long)

Figure 19.

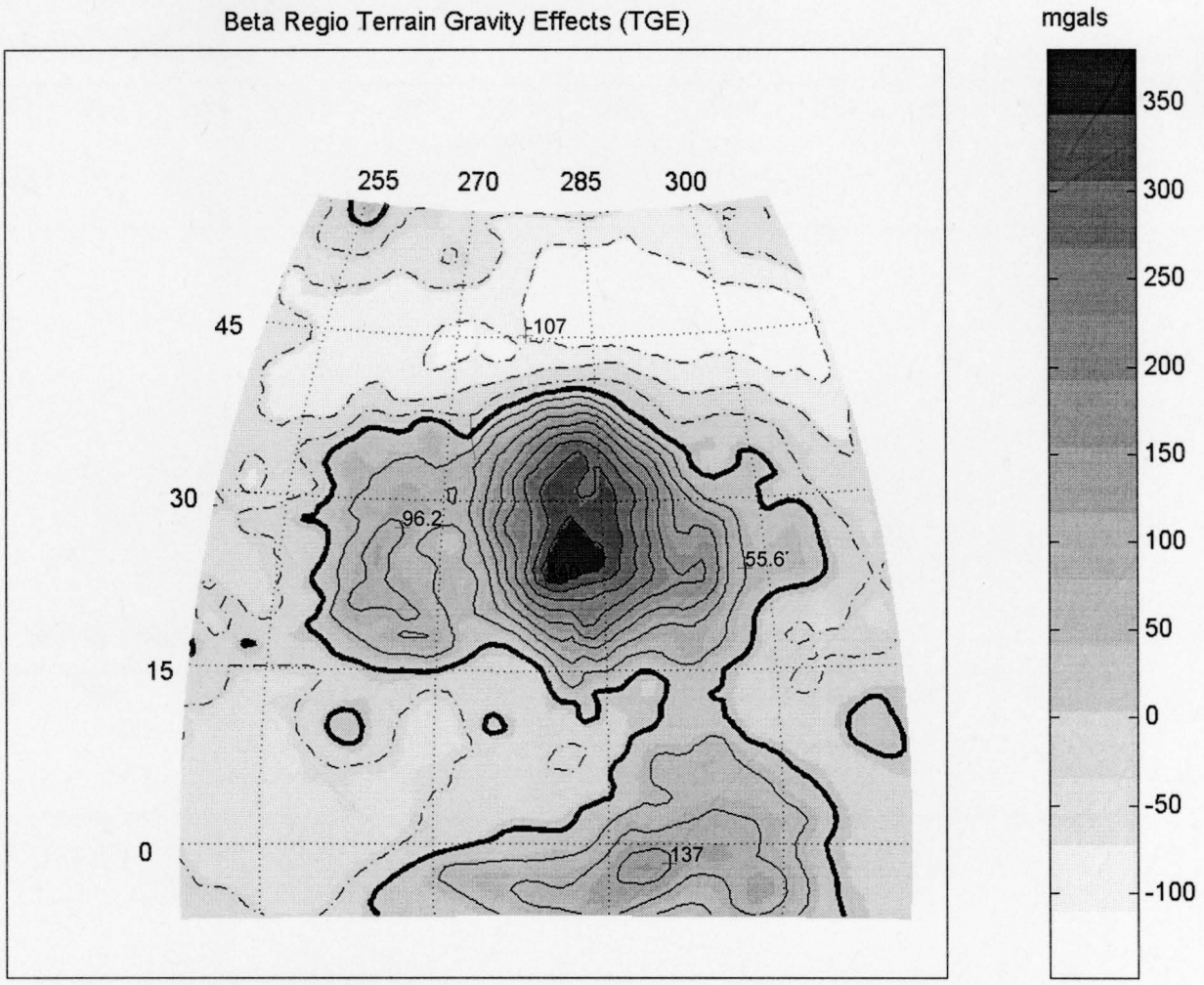

AR=-147.47; 380.41, AM=2.6211, ASD=93.7246, AU=mgal, Z=100km, GI=1x1deg (lat/long)

Figure 20.

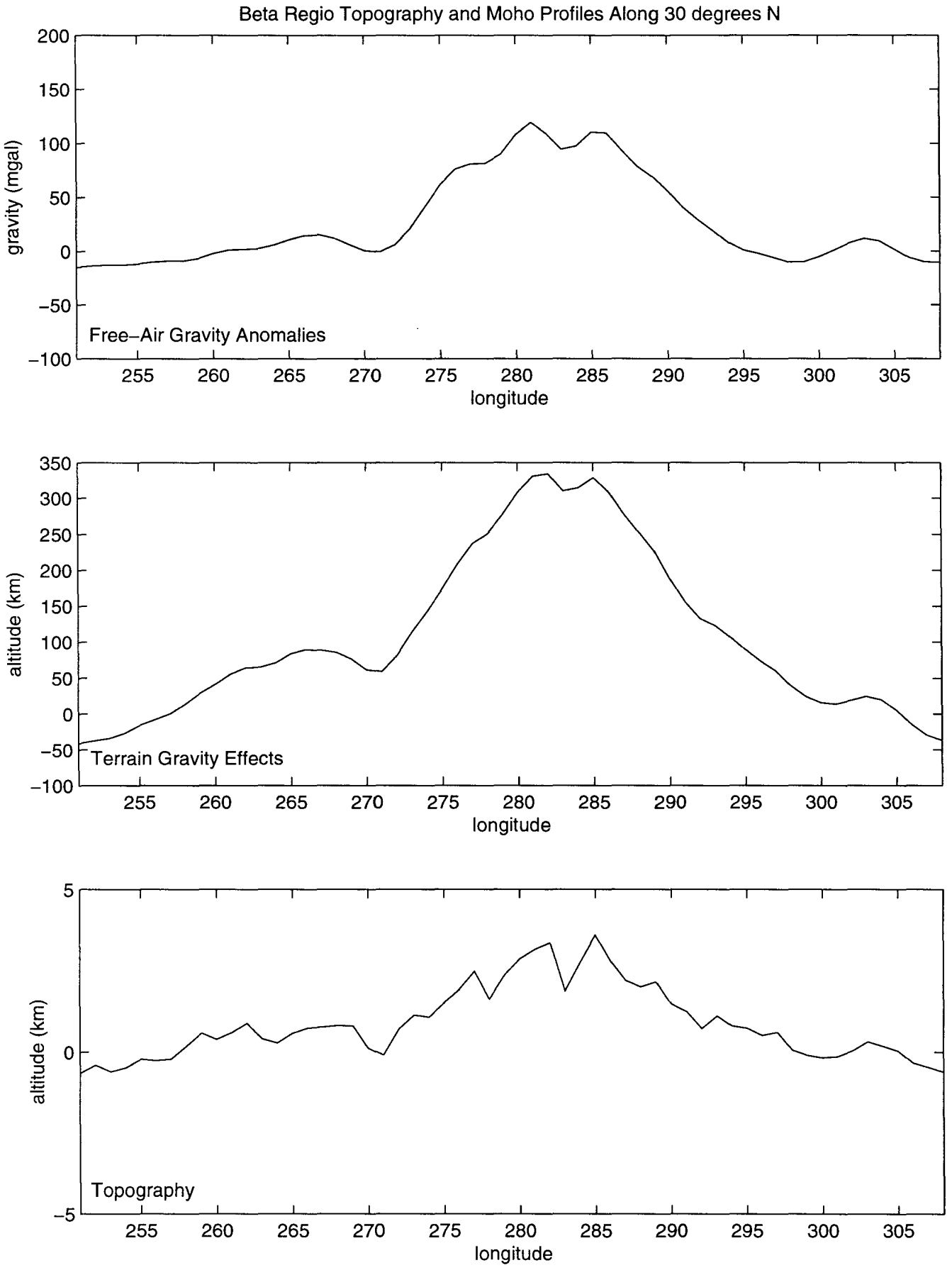
Beta Regio Topography and Moho Profiles Along 30 degrees N
gravity (mgal)
200
150
100
50
0
−50
−100
Free−Air Gravity Anomalies
255
260
265
270
275
280
285
290
295
300
305
longitude
altitude (km)
350
300
250
200
150
100
50
0
−50
−100
Terrain Gravity Effects
255
260
265
270
275
280
285
290
295
300
305
longitude
altitude (km)
5
0
−5
Topography
255
260
265
270
275
280
285
290
295
300
305
longitude

Figure 21.

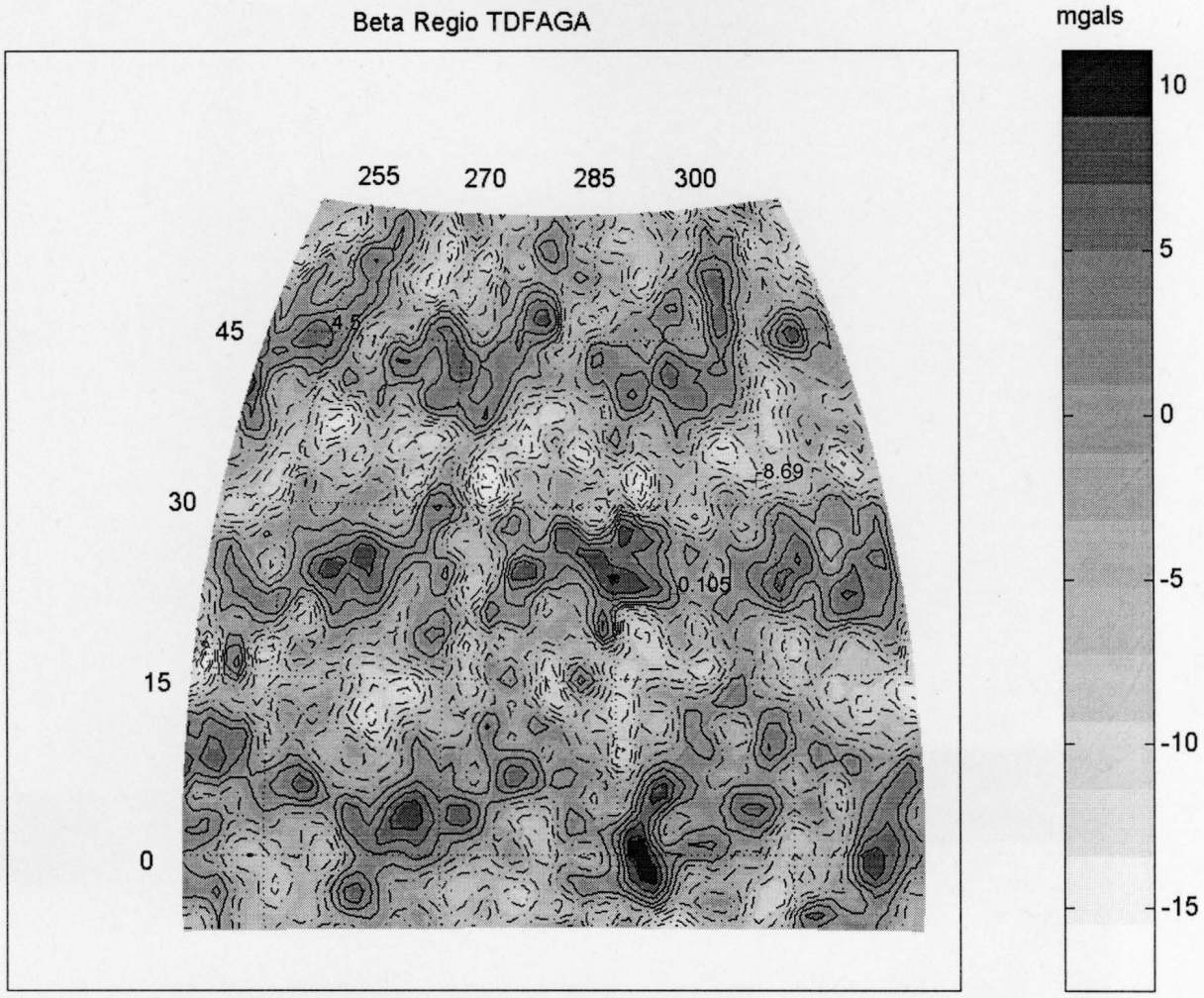

AR=-17.49; 11.10, AM=(-2.2786), ASD=4.4285, AU=mgal, Z=100km, GI=1x1deg (lat/long)

Figure 22.

Theia Mons: Central Beta Regio (F–MIDR f25n278)

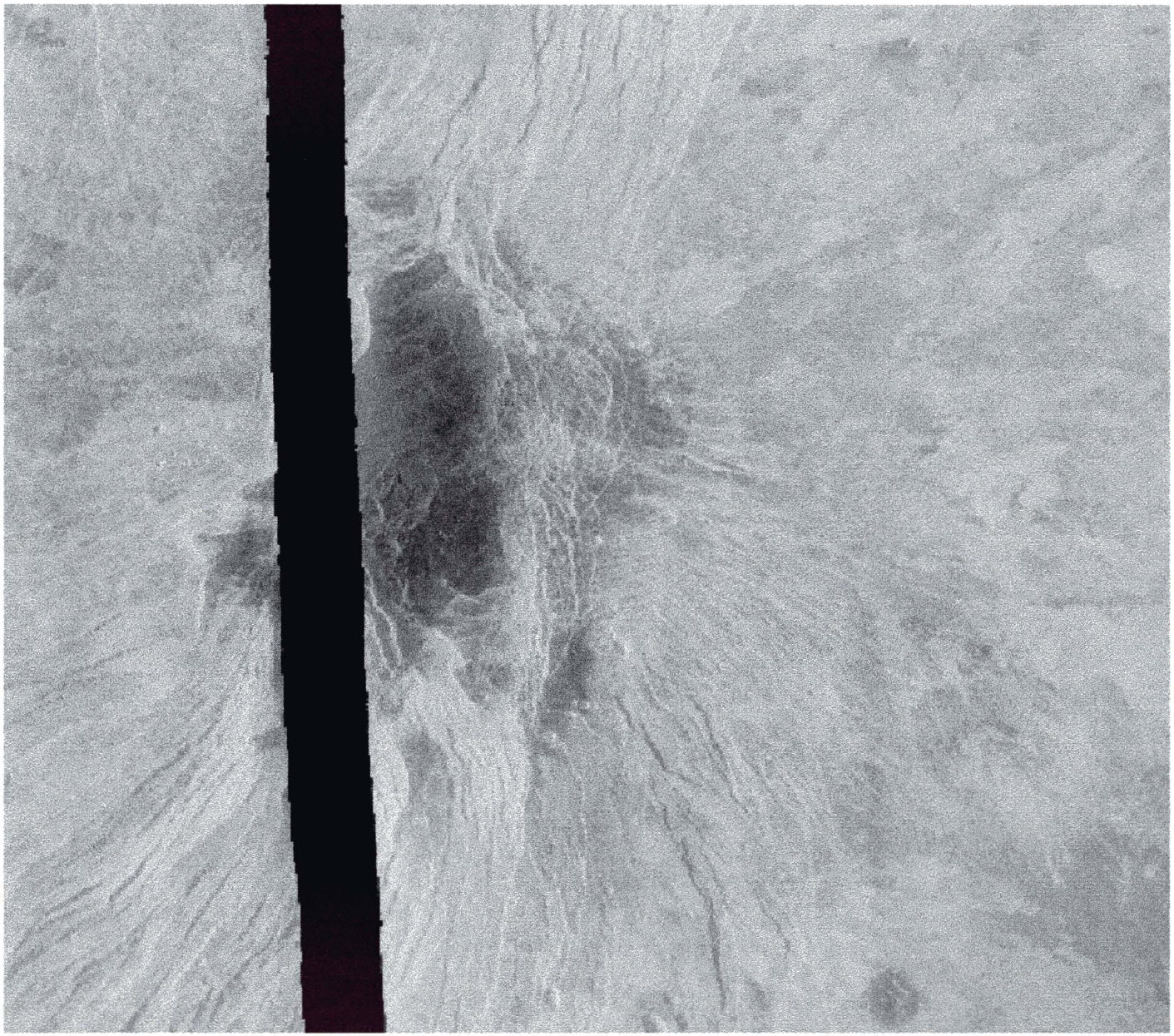

Figure 23

Beta Regio Local Favorability Indices

Summed Local Favorability Indices

Differenced Local Favorability Indices

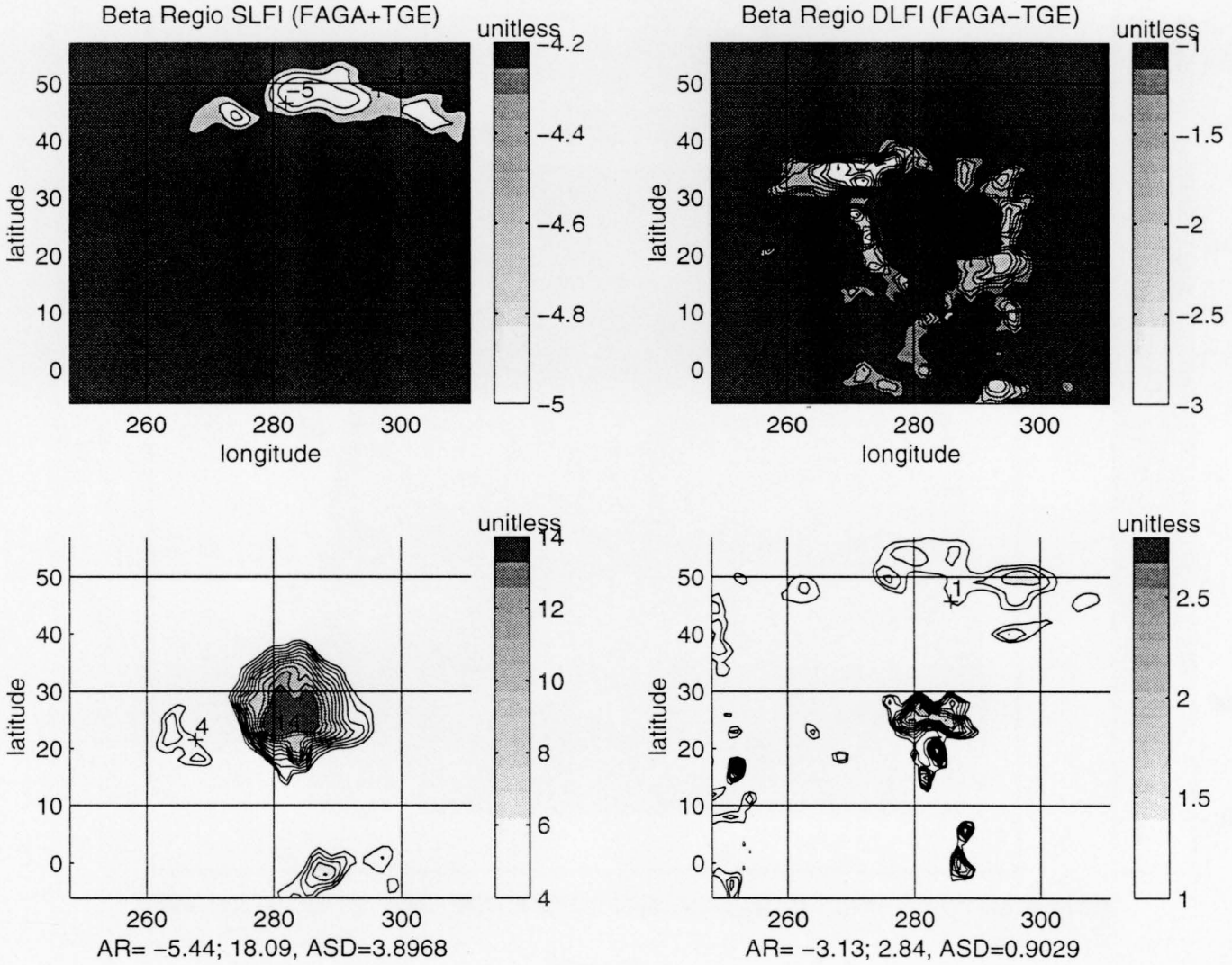

Figure 24.

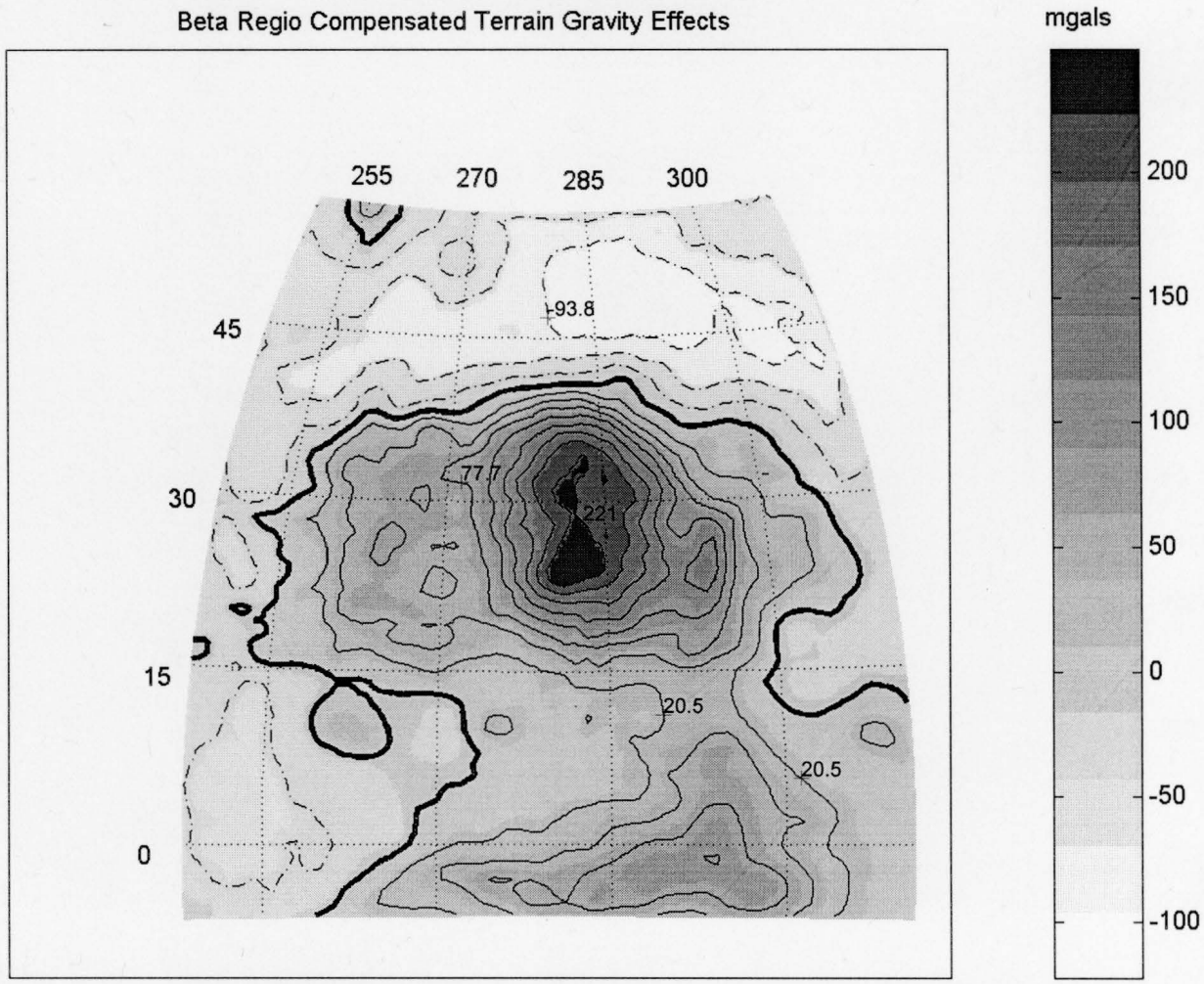

AR=-122.38; 249.13, AM=2.5925, ASD=70.1044, AU=mgal, Z=100km, GI=1x1deg (lat/long)

Figure 25.

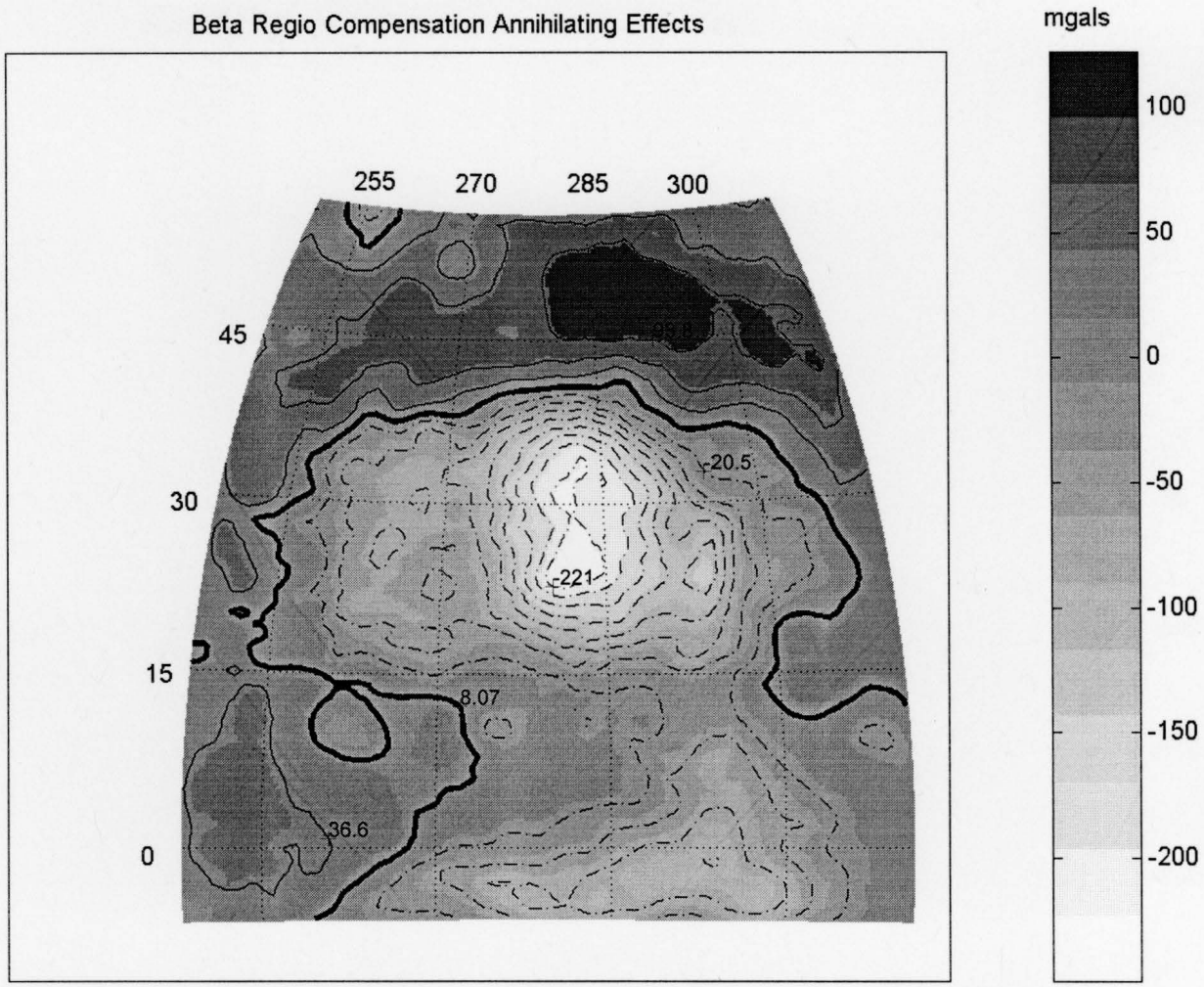

AR=-249.13; 122.38, AM=-2.5925, ASD=70.1044, AU=mgal, Z=100km, GI=1x1deg (lat/long)

Figure 26.

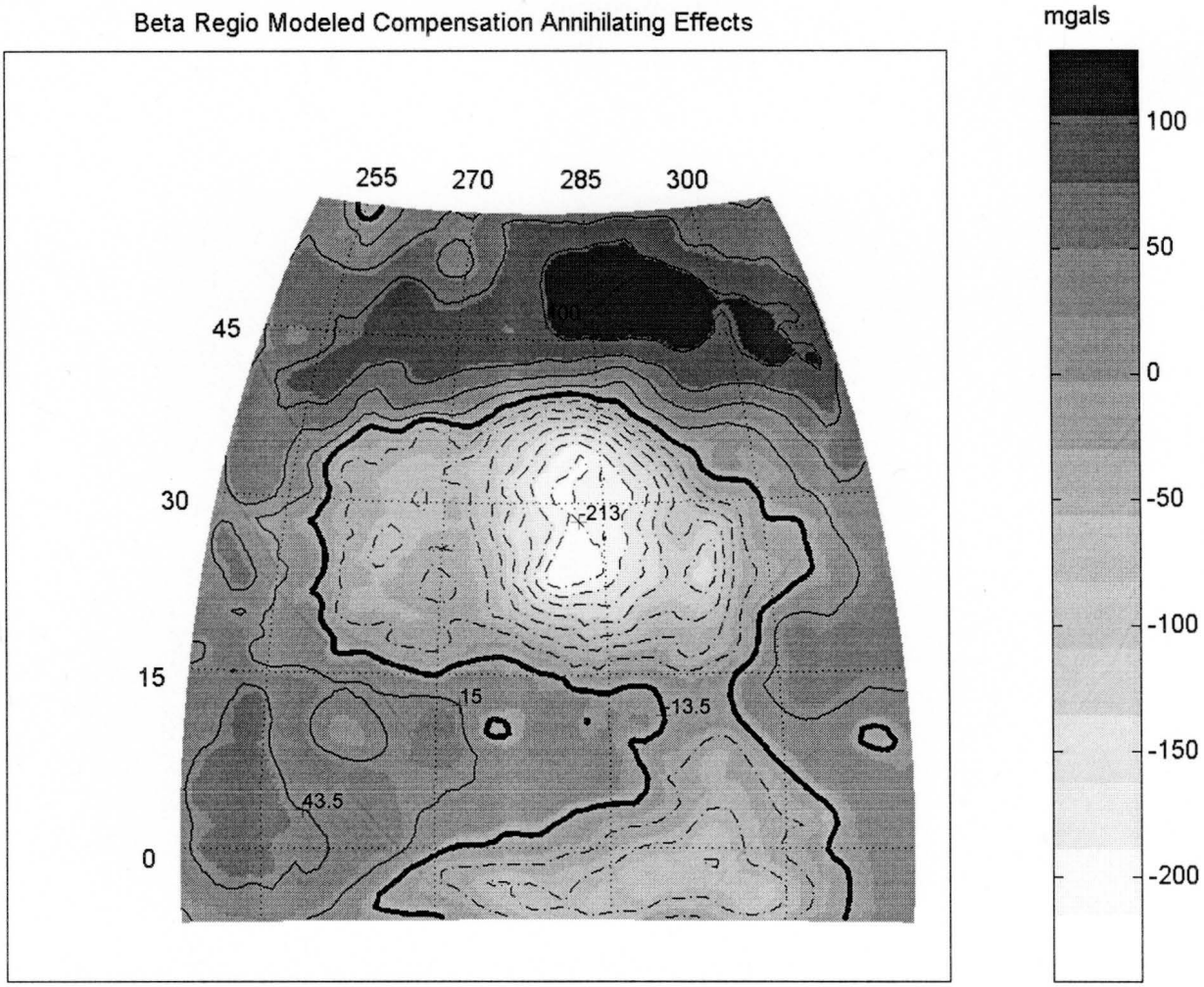

AR=-241.26; 128.87, AM=-0.2698, ASD=74.0149, AU=mgal, Z=100km, GI=1x1deg (lat/long)

Figure 27.

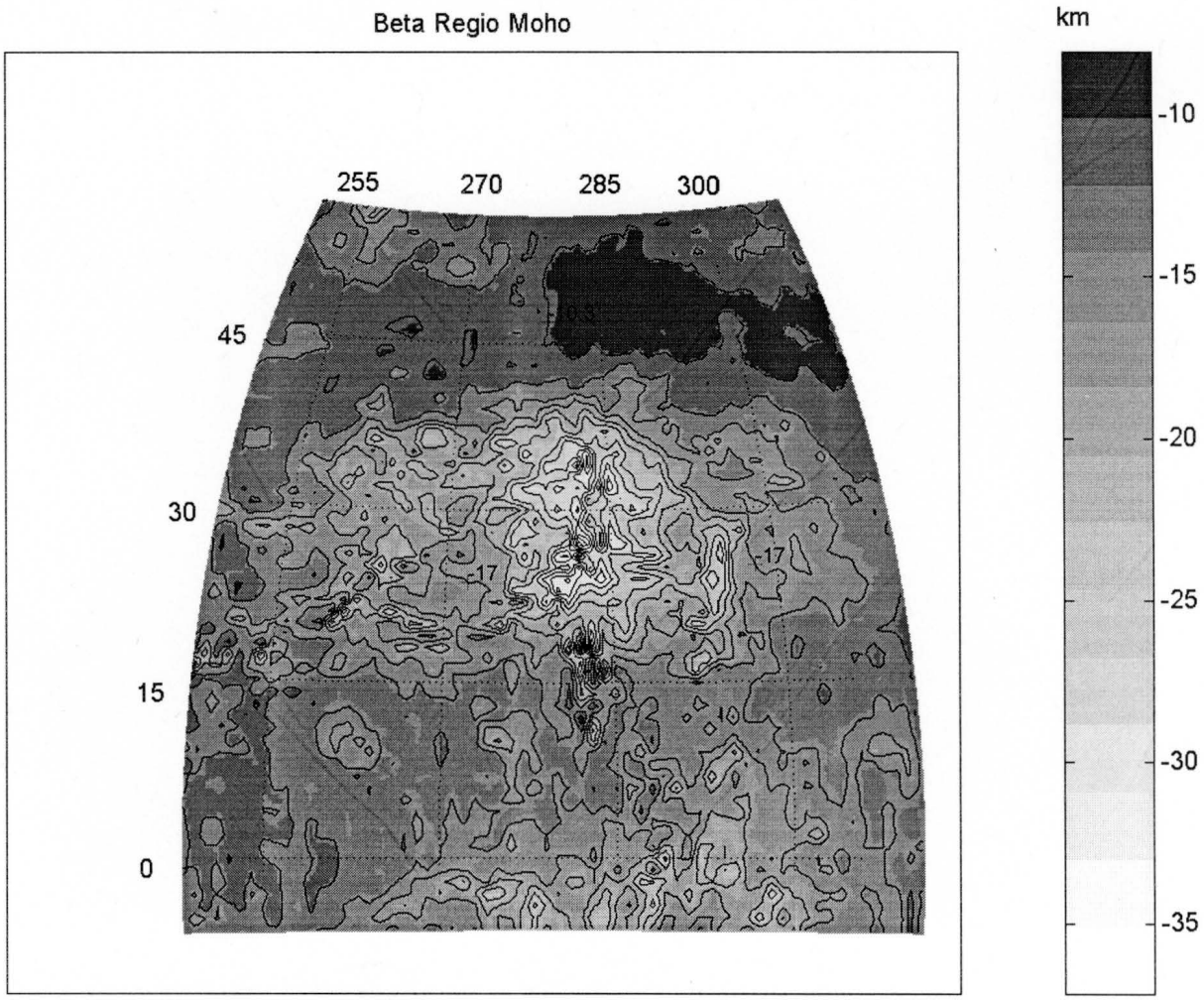

AR=-37.15; -8.07, AM=-15.1709, ASD=4.2303, AU=km, Z=6052km, GI=1x1deg (lat/long)

Figure 28.

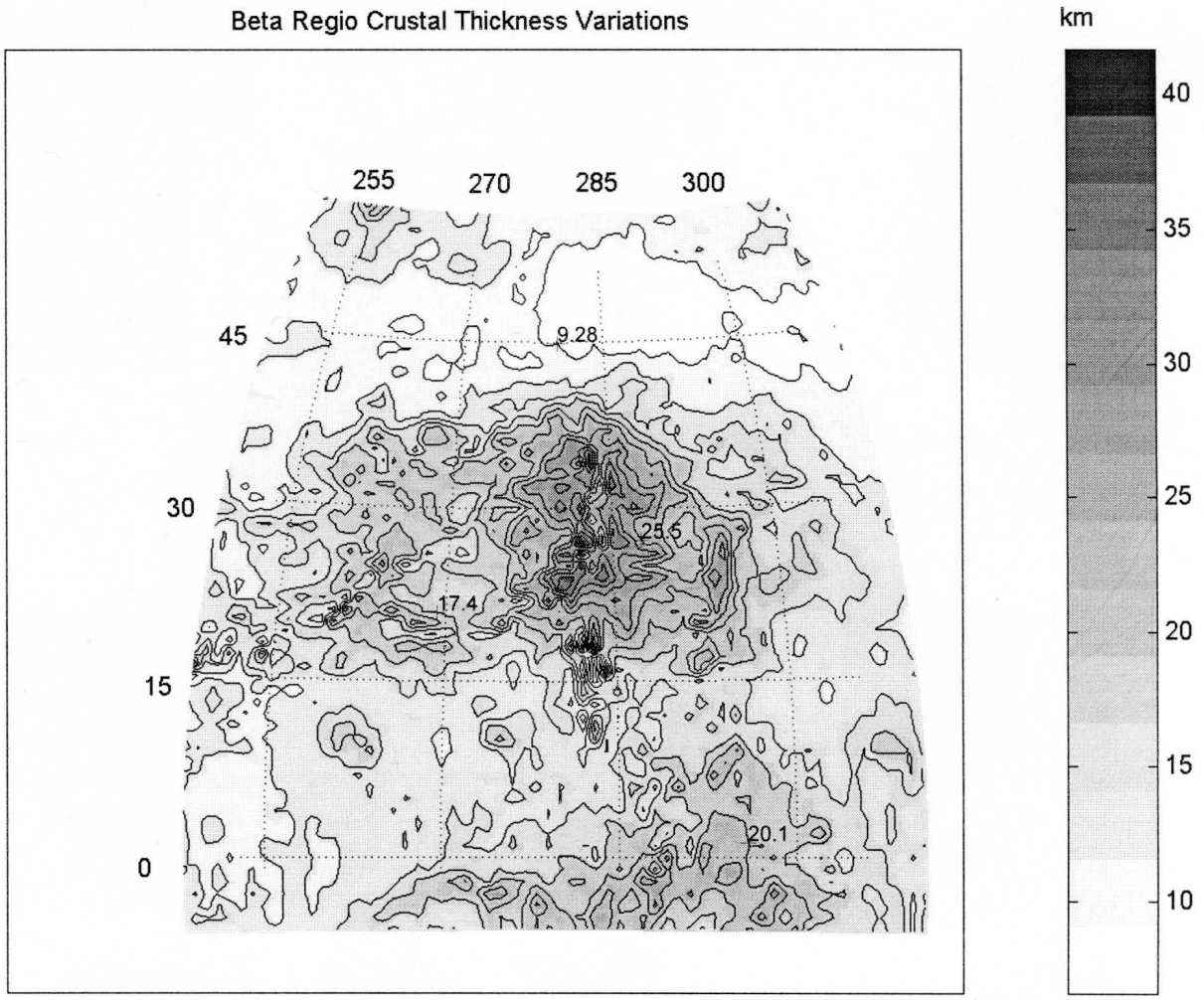

AR=6.58; 41.69, AM=15.1088, ASD=5.217, AU=km, Z=6052km, GI=1x1deg (lat/long)

Figure 29.

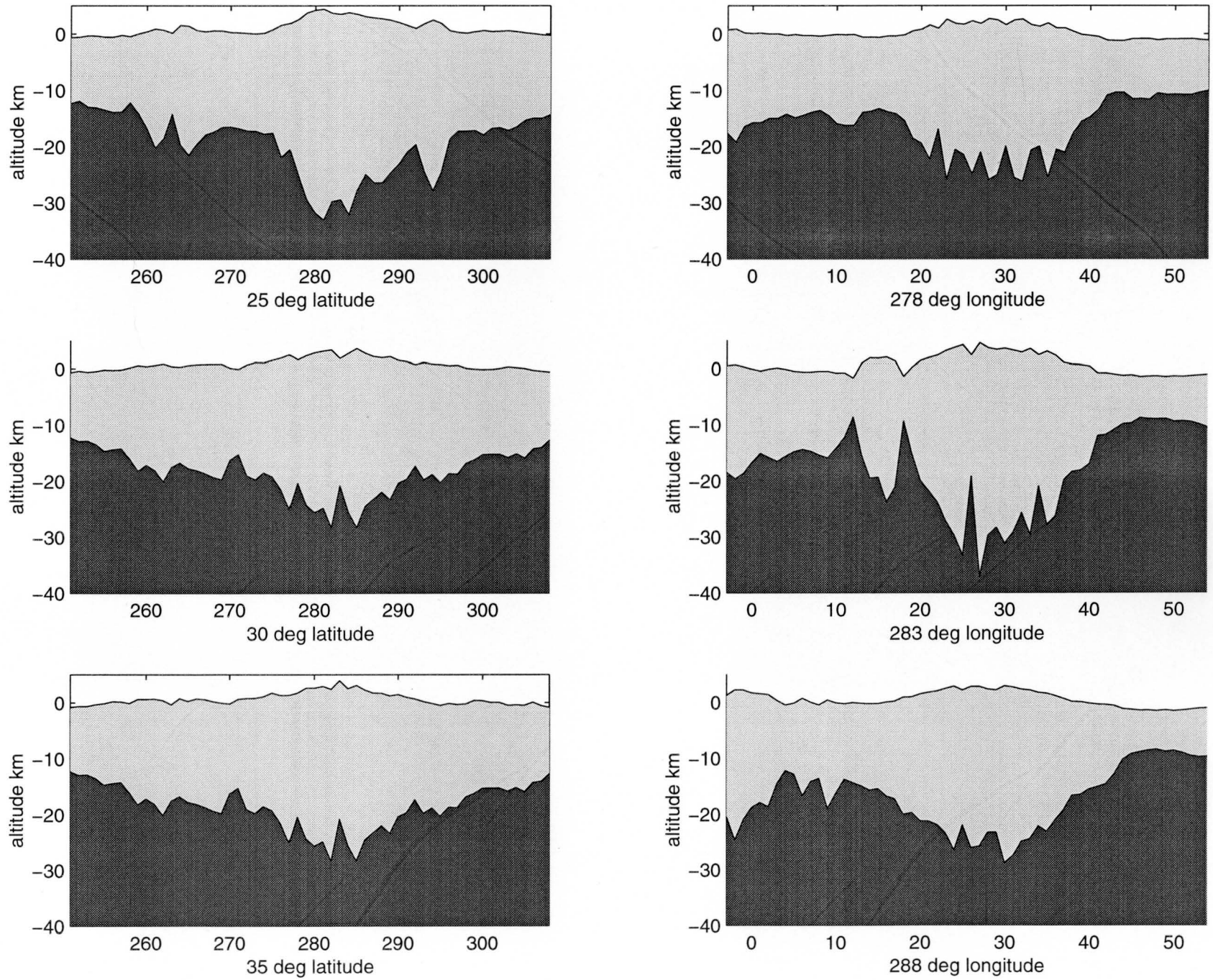
Crustal Thickness Profiles Across Selected Latitudes and Longitudes Trough Beta Regio
altitude km
0
−10
−20
−30
−40
260
270
280
290
300
25 deg latitude
0
10
20
30
40
50
278 deg longitude
30 deg latitude
283 deg longitude
35 deg latitude
288 deg longitude

Figure 30.

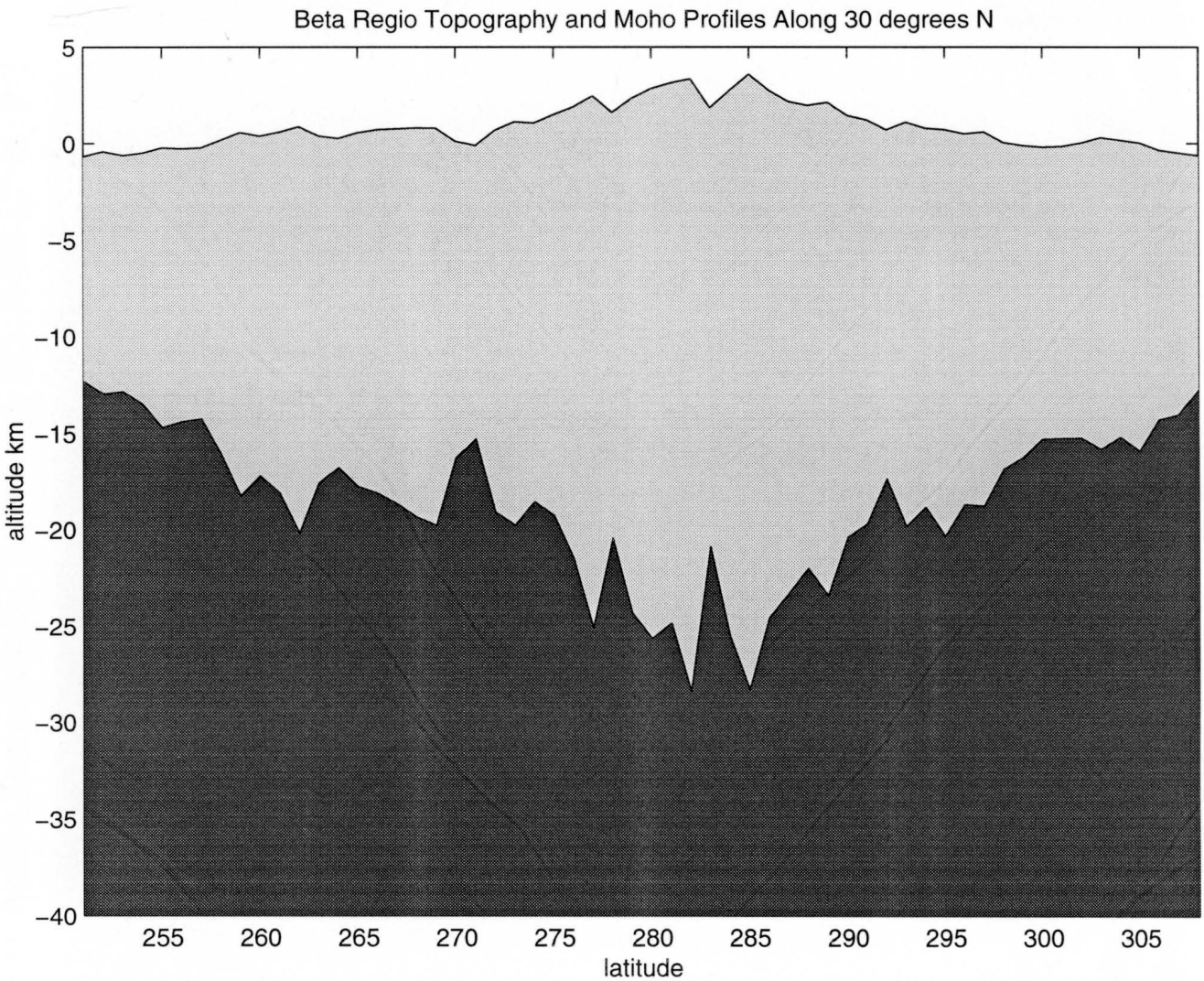
Beta Regio Topography and Moho Profiles Along 30 degrees N
5
0
−5
−10
−15
−20
−25
−30
−35
−40
altitude km
255
260
265
270
275
280
285
290
295
300
305
latitude

Figure 31.

Hemisphere Encompassing Thetis Regio (C3-MIDR c314s180)

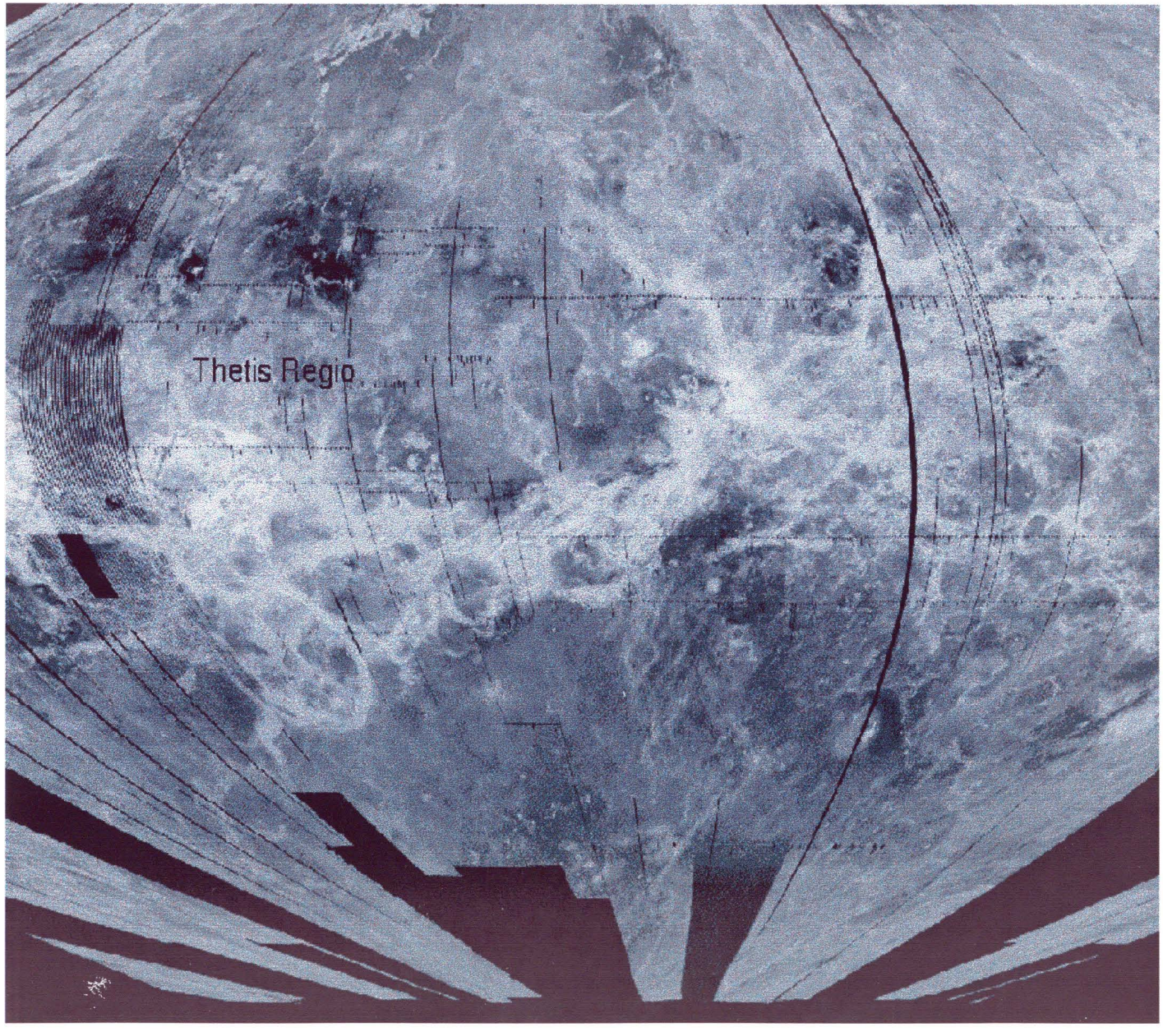

Figure 32.

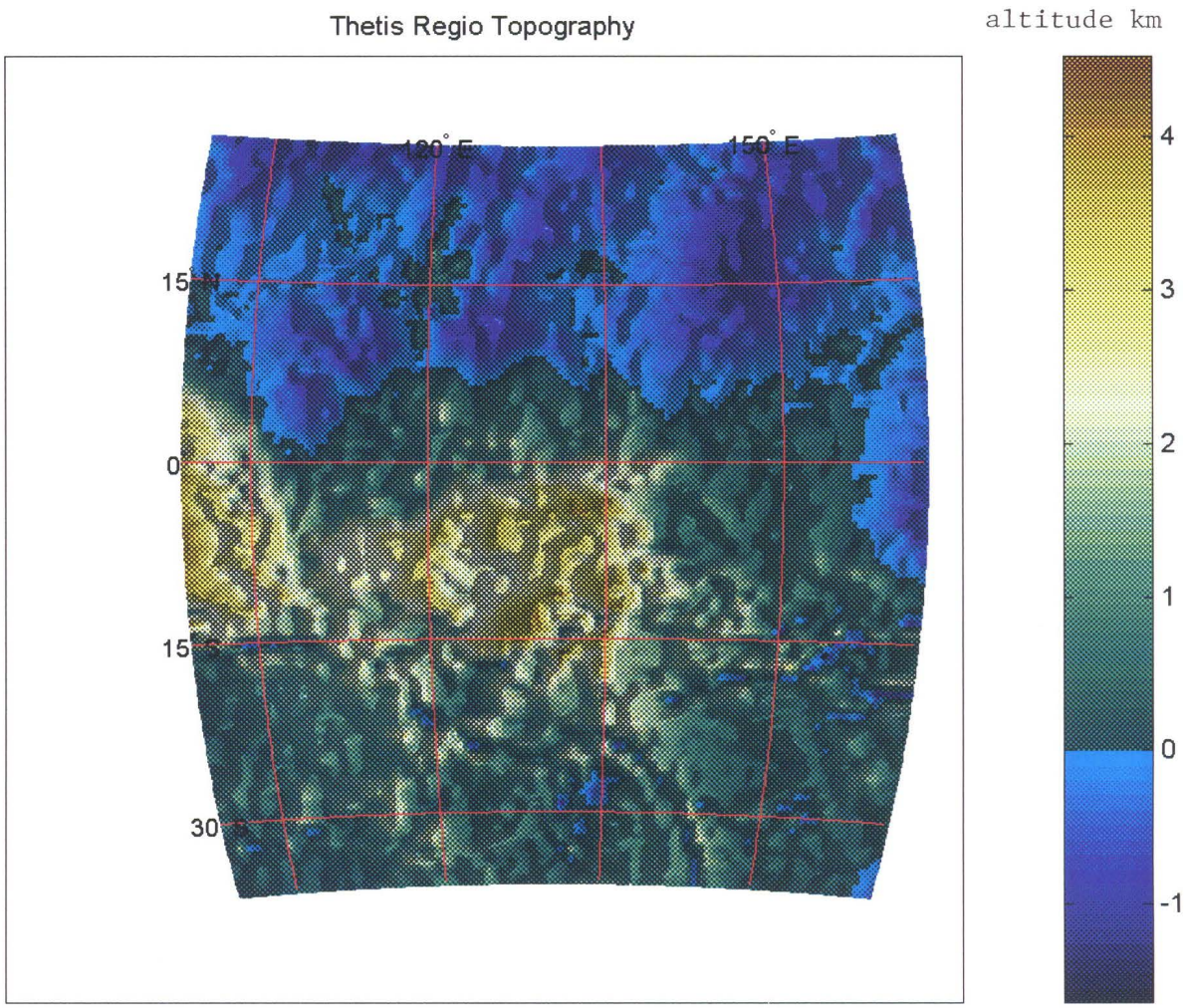

AR= -1.64; 4.43, AM=0.6176, ASD=1.0961, AU=km, Z=6052km, GI=1x1 deg (lat/lon)

Figure 33.

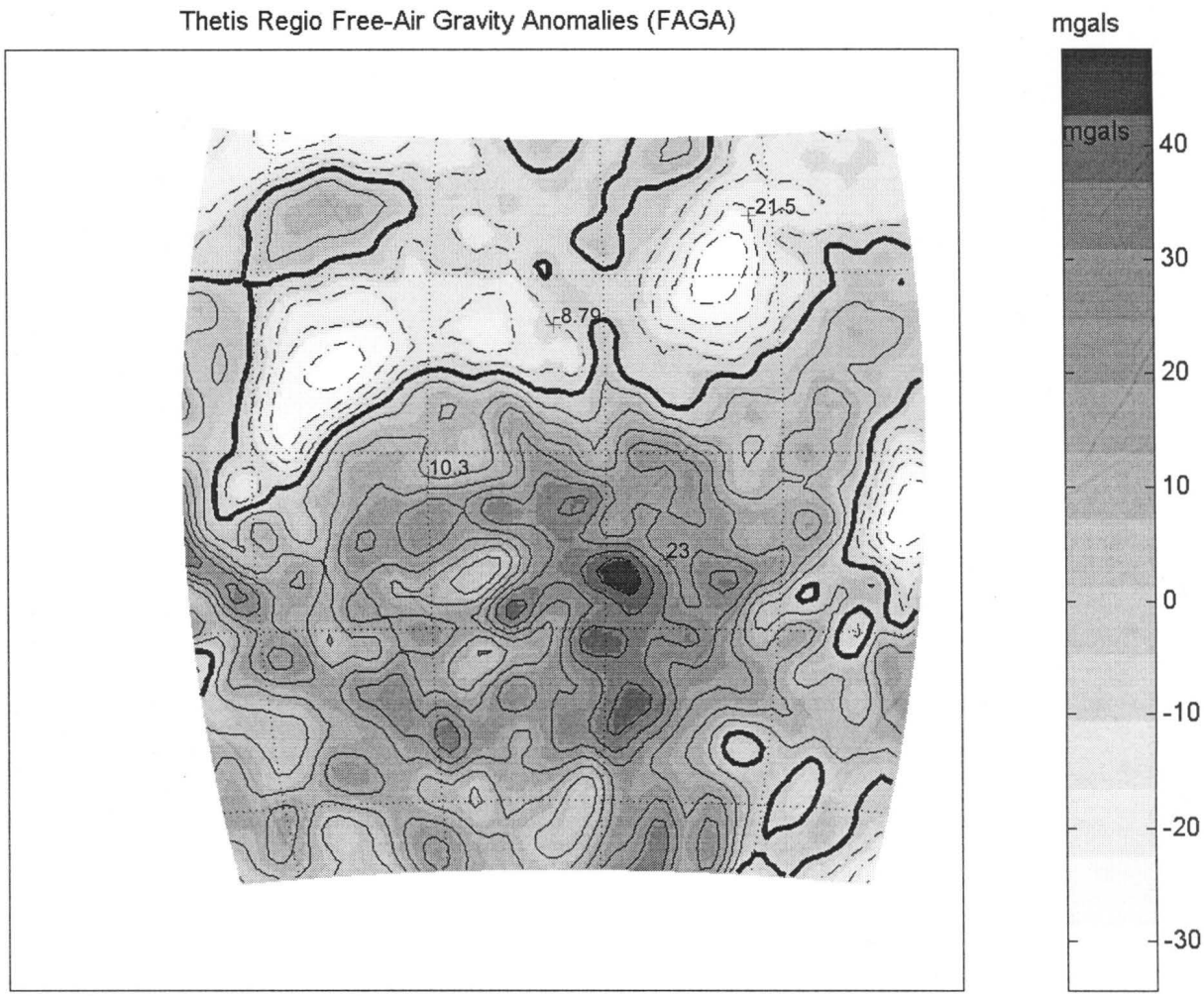

AR=-34.24; 48.46, AM=4.7442, ASD=14.7281, AU=mgal, Z=100km, GI=1x1deg (lat/long)

Figure 34.

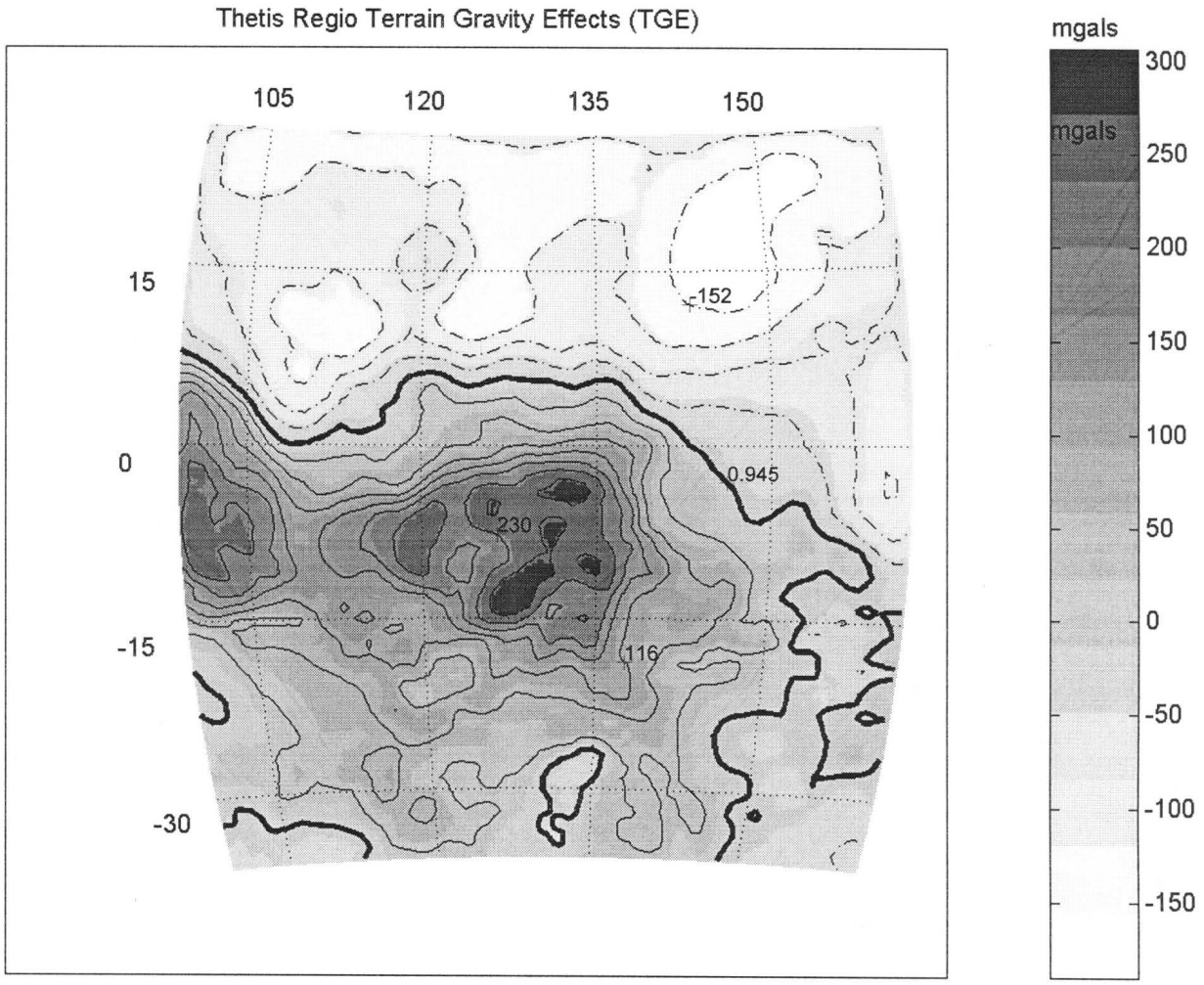

AR=-190.01; 306.47, AM=4.5630, ASD=109.6558, AU=mgal, Z=100km, GI=1x1deg (lat/long)

Figure 35.

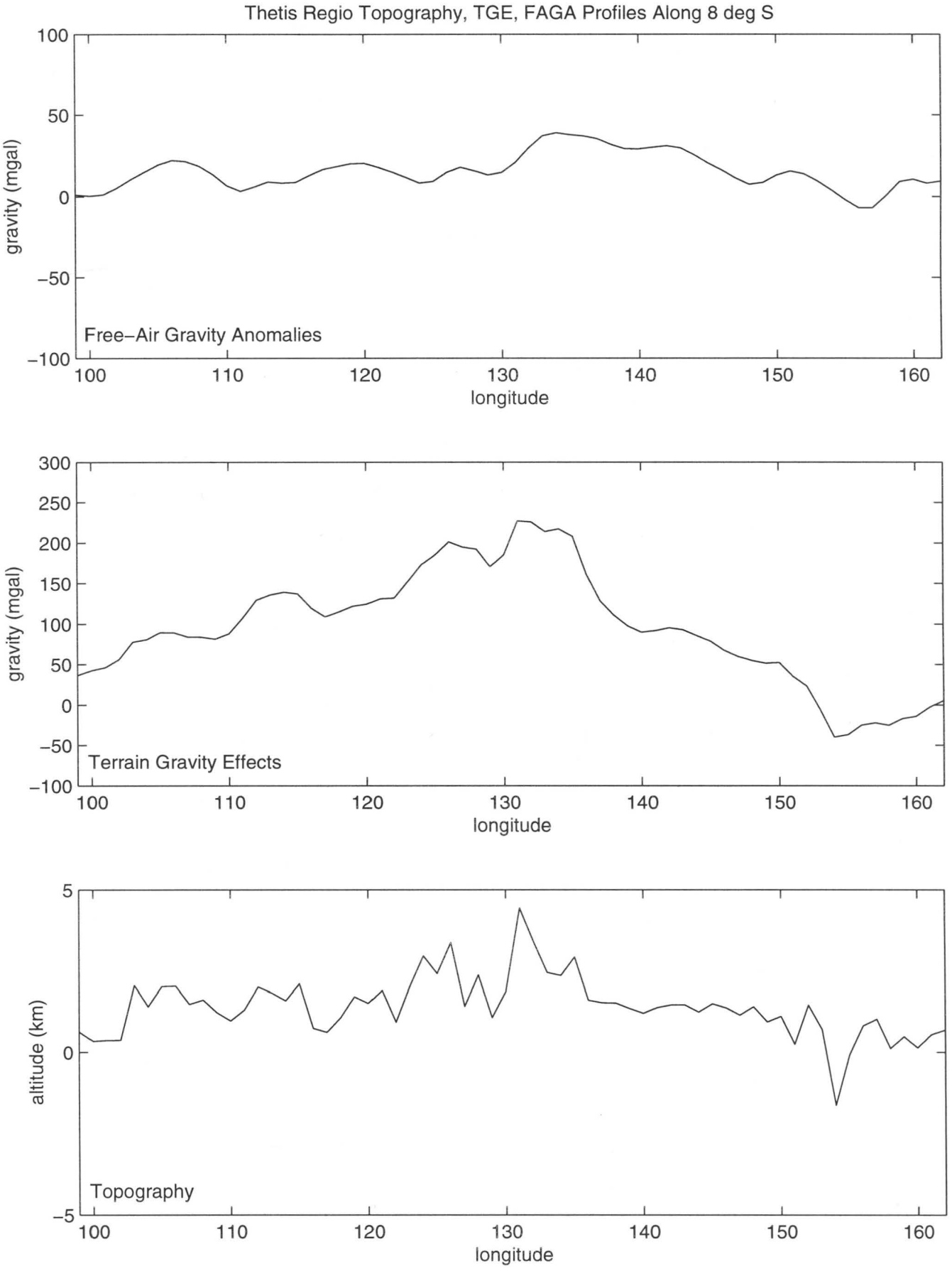
Thetis Regio Topography, TGE, FAGA Profiles Along 8 deg S
gravity (mgal)
100
50
0
−50
−100
Free−Air Gravity Anomalies
100
110
120
130
140
150
160
longitude
gravity (mgal)
300
250
200
150
100
50
0
−50
−100
Terrain Gravity Effects
100
110
120
130
140
150
160
longitude
altitude (km)
5
0
−5
Topography
100
110
120
130
140
150
160
longitude

Figure 36.

Thetis Regio Local Favorability Indices

Summed Local Favorability Indices

Differenced Local Favorability Indices

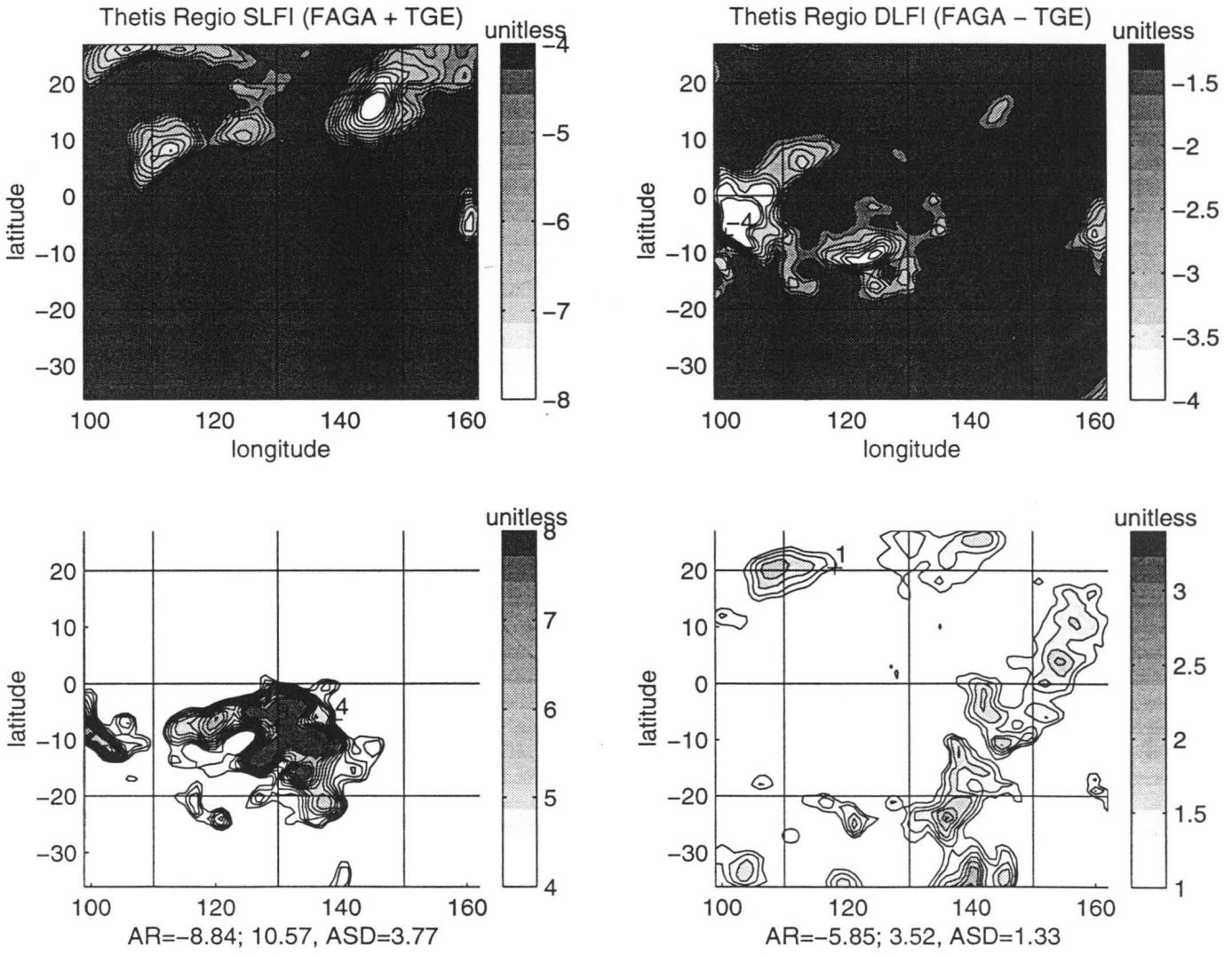

Figure 37.

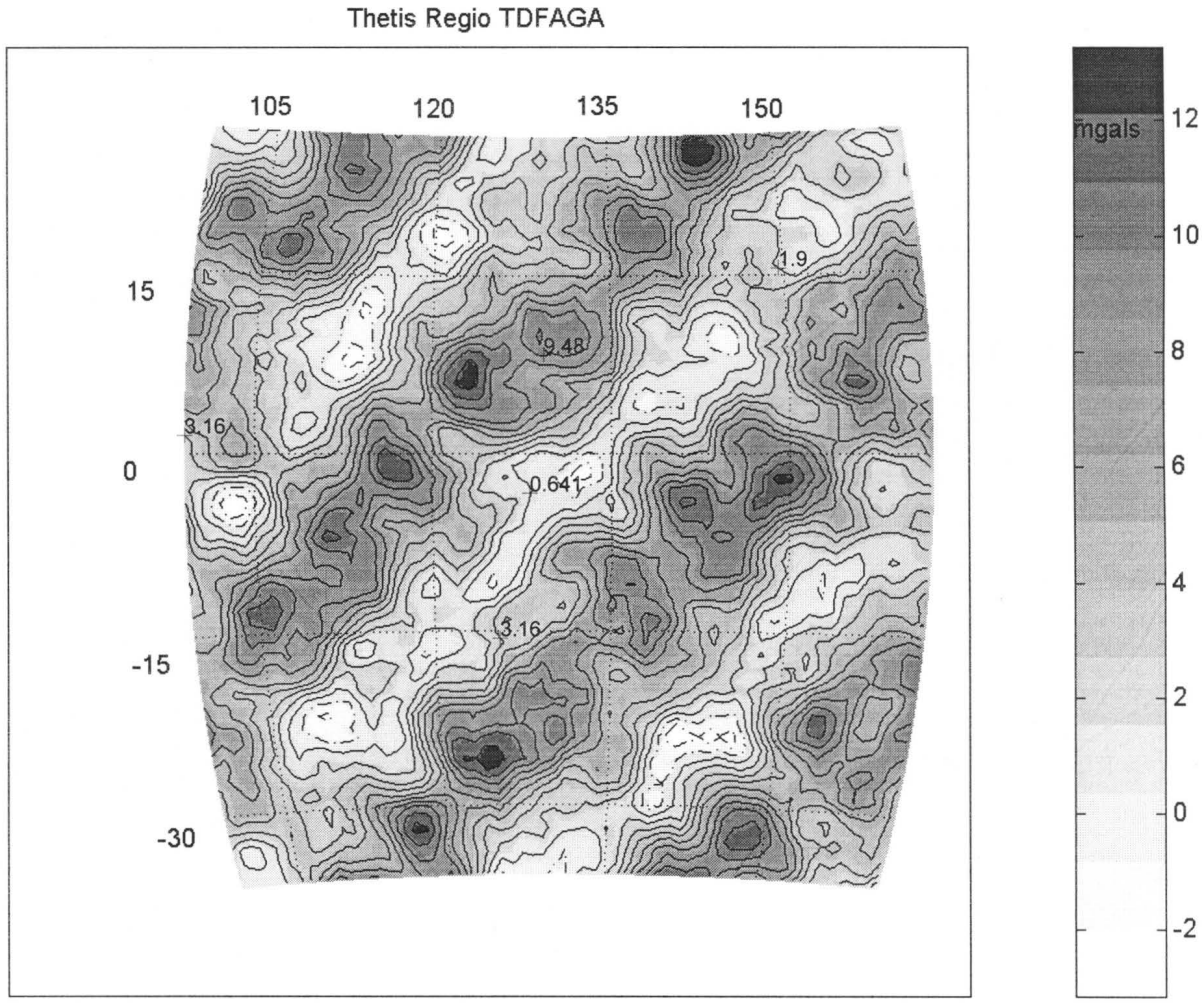

AR=-3.15; 13.26, AM=(4.7442), ASD=3.1932, AU=mgal, Z=100km, GI=1x1deg (lat/long)

Figure 38.

Southeast Thetis Regio (C3-MIDR c314s180)

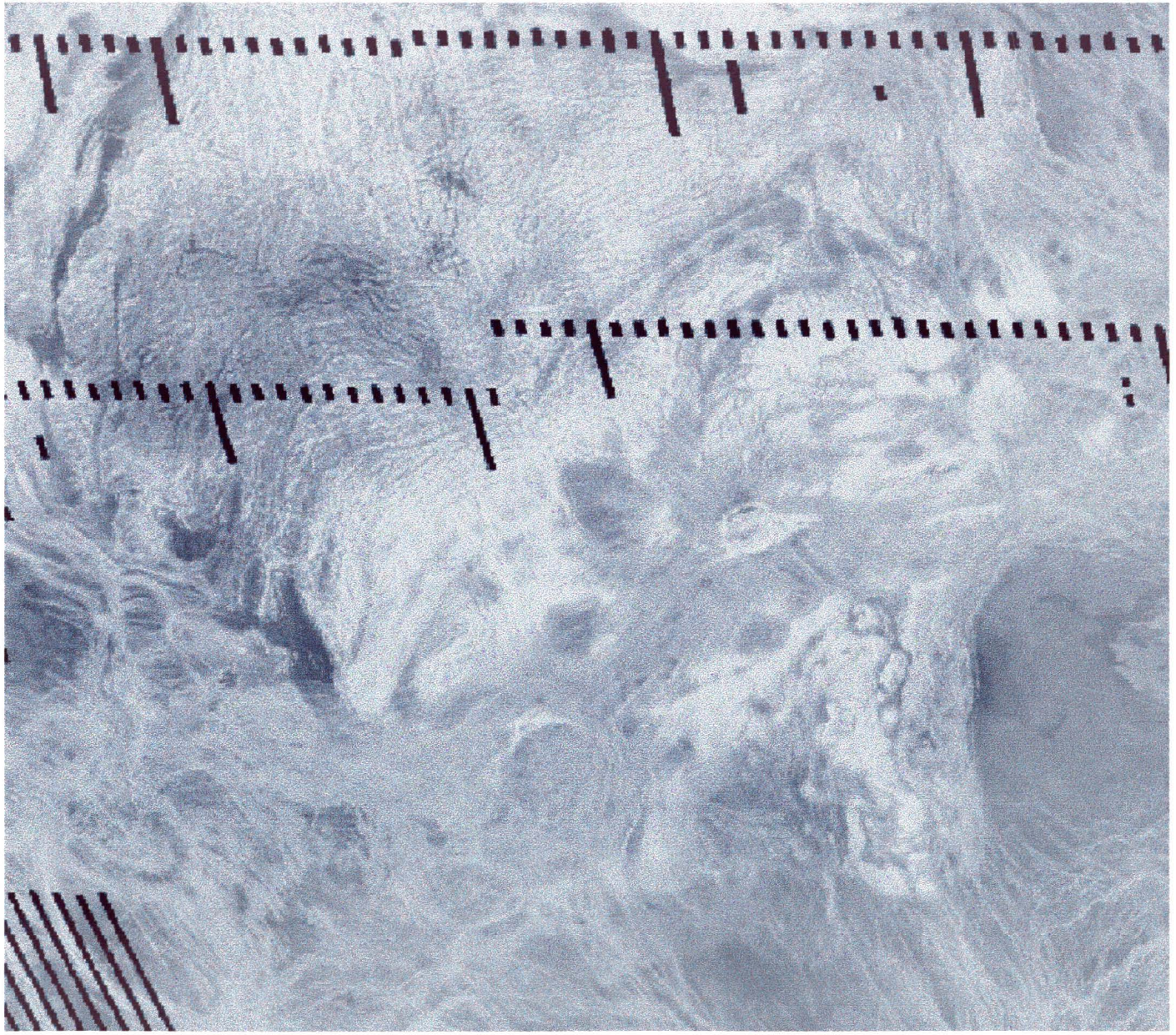

Figure 39.

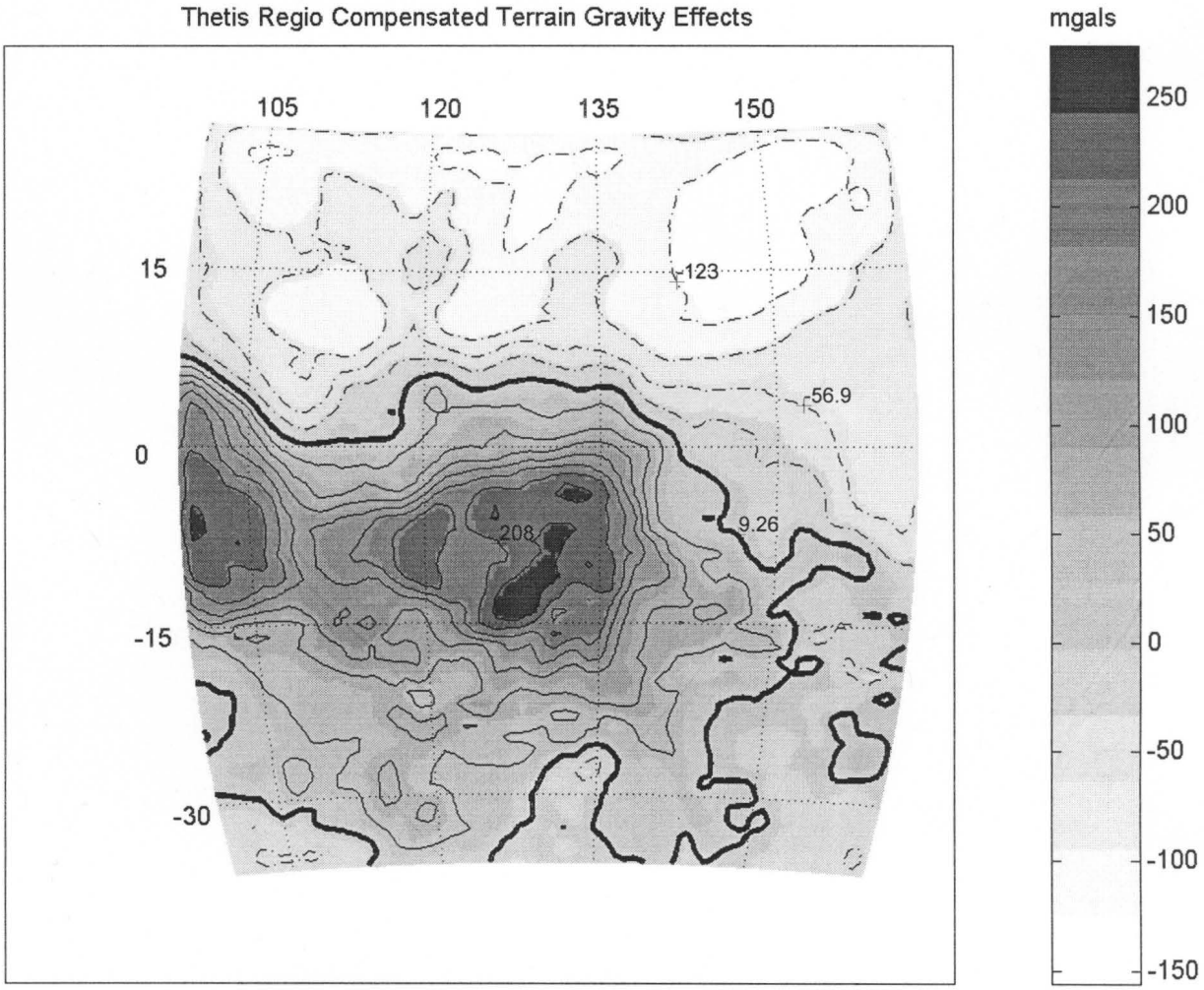

AR= -156.09; 273.83, AM=4.5630, ASD=98.6083, AU=mgal, Z=100km, GI=1x1deg (lat/long)

Figure 40.

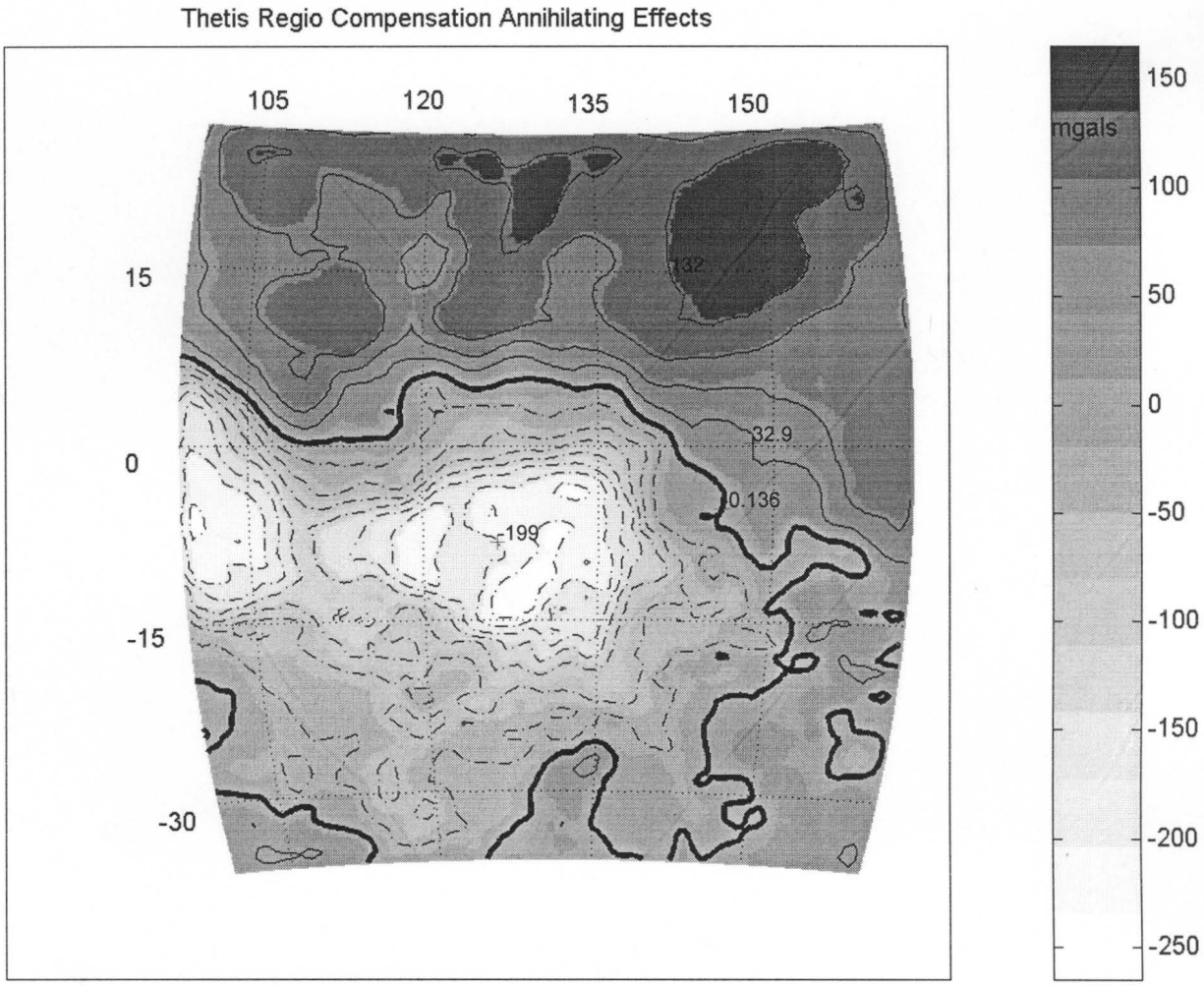

AR=-273.83; 156.09, AM=(-4.5630), ASD=98.6083, AU=mgal, Z=100km, GI=1x1deg (lat/long)

Figure 41.

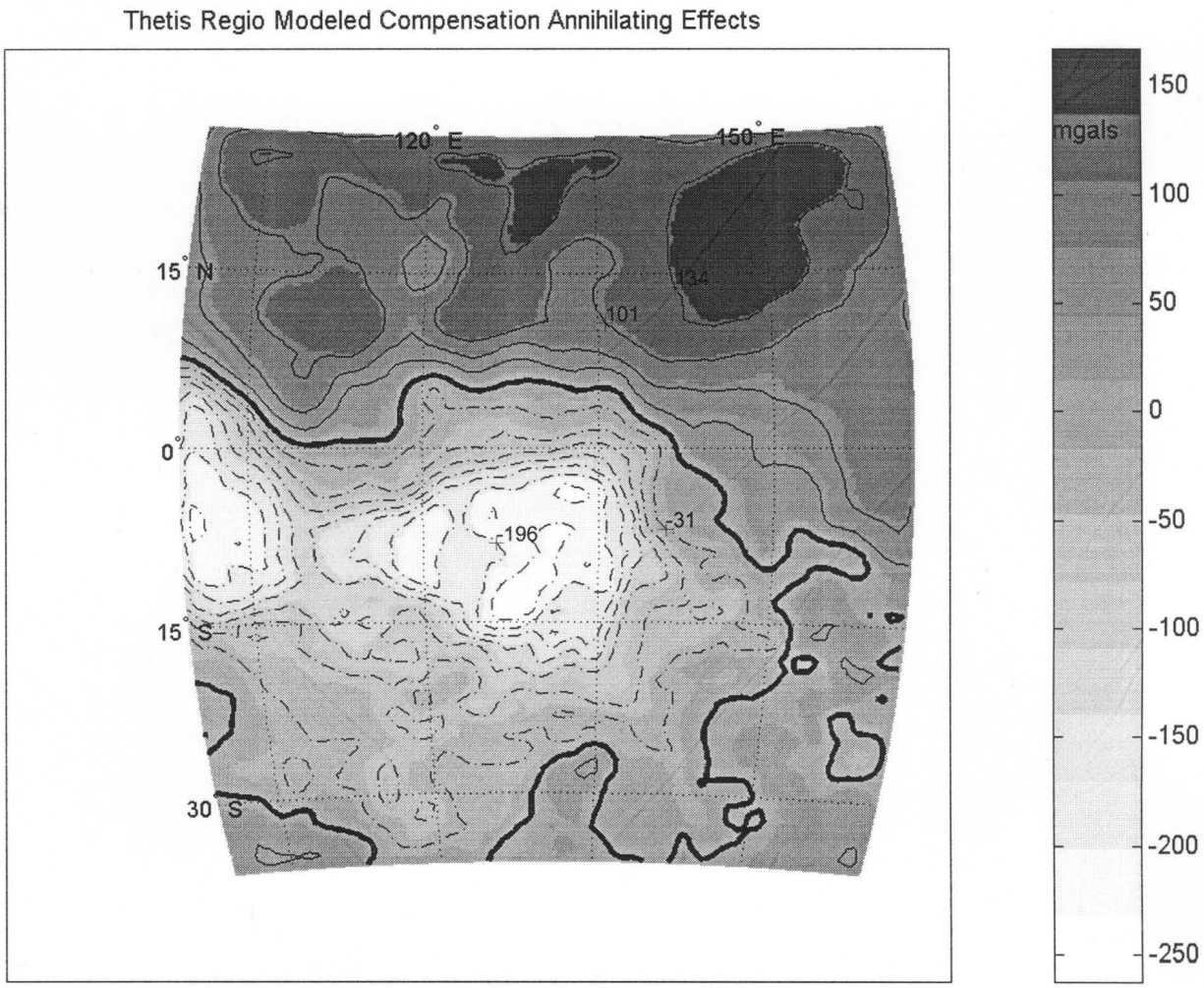

AR=-262.24; 167.14, AM=-0.6958, ASD=101.7862, AU=mgal, Z=100km, GI=1x1deg (lat/long)

Figure 42.

Thetis Regio Moho

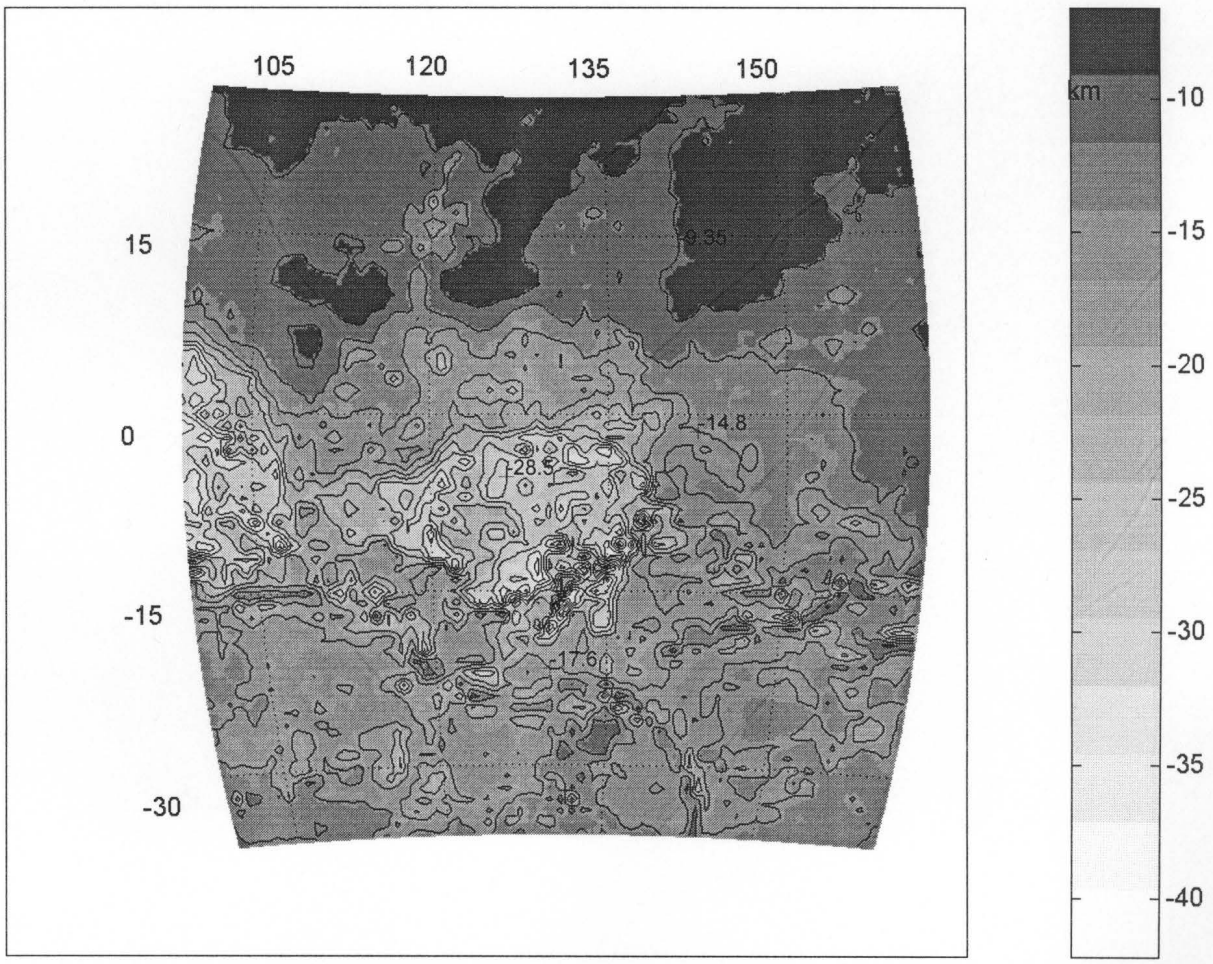

AR= -42.18; -6.61, AM=-15.2540, ASD=5.6063, AU=km, Z=6052km, GI=1x1deg (lat/long)

Figure 43.

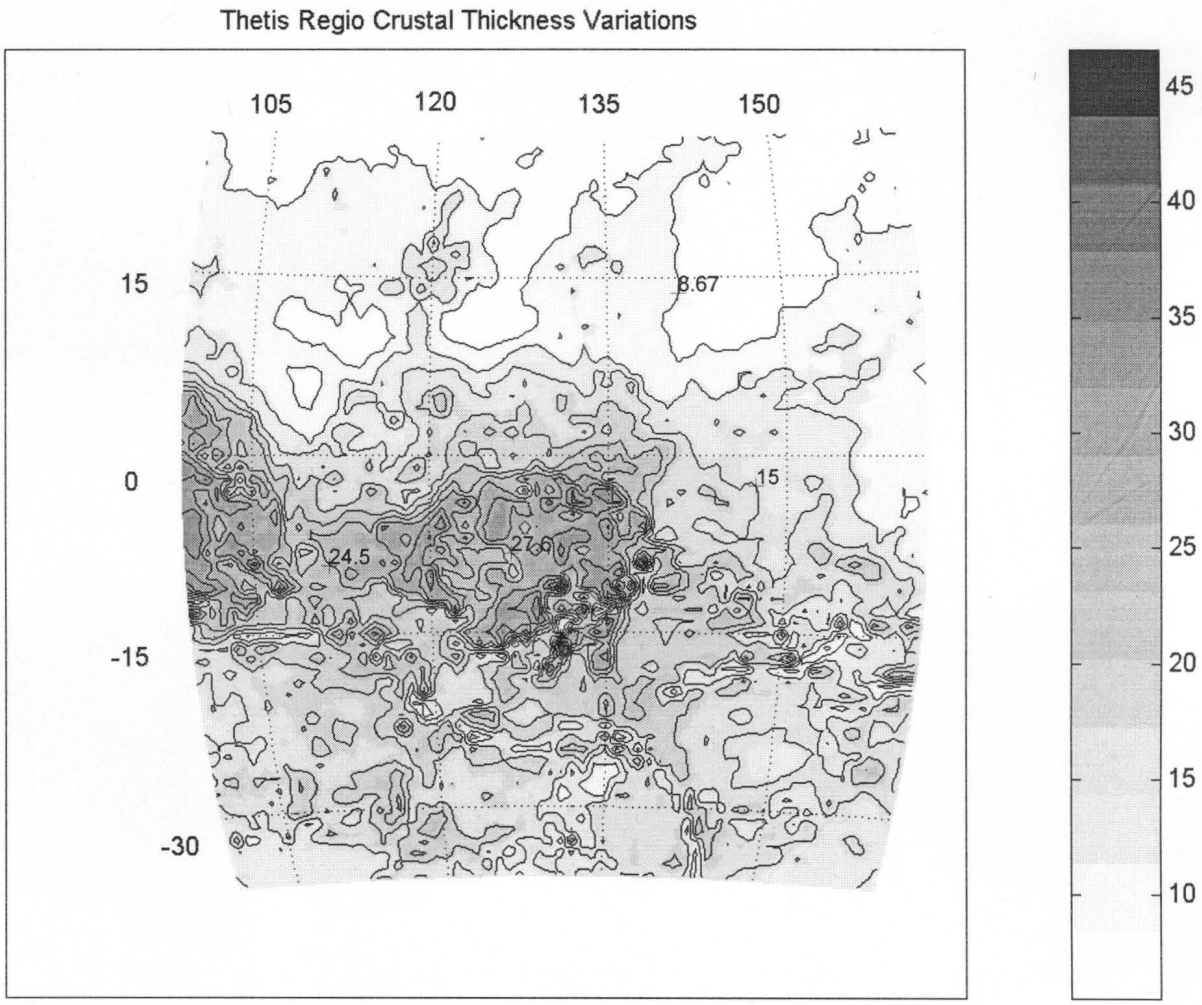

AR= 5.51; 46.62, AM=15.9599, ASD=6.6906, AU=km, Z=6052km, GI=1x1deg (lat/long)

Figure 44.

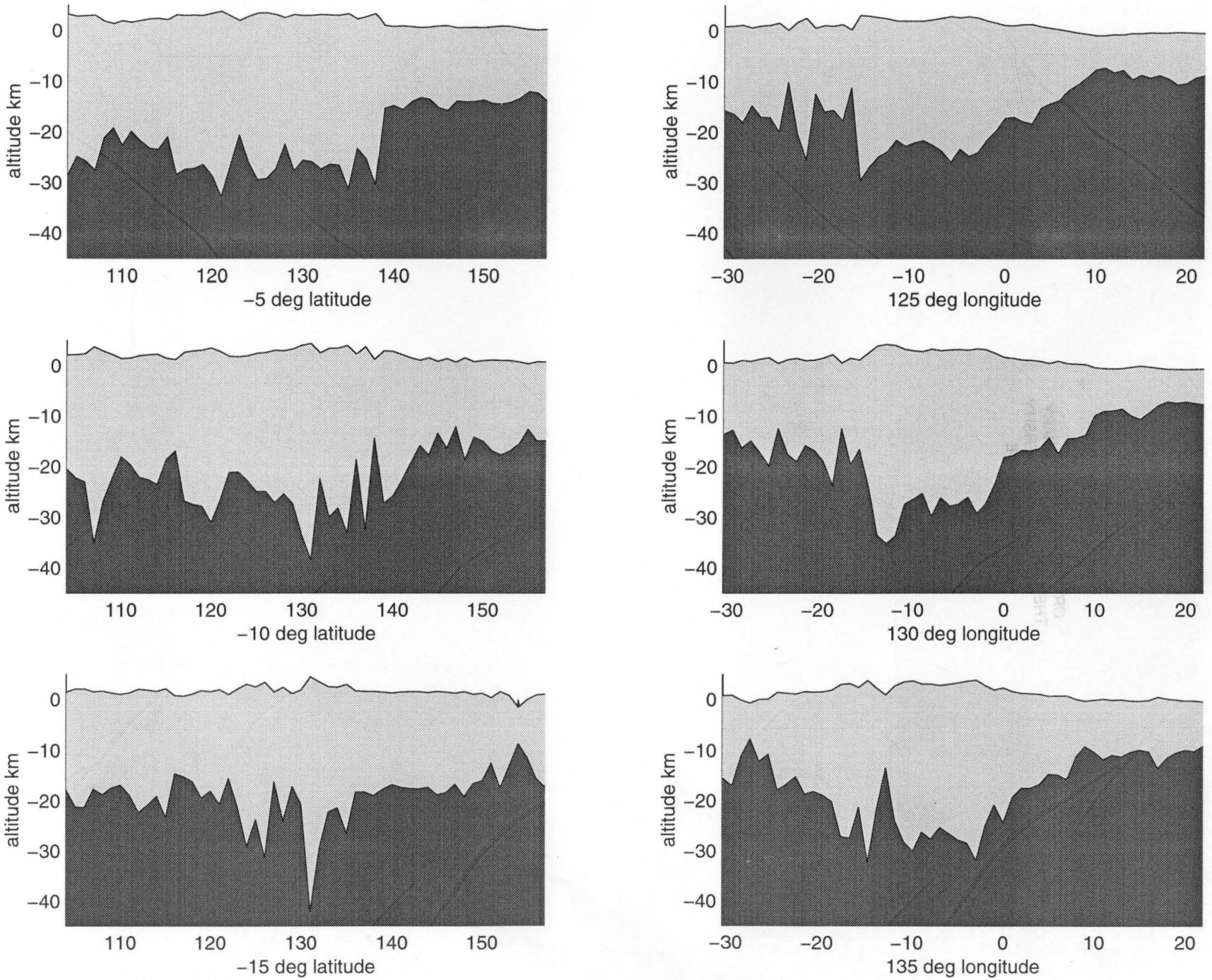
Crustal Thickness Profiles Across Selected Latitudes Through Thetis Regio
altitude km
0
−10
−20
−30
−40
110
120
130
140
150
−5 deg latitude
−10 deg latitude
−15 deg latitude
−30
−20
−10
0
10
20
125 deg longitude
130 deg longitude
135 deg longitude

Figure 45.